Alma Mater Studiorum - Università di Bologna

DIPARTIMENTO DI ASTRONOMIA
Corso di Dottorato di Ricerca in Astronomia
Ciclo XXII (2007-2009)
Esame finale anno 2010

Development of a new galaxy classification technique and its application to the zCOSMOS survey

Dottorando:
Graziano Coppa

Relatore e correlatori:
Ch.mo Prof. Bruno Marano
Dott. Marco Mignoli
Dott. Giovanni Zamorani

Coordinatore:
Ch.mo Prof. Lauro Moscardini

Scuola di Dottorato in Scienze Matematiche, Fisiche e Astronomiche
Settore Scientifico Disciplinare: Area 02 - Scienze Fisiche
FIS/05 Astronomia e Astrofisica

Contents

Introduction

It is well known that galaxies show a large assortment of observational and intrinsic features. In the local and near universe, [up to $z \sim 1$, Bell et al., 2004] many of these properties, such as optical colours [Strateva et al., 2001, Ball et al., 2006], morphological parameters [Driver et al., 2006], and spectral indices [Kauffmann et al., 2003a, Balogh et al., 2004], are known to come in a bimodal fashion. The origin of these bimodalities is not clear yet, in terms of galaxy evolution [Blanton et al., 2003].

The existence of two different groups has been explained in the past as a matter of different of initial conditions (galaxies having different mechanisms of formation), whether it would be a dissipationless collapse, leading to the formation of an elliptical galaxy and the dispersion of its gas content, or a dissipative one, giving as a result a spiral galaxy which retained its gas and could subsequently maintain its star formation [Ellis et al., 2005].

The most accepted current cosmological models, however, predict that the formation of galaxies is mostly hierarchical, massive ellipticals being the result of a series of major mergers between smaller spiral galaxies [Cole et al., 1994a, Baugh et al., 1996, Schweizer, 2000, for a review]. For these reasons the widely accepted scenario to explain the bimodal segregation of the galaxy properties is an evolutive one: galaxies in different phases of their evolution show different colours, different star formation rates, different morphologies. How these different parameters are connected is still a matter of debate [Conselice, 2006]; it appears clear, however, that a better knowledge of these connections would help develop a deeper understanding of the physical processes behind galaxy evolution.

The purpose of this Thesis is to develop a robust and powerful method to classify galaxies from large surveys, in order to establish and confirm the connections between the principal observational parameters of the galaxies (spectral features, colours, morphological indices), and help unveil the evolution of these parameters from $z \sim 1$ to the local Universe.

The Thesis is organized as follows: in Chapter 1 we will present

an overview of our current knowledge in galaxy evolution, focusing in particular in the bimodal galaxy properties and their evolution, how they relate each other and the mechanisms that drive the bimodal behaviour in galaxies. In Chapter 2 we will present a first attempt at building a reliable classification method, the *classification cube* method, which exploits the spectral, photometric and morphological bimodalities of the galaxies in separate ways, and then combines those dataset to give a more complex classification. In Chapter 3 we will present the *PCA+UFP* clustering method, which is a newly devised and original method of classification that makes use of statistical tools like the Principal Component Analysis and the Unsupervised Fuzzy Partition method to classify galaxies, relying in their overall characteristics in a more organic and comprehensive way. In Chapter 4 we will provide some physical interpretation of the results, focusing on the evolution of the different galaxy populations from $z \sim 1$ to the local Universe, and we will analyse some properties of other interesting subpopulations. Finally, in Chapter 5, we will present a brief summary and conclusion of the work.

CHAPTER 1

Galaxy properties

This chapter aims at providing a brief overview of the general properties of the galaxies, from both the observational and theoretical sides, with particular emphasis on the bimodal nature of many of their observational features. We will describe their morphologies, spectro-photometric features, masses and luminosities and their distribution in the Universe. We will also address the issue of their birth, present the most important models of galaxy formation and briefly review some of the mechanisms that trigger, quench and regulate the creation of new stars.

SECTION 1.1

Bimodalities in galaxy systems properties

At the beginning 20th century the knowledge of the Universe was limited to our own star system, the Milky Way. It was Edwin Hubble, in the early 1920s, who established the nature of the then-called *spiral nebulae* as self-bound stellar systems similar to our own. Galaxies are now known to be the places where stars form and evolve, in constant interaction with other galaxies in groups and clusters, and with the interstellar medium (ISM), a complex mix of gas and plasma, dust, relativistically moving atomic and subatomic particles, photons and magnetic fields. The ISM is an important component in galaxy systems, accounting in some galaxies for more mass than stars, and with a fundamental role for star-formation. Most of the gas mass is contained in neutral unstable HI clouds ($10^2 < T < 10^4$ K) and in dense, cold molecular clouds ($T < 10^2$ K) which are the actual places where stars form,

while a great part of the ISM volume is occupied by diffuse ($n \sim 0.1$ cm^{-3}), warm/hot ($T \sim 10^4 - 10^5$ K) turbulent gas that confines clouds by pressure.

There are many different possible mechanisms for star formation triggering, which will be presented briefly in §1.3.1. All these mechanisms cause large-scale compression of the diffuse ISM and the molecular clouds, causing the latter to collapse and begin the processes that will lead to the formation of stars.

In the centre of possibly every galaxy a massive black hole (BH) can be found; when the surrounding material from its accretion disc falls into it, the galaxy can experience a temporary condition during which it releases, through powerful plasma jets and winds, the largest amount of energy known among astronomical objects. This phenomenon is called "Active Galactic Nucleus" (AGN), and it is now thought to play an important role in the evolution of the host galaxy.

Stars, gas, AGN, and all the luminous matter of galaxy constitute only a small (1-5%) fraction of the total mass. Under the assumption of Newtonian gravity, the observed kinematics of galaxies indicate the presence of enormous amounts of unseen mass, the dark matter (DM), whose presence can be inferred only indirectly from its gravitational influence. In their central regions galaxies are baryon-dominated and DM dominates only at large radii. Recently, from statistical analyses, it results that a typical galaxy with stellar mass $M \sim 6 \times 10^{10}$ M$_\odot$ is surrounded by a DM halo of $\sim 2 \times 10^{12}$ M$_\odot$ [Mandelbaum et al., 2006], and $\sim 200 - 250$ kpc in extent. The baryonic mass represents only $3 - 5\%$ of the DM mass in the halo. This fraction could be even lower for dwarf and very luminous galaxies.

Galaxies possess a very wide range of observable properties, which will be addressed in the next subsection. The most important are:

- morphology and light distribution;
- spectral energy distribution and features;
- photometric properties (luminosity and colours);
- size and mass;
- distribution in space.

1.1.1 Morphologies

The publication of Edwin Hubble's "The realm of the nebulae" in 1926 was the first attempt at a galaxy classification based on their morphological properties. Depending on their shape, Hubble grouped galaxies into three

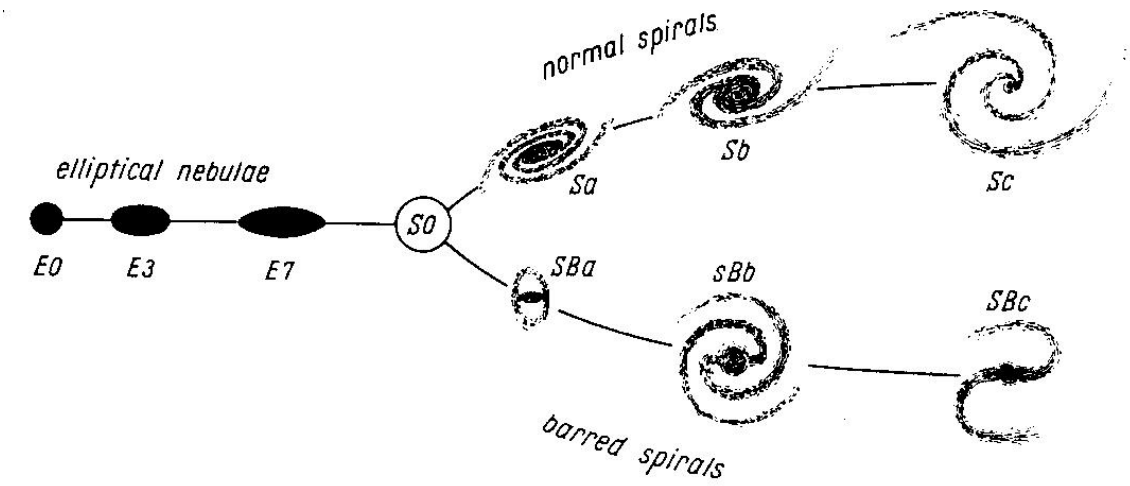

Figure 1.1: Hubble's tuning-fork diagram for the morphological classification of galaxies.

fundamental categories (ellipticals, spirals and irregulars), and arranged them in what will be called "Hubble tuning-fork diagram". This led to the morphological sequence known as the "Hubble sequence": Hubble placed the morphological types into a fork-shaped diagram, shown in Fig. 1.1, in which ellipticals lie in the leftmost sequence, while spiral galaxies were divided on the two branches on the right according to the presence or not of a central bar.

The elliptical galaxies appear smooth (see Fig. 1.2) and almost without structures; they are given a label En, where the index n, defined as $n = 10[1 - (b/a)]$ (with b/a being the apparent axial ratio), describes their elongated shape. The index n typically ranges between 0, for apparently round galaxies, and 7 for the most elongated galaxies. In the past it was believed that these galaxies were just simple oblate stellar systems flattened by rotation; however it was later shown that elliptical galaxies show no or little rotation, suggesting the necessity for a formulation of more complex kinematic model in order to explain their shape.

Spiral galaxies have a disk structure formed by a central bulge from which depart spiral arms. They are morphologically divided into normal spirals (S, see Fig. 1.3) and barred spirals (SB, Fig. 1.4). Each of these classes can be separated into a finer classification: Sa, Sab, Sb, Sbc, Sc (and SBa, SBab, SBb, SBbc, SBc) according to the prominence of the central luminous bulge to the surrounding disk in producing the overall light distribution of the galaxy, the tightness with which the spiral arms are wound; and the distribution of stars in the arms. Sa and SBa galaxies have luminous bulges ($L_{bulge}/L_{disc} \sim 0.3$), and spiral arms tightly wound, and an uniform distribution of star towards the arms. Passing from a to c the bulge become less prominent

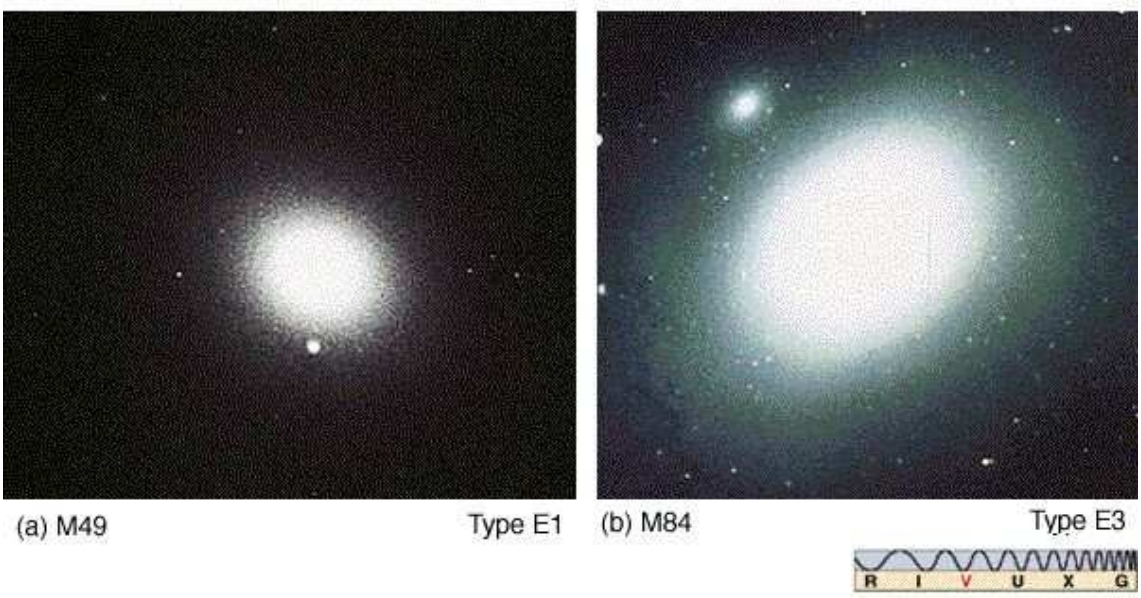

Figure 1.2: Two elliptical galaxies, with different n index.

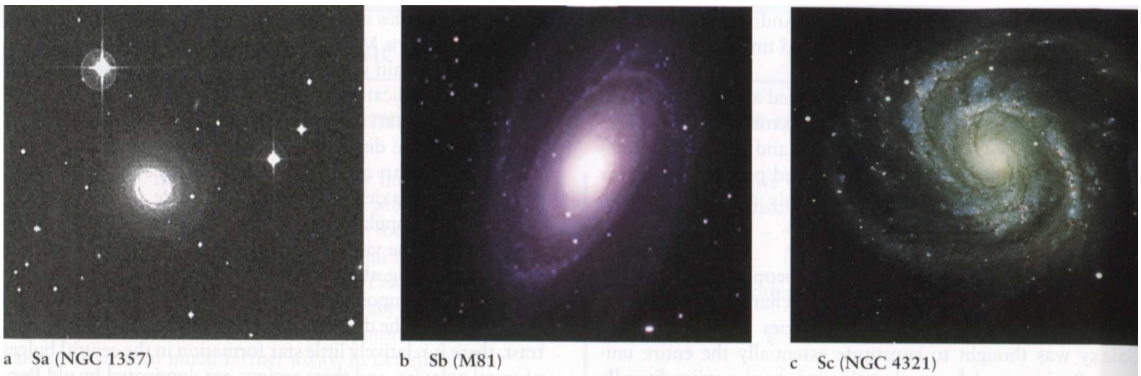

Figure 1.3: Three spiral galaxies, with different bulge-to-disc ratios.

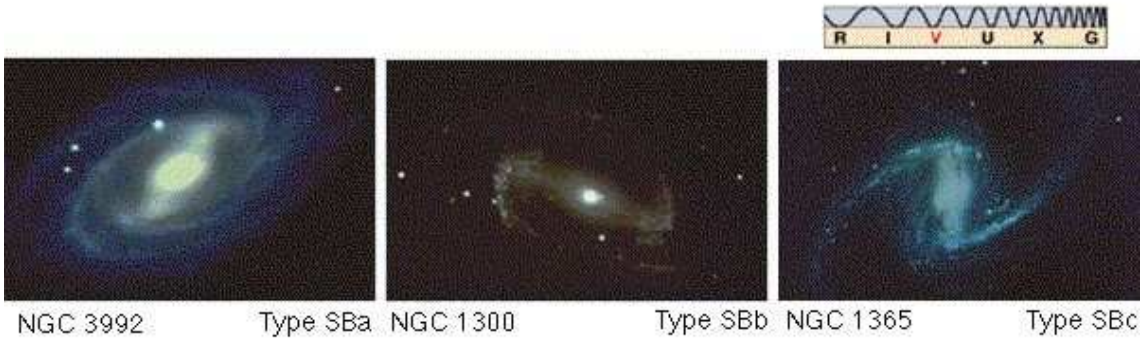

Figure 1.4: Three barred spiral galaxies, with different bulge-to-disc ratios.

($L_{bulge}/L_{disc} \sim 0.05$), the spiral arms widen out and the stars are more clumpily distributed.

At the junction of the ellipticals and spirals, in the middle of Hubble's tuning-fork diagram, there is a class of galaxies known as lenticulars (Fig. 1.5). These galaxies are designated as S0 (or SB0 if they do possess a central bar). The S0 galaxies are characterized by a central brightness condensation, which is similar to an elliptical and is called *bulge* or spheroidal component, surrounded by a disk, which has a different brightness profile with respect to the spheroidal component, being characterized by an intensity which decreases more rapidly with radius. Typically the disk component of the lenticulars is characterized by the presence of a dust lane in such a way that the family of S0s is subdivided into three classes, S01, S02, S03, according to the growing strength of dust absorption. Also the barred lenticulars are divided into three classes: SB01, SB02 and SB03; but the division is made according to the prominence of the bar rather than to the dust strength.

Hubble interpreted his tuning-fork diagram as an evolutionary sequence on galaxies evolving from left to right, that is, from the ellipticals towards the spirals. Nowadays this interpretation has been discarded even if it survives in

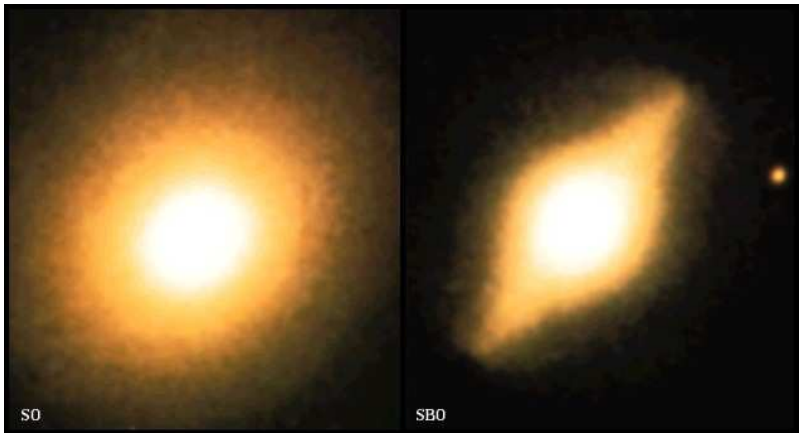

Figure 1.5: Two lenticular galaxies, one normal and one barred.

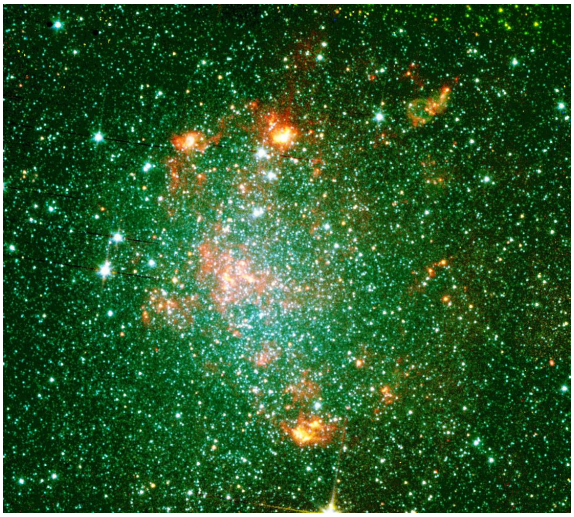

Figure 1.6: NGC 6822, an irregular galaxy.

the terminology: elliptical and lenticular galaxies are still called “early-type” galaxies, while spirals are often referred to as “late-type” galaxies.

This tuning fork diagram has been reviewed and corrected several times [e.g. de Vaucouleurs, 1959, who introduced rings and lenses in the description of the morphologies], but in its essence it is still used as it was designed by Hubble almost a century ago. One addition that does not fit easily in the scheme is made by the irregular galaxies (Fig. 1.6), labelled as I, which are essentially low-mass disorganised and amorphous structures.

Morphological parameters

Although trust in visual classification remains for both low- and high-redshift datasets [e.g., Schawinski et al., 2007, Ferreras et al., 2005], the hope was that new structural classification schemes would also be suitable to describe the various kinds of peculiar galaxies in an appropriate way [Abraham et al., 1994, 1996b], and to separate them from the more familiar galaxy classes.

"Non-parametric" structural measures that have been developed in this context are the concentration index C [among others Abraham et al., 1994, Conselice, 2003] defined as the ratio the amount of light comprised within two different Petrosian radii, the asymmetry index A [Abraham et al., 1996a, Conselice et al., 2000a] which quantifies the degree of rotational symmetry of the light distribution, and the clumpiness index S [Conselice, 2003], which is a measure of the ratio between the amount of light in high spatial frequency structures and the total light of the galaxy. These three are known as the CAS parameters. Two further parameters that are frequently used are the Gini coefficient G [Gini, 1912, Lotz et al., 2004] and the M_{20} parameter [Lotz et al., 2004]. G describes the distribution of flux values among the pixels of an object's image, while M_{20} quantifies the distribution of the brightest 20% of pixels. As opposed to the CAS parameters, neither G nor M_{20} require the centre of a galaxy to be defined, and thus do not need to assume that a well-defined visible centre exists at all. All these parameters are commonly dubbed "non-parametric", since they do not rely on certain model parameter fits, such as the Sérsic index [Sérsic, 1963] in models of radial surface brightness profiles (see next paragraph). Many of this parameter are also clearly correlated (Fig. 1.7).

The Gini coefficient was found to correlate strongly with stellar mass [Zamojski et al., 2007]. They claim that G traces the overall structure of a galaxy better than any other morphological parameter of their study. Apart from describing the overall structure, the G coefficient was also used to identify substructure in galaxies: Lisker et al. [2006] presented a preliminary method to automatically identify large bars, using the radial variation of G within a galaxy.

Kauffmann et al. [2003b] showed that concentration index C as function of stellar mass is bimodal and they interpreted this trend as a correlation between stellar mass and morphology. Strateva et al. [2001], using a by-eye morphological classification, showed that there is a strong correlation between C and galaxy type, whereby systems with $C < 2.6$ are preferentially late-type, while galaxies with $C > 2.6$ are mostly early-type. When higher

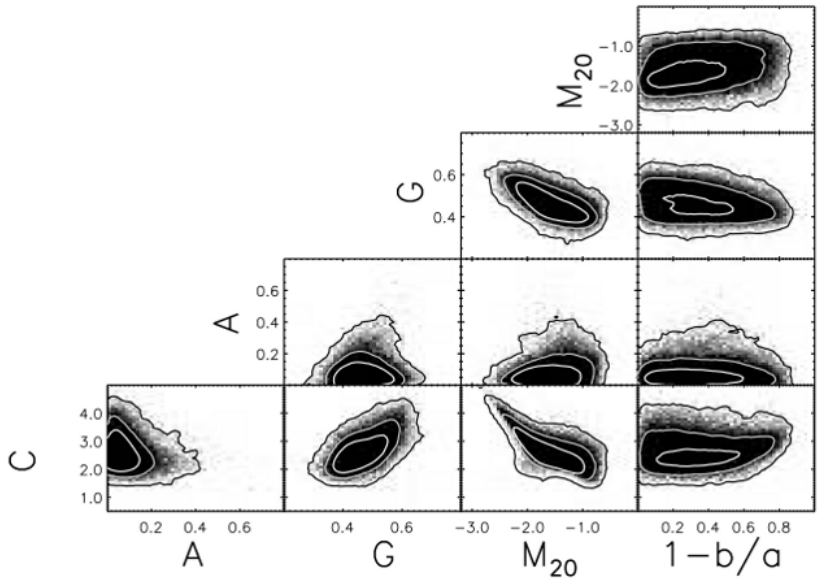

Figure 1.7: Relations between some of the non-parametric diagnostics described in text (M_{20}, G, A, C) and the ellipticity $1-b/a$, for ~ 56000 galaxies of the COSMOS survey. Contours enclose $\sim 30\%$ (white contour), 80% (grey contour), and 98% (black contour) of the galaxies. The main correlations among some of the parameters, such as M_{20}, C, and G, are clearly visible [Scarlata et al., 2007].

mass bins are considered, the distribution shifts towards higher C values: in the most massive bin more than 90% of galaxies have $C > 2.6$. This result implies that, in general, the bulge-to-disk ratio is observed to gradually decrease with decreasing mass: low-mass blue galaxies are disc-dominated, while red massive galaxies are principally spheroids.

Models of galaxies often assume that the mass distribution of a galaxy is symmetric. Galaxies are, to first order, dynamically relaxed systems. Understanding how and in what manner the distribution of galaxy light is asymmetric can help reveal dynamical processes in galaxies. For example, galaxies disturbed by interactions or mergers will tend to have large asymmetries. Attempts to characterize asymmetry for nearby galaxies, and its usefulness as a morphological parameter within existing frameworks, was first carried out by Conselice [1997]. They showed that asymmetry increased with Hubble type, but with a large spread. Potentially more important was the strong correlation found between colour and asymmetry, and a lack of a strong correlation between luminosity and asymmetry for the narrow absolute magnitude of their sample.

The clumpiness of a galaxy's light distribution correlates with the amount

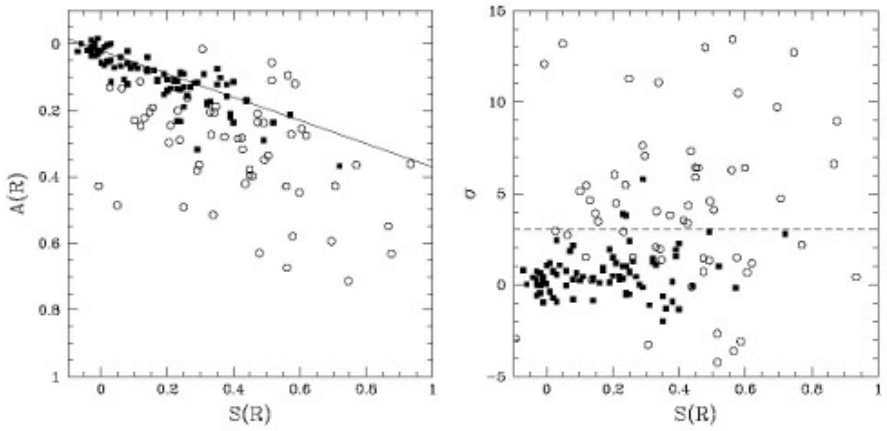

Figure 1.8: The relationship between the asymmetry index A and the clumpiness index S. Higher A and S values indicate galaxies that are more asymmetric and have a higher fraction of clumpy light, respectively. For normal galaxies (black squares, left panel) there is a strong correlation between A and S such that $A = (0.35 \pm 0.03) \times S + (0.02 \pm 0.01)$. The galaxies which deviate from this relationship are the ongoing major mergers, shown in the left panel as open circles. The right panel shows the deviation from the $A - S$ relationship in units of the scatter of the asymmetry values of the normal galaxies (σ). Generally, only the mergers deviate from this relationship by more than 3σ [Conselice, 2003].

and the location of star formation [e.g. Takamiya, 1999, Conselice, 2003]. This trend can be demonstrated by the strong correlation between the clumpiness index S and Hα equivalent widths and colours of star forming galaxies. There is also a strong relationship between the dynamical state of a galaxy and the presence of a merger. Generally, merging galaxies are asymmetric, while non-mergers are not. This has been shown in numerous ways, including empirical methods and the correlation of internal HI dynamics and asymmetries of stellar distributions [Conselice et al., 2000a]. As shown in Conselice et al. [2000b], asymmetric light distributions can also be caused by star formation. However, by decomposing light and kinematic structures in galaxies, it is possible to show that primary asymmetries are not the result of star formation, which forms in clumps, but from large scale lopsidedness on the order of the size of the galaxy itself. Likewise, there is a strong correlation between the asymmetry parameter and the clumpiness parameter for normal star forming galaxies (Fig 1.8). Galaxies with high clumpiness values S, which correlates with high amounts of star formation, have correspondingly higher asymmetry values. However, this correlation breaks down for systems involved in major mergers, such as nearby ultra-luminous infra-red galaxies. The nature of this deviation is such that a galaxy undergoing a merger has too

high an asymmetry for its clumpiness, demonstrating that large asymmetries are produced in large scale features and not in clumpy, star formation like regions.

The definition of M_{20} is similar to that of C, but it differs in two important respects. First, M_{20} is more heavily weighted by the spatial distribution of luminous regions. Second, unlike C, M_{20} is not measured within circular or elliptical apertures, and the centre of the galaxy is a free parameter. Lotz et al. [2004], who introduced the definition of M_{20}, showed that this index can be very successful in the search for galaxy mergers.

Surface brightness distribution

Tightly tied to the morphology of a galaxy is its surface brightness, which is defined as the energy emitted per unit of time, surface and solid angle. Several attempts have been made to find a suitable empirical law describing the light profiles of ellipticals galaxies and of the spheroidal components of lenticulars and spirals. In 1948, Gerard de Vaucouleurs described the brightness profile with the following law:

$$I(R) = I_e e^{-7.67[(R/R_e)^{1/4}-1]}, \tag{1.1}$$

where, I_e, called the effective surface brightness, is the surface brightness at R_e, which is called the effective radius; that is, the radius of the isophote containing half of the total galaxy luminosity. More recent photometric data have shown, however, that for a large fraction of elliptical galaxies and of bulges the de Vaucouleurs' law is only an approximation of the radial brightness profile and, in particular, systematic deviations from this law have been observed. These deviations from the $R^{1/4}$ law have prompted a search for other representations of the brightness profile of early-type galaxies.

A generalization of the de Vaucouleurs' law, proposed by Sérsic in 1963, has been subsequently widely used. Sérsic's law can be written as:

$$I(R) = I_e e^{-b_n[(R/R_e)^{1/n}-1]}, \tag{1.2}$$

where the exponent 1/4 has been replaced by $1/n$, with n being the so-called Sérsic index parameter, which determines the shape of the light profile (see Fig. 1.9). The figure shows that the profiles with higher values of the Sérsic index are characterized by a distribution of light decreasing more rapidly with the distance from the centre, that those with lower Sérsic index. The constant b_n is analogous to the 7.67 constant in de Vaucouleurs' law, but it is function of n. Sérsic's law is often written in logarithm form:

$$\mu(R) = \mu_e + c_n[(R/R_e)^{1/n} - 1]. \tag{1.3}$$

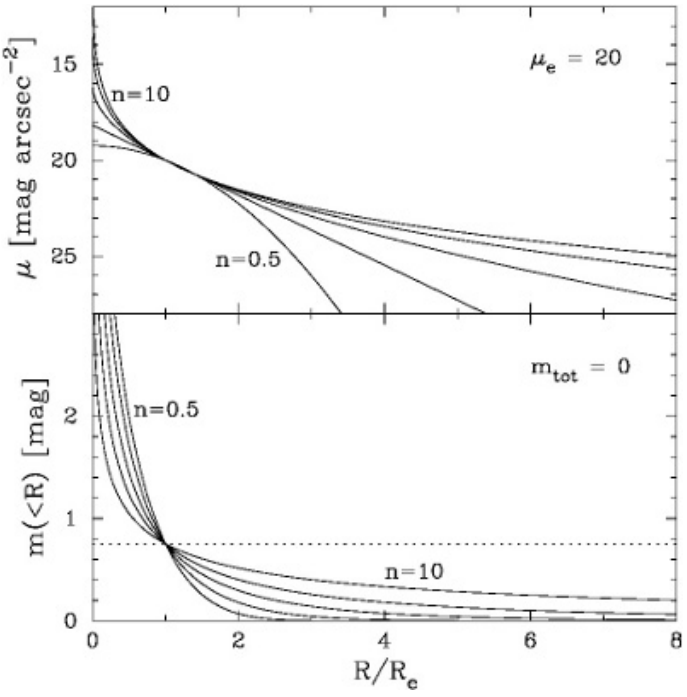

Figure 1.9: Top panel: Sérsic surface brightness profiles for n=0.5, 1, 2, 4, and 10. The profiles have been normalised at $\mu_e = 20$ mag arcsec^{-2}. Bottom panel: Sérsic aperture magnitude profiles, normalised such that the total magnitude equals zero. The dotted line is offset by 0.75 mag (a factor of 2 in flux) from the total magnitude [Graham and Driver, 2005].

If the shape parameter $n = 1$, the Sérsic law assumes an exponential form which models well the brightness profile of the disk component present in the lenticular galaxies.

1.1.2 Mass

Elliptical and spiral galaxies have a large range of masses, although on average the ellipticals are more massive than the spirals: the characteristic mass scale which distinguishes the two families is $M_{\rm cross} \sim 3 \times 10^{10} {\rm M}_{\odot}$ [Kauffmann et al., 2003b].

This bimodal behaviour of the galaxy population as function of mass is particularly evident in some relations such as the luminosity function, the scaling relations, and in particular features such as colour, morphologies, and the mean stellar age.

Elliptical galaxies

Elliptical galaxies span a wide range of mass and luminosity from the gigantic cD galaxies, through normal and dwarf ellipticals, to the least massive

galaxies in the Universe, the dwarf spheroidals.

cD ellipticals are enormous structures, with diameter up to ~ 1 Mpc, found at the centre of galaxy clusters. They are characterised by a central component that resembles an elliptical galaxy with a surrounding diffuse halo made of stars whose surface brightness is lower than the central component. The magnitude of this objects can reach $M_{\mathrm{B}} = -25$ and their mass $10^{14}\,\mathrm{M}_{\odot}$.

Normal ellipticals show strong stellar concentrations in the central regions, which can produce luminosities as high as $M_{\mathrm{B}} = -23$. The mass of these systems can reach $10^{13}\,\mathrm{M}_{\odot}$. Their light profiles are well described by Sérsic's law with $n > 2$.

Dwarf ellipticals are strongly different from the "normal" ellipticals being much more compact and of lower luminosity. The surface brightness distribution can be described by a Sérsic profile with $n < 2$, indicating the presence of a shallow potential well. The total mass can reach $10^{9}\,\mathrm{M}_{\odot}$ and the dimension does not exceed 10 kpc.

Dwarf spheroidals are the lowest mass galaxies in the Universe, and while they may have extremely low luminosities (reaching $M_{\mathrm{V}} \sim -3$) and surface brightnesses, they appear to have a minimum DM halo mass of $\sim 10^{7}\,\mathrm{M}_{\odot}$.

Spiral galaxies

Differently from elliptical galaxies, spiral galaxies do not cover such a wide range of total mass, spanning from $10^{9}\,\mathrm{M}_{\odot}$ to $10^{12}\,\mathrm{M}_{\odot}$, against the seven orders of magnitude cover by ellipticals from $10^{7}\,\mathrm{M}_{\odot}$ to $10^{14}\,\mathrm{M}_{\odot}$ but, on the contrary show strong differences in dimensions. In fact, the dimension of the disc can vary from 5 kpc of diameter to 100 kpc. However, for spiral galaxies it is necessary to distinguish between the bulge component and the disc. The surface brightness distribution of the bulge follows a de Vaucouleurs' profile, while the disk is well described by an exponential law.

1.1.3 Photometric properties

It has been known at least since the late 1930s that colours of galaxies reflect their dominant stellar populations. The HR diagram by Ejnar Hertzsprung and Henry Norris Russell in the 1910s showed that the luminosity of the main sequence stars, which are the large majority of the stars in a galaxy, is directly related to their colours: the most luminous stars are blue, while

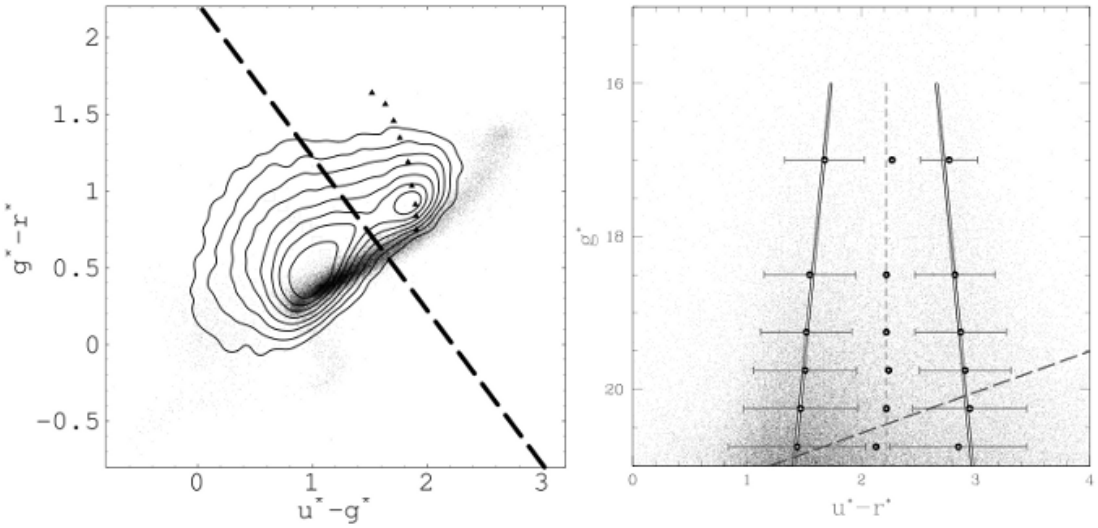

Figure 1.10: Left panel: distribution of galaxies (contours) and stars (dots) in the $u^* - g^*$ vs. $g^* - r^*$ colour-colour diagram. Right panel: $u^* - r^*$ vs. g^* colour-magnitude diagram. Dashed lines in both panels are the $u^* - r^* = 2.22$ separator [Strateva et al., 2001].

the smallest ones lie in the red side of the diagram. The understanding of the physical processes that allow stars to shine led to the concept of the mass being the main driver of a star's evolution; more massive stars have surface temperatures $T > 10000$ K and therefore blue colours, and consume their atomic fuel very rapidly, until the final supernova explosion. Less massive stars, on the other hand, have lower temperatures and emit mainly in the red part of the visible spectrum and in the infra-red. Their life in the main sequence is considerably longer, comparable with the age of the Universe so a large part of these low-mass stars are essentially unevolved. Low-mass stars are also much more common than high-mass stars: given a Salpeter IMF [Salpeter, 1955], where the number of stars for a given mass $\xi(M) \propto M^{-2.35}$, stars like the Sun should be 1000 times more frequent than $20\,\mathrm{M}_\odot$ stars. High-mass stars, however, are much more luminous so that, if present, they dominate the overall colour of a galaxy. In summary, colours can give a hint on the star formation rates of a galaxy: red galaxies are dominated by small stars still burning hydrogen in the main sequence phase and large stars, the red giants, which are evolved intermediate-mass objects. The population of these galaxies is therefore old, meaning that there is small or no star formation ongoing. Blue galaxies, on the other hand, are dominated by the light of the most massive stars, whose life is only few Myrs long: their star formation is therefore very recent and most probably strong and still present.

Since the era of large surveys like SDSS, galaxy colours are known

to come in a bimodal way. Strateva et al. [2001] have shown that the distribution of the $u^* - r^*$ colour in their sample is peaked in two different regions (Fig. 1.10): the red sequence and the blue cloud. The red sequence is defined roughly by early-type galaxies. Along this red sequence, integrated colours of galaxies become progressively redder at bright magnitudes. Late-type galaxies, instead, populate the wider and more dispersed blue cloud [Tully et al., 1982].

Baldry et al. [2004] confirmed that the colour distribution of galaxies (Fig. 1.11 and Fig. 1.12) can be approximated by a bimodal function made by the sum of two Gaussian functions. This trend is evident across seven magnitudes and it is not strongly dependent on redshift

As we already pointed out, Fig. 1.10 shows the colour bimodality found in large samples of galaxies: galaxies are distributed in a bimodal way, with galaxies possessing younger stellar population peaking in the blue part of the distribution and galaxies with older stars distributed mainly in the red part. As a blue star forming galaxy ages, and its star formation is being quenched for whatever reason, galaxies do migrate toward the red part of the colour-magnitude diagram, as illustrated in Fig. 1.13.

In recent years the notion of "green valley" has arisen: galaxies in the intermediate region of the colour-magnitude diagram are thought to be transitional galaxies, object with quenched star formation that begin their voyage toward the red sequence. Recent observations of the host galaxies of AGN both in the nearby universe and at redshifts out to $z \sim 1$ have shown that the rest-frame optical colours of the host galaxies peak in the green valley [Schawinski et al., 2007, Nandra et al., 2007, Silverman et al., 2008]. This observation has led to the suggestion that these green valley AGN host galaxies represent a population in transition from the blue cloud to the red sequence that continuously build up the red sequence across a large range in cosmic time [Faber et al., 2007, Bundy et al., 2008].

However, the interpretation of green or intermediate host galaxy colours is not necessarily unique [Schawinski, 2010]. In general, green or intermediate optical colours can arise from a number of scenarios. The three main scenarios are (1) the recent, rapid suppression of star formation; (2) the slow, gentle fading of star formation; and (3) an enhanced dust screen covering a regular blue cloud star-forming galaxy. Thus the observation that AGN host galaxies exhibit green optical colours is consistent with a scenario where a recent catastrophic event (such as the AGN phase) has shut down star formation.

If the green colours of AGN host galaxies are due to a recent, rapid

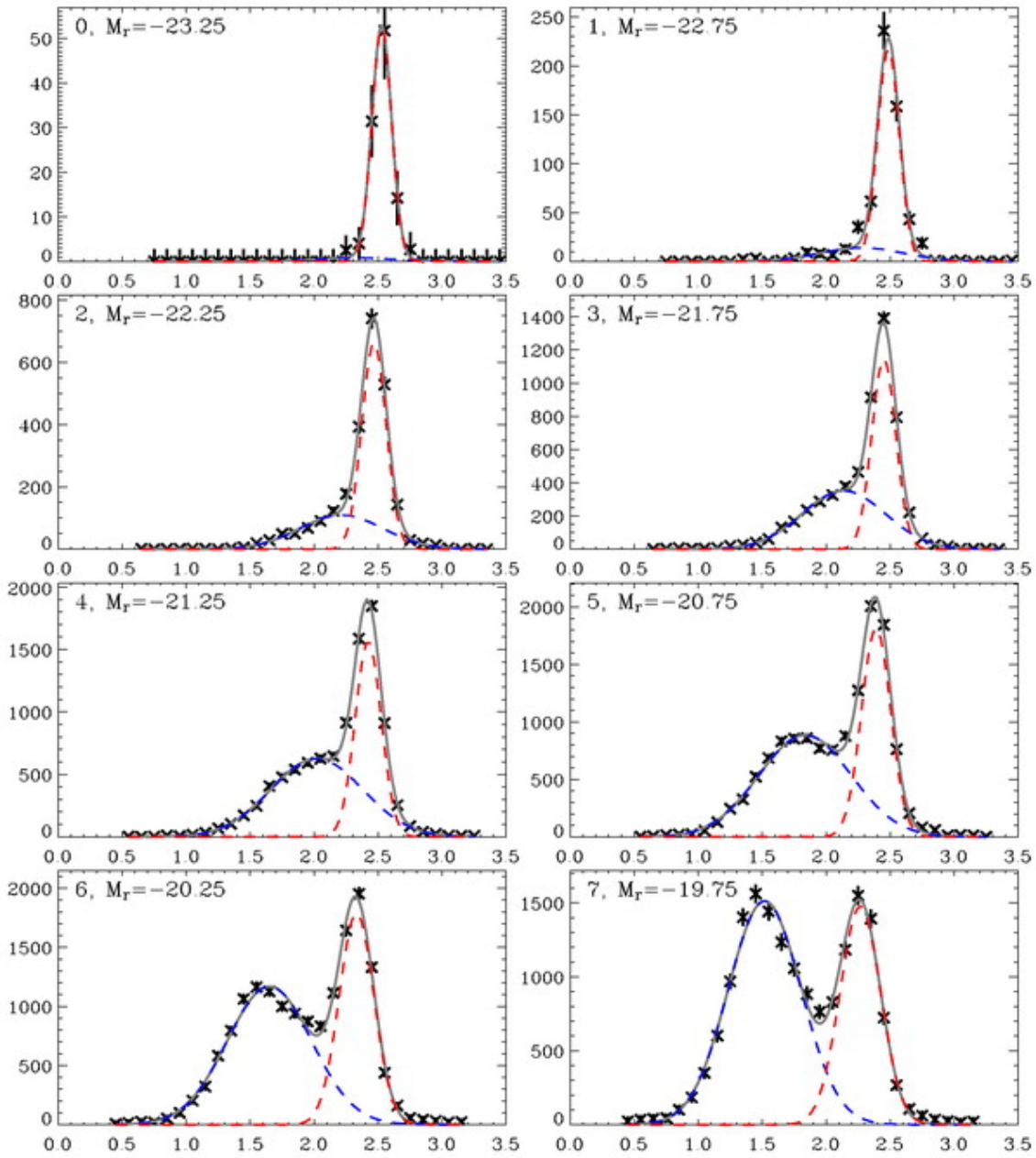

Figure 1.11: Colour $u-r$ distributions in bins of absolute magnitude $-23.25 \leq M_r \leq -19.75$. Blue and red dashed lines are the Gaussian fits of the blue and red distributions, while the solid lines are the convolution of the two single fits [Baldry et al., 2004].

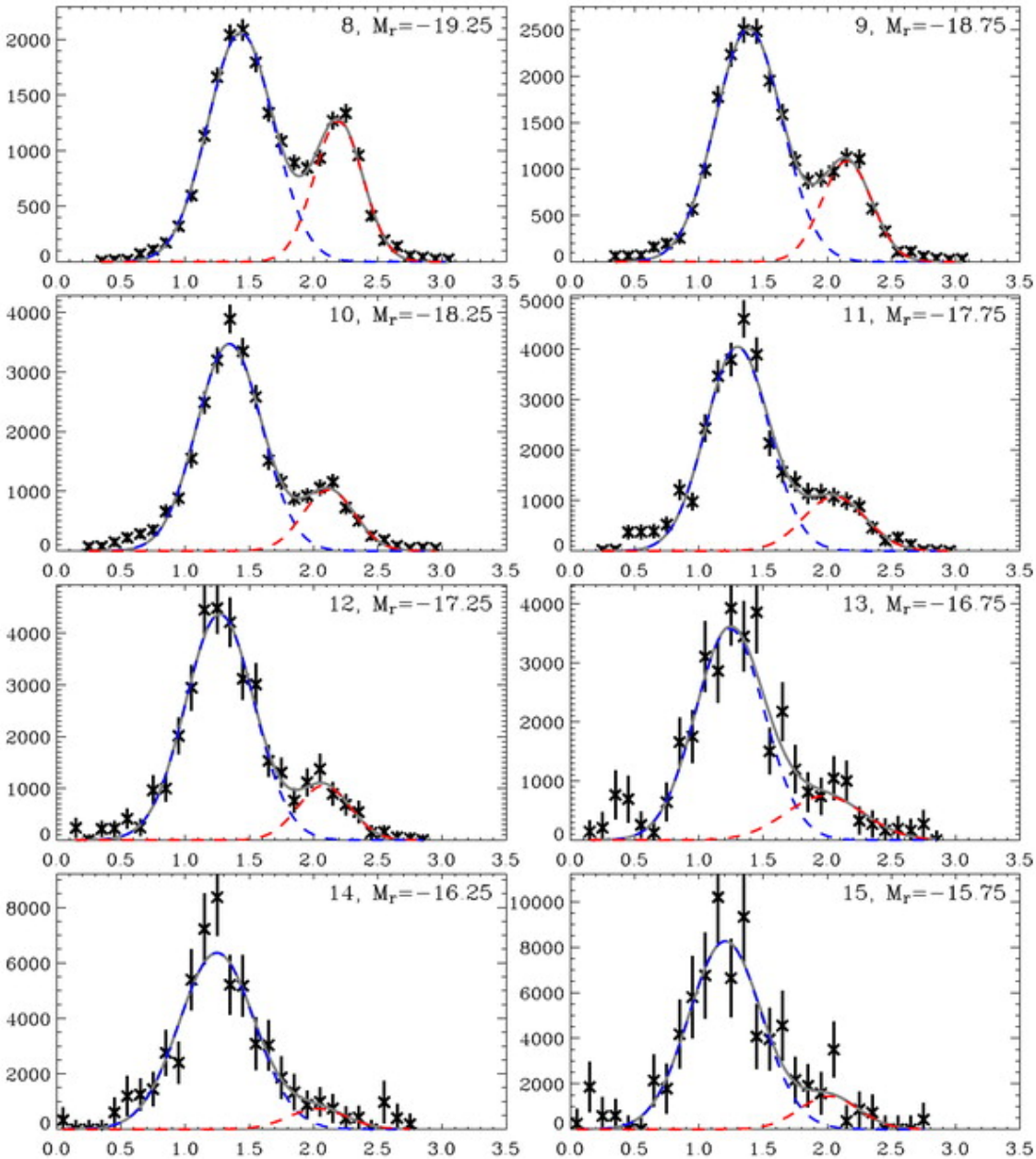

Figure 1.12: Same of Fig. 1.11, in bins of magnitude $-19.25 \leq M_r \leq -15.75$.

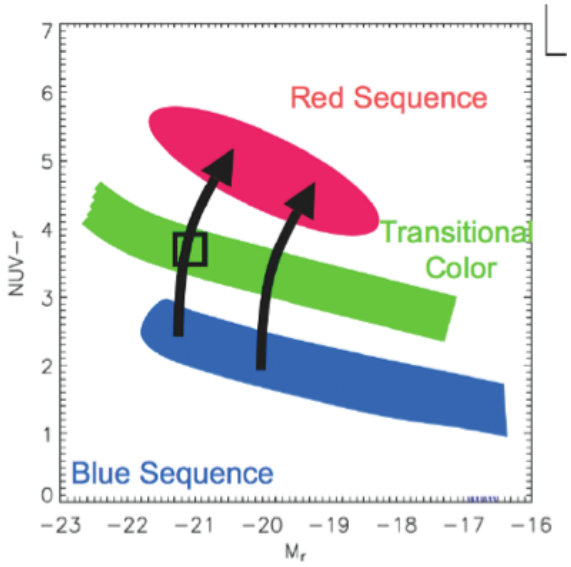

Figure 1.13: Sketch of a colour-magnitude diagram. Emphasized are the "blue sequence" (also known as "blue cloud"), the "red sequence" and the "transitional colour" region also known as "green valley".

suppression of star formation, then the fact that the host galaxies are "green" leads to a time scale problem. Intermediate colours in such a suppression scenario imply that the event that led to the suppression of star formation is already significantly in the past. The minimum amount of time elapsed since the suppression event in the case of instantaneous suppression is set by the lifetime of OB stars that dominate the ultraviolet-optical spectral energy distribution of young stellar populations. Thus, if there are no AGN host galaxies with blue host galaxy colours, then the AGN population detected in the green valley cannot be responsible for the suppression of star formation.

Martin et al. [2007] have studied this by measuring how fast galaxies move from one end to the other. By using SDSS spectra, one can infer the star formation histories of individual galaxies. To this end, spectroscopic indices – more specifically, $D4000$ and Hδ – were measured for a large number of green valley galaxies. While evolving, galaxies trace a path through the $D4000$-Hδ plane, and this path is strongly dependent on the speed through which star formation is quenched. By measuring masses and number densities of the green valley galaxies, one can infer how much mass is going through the valley at a given time.

Martin and collaborators have found that the mass going through the green valley is consistent with the build-up of the red sequence, with quenching times-scales of a few hundred million years for most galaxies.

In addition, they have found the fraction of AGN in the green valley is the highest across the colour-magnitude plot, which could indicate active nuclei play a prominent role in quenching star formation. The galaxies studied by them are at $z \sim 0.2$. However, we know the process of galaxy formation and evolution is strikingly different across cosmic time, from $z \sim 10$ (or more) until today, and that most stars in the present universe were formed at $z \sim 2-3$. Therefore, one would expect the quenching to be different at different ages of the cosmos.

1.1.4 Spectral properties

Galaxy spectra constitute a mine of information about the properties of stellar populations, such as the age, metallicity, chemical composition and star-formation history. By comparing observed spectra and, in particular, the equivalent widths of absorption and emission lines to synthetic spectra from models of simple stellar populations (SSPs), it is possible to obtain information of these stellar population parameters.

For example, the strong absorption of Balmer lines (Hα, Hβ, Hδ) is characteristic of A-type stars, and stellar populations dominated by a burst of star-formation that ended less than 1 Gyr ago, at an age when A-type stars dominate the optical emission of SSPs. Hence high value of Balmer lines are indicative of recent star-formation while low values characterize galaxies with old stellar populations.

The index $D4000$ is the measure of the discontinuity observable at 4000Å in the spectrum. The break occurring at 4000Å is the strongest discontinuity in the optical spectrum due to the accumulation of many spectral lines in a narrow wavelength range. The principal contribution to the opacity of stellar photospheres comes from the ionized metals. In hot stars, due to their high temperatures, the elements are multiply ionized and the opacity decreases, so the 4000Å break will be small for young stellar populations and larger for old and metal-rich galaxies. This index has been extensively used by many authors since the 1960s [among the first, Wildey et al., 1962, van den Bergh, 1963, van den Bergh and Sackmann, 1965] as indicator of an old stellar population, and is defined as the ratio between the average flux density in the bands 4050–4250Å and 3750–3950Å [Gorgas et al., 1999].

The analysis by Kauffmann et al. [2003b] of $\sim 122\,000$ galaxies from the Sloan Digital Sky Survey underlined that the distribution of mean stellar age as function of stellar mass $M_\star$ is strongly bimodal. In Fig. 1.14 are reported the density distributions of $H\delta_A$ and D_n4000, which is a narrower band definition of $D4000$ [Balogh et al., 1999], as function of logarithm of

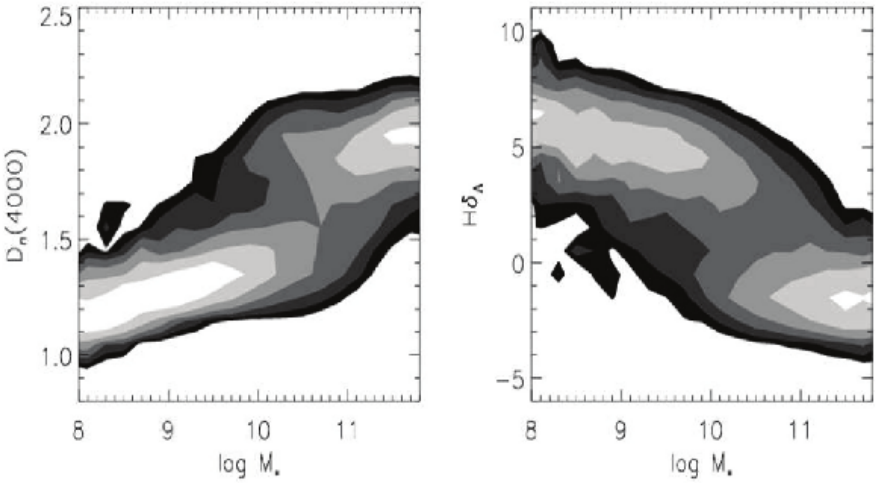

Figure 1.14: The density distribution of stellar age indicators D_n4000 and Hδ as functions of the logarithm of stellar masses, showing trend and bimodalities [adapted from Kauffmann et al., 2003b].

stellar mass. The grey-scale indicates the fraction of galaxies in a given logarithmic mass bin that fall into each age-indicator bin. The contours are separated by factors of two in population density. It shows the clear strong bimodality between stellar mass and mean stellar age: massive galaxies are characterized by older stellar population having typically lower values of Hδ and higher values of D_n4000. At a mass value $M_{\rm cross}$ a transition towards younger stellar populations begins to take effect.

Galaxy bimodality is observed also in the relation involving metallicity Z. As first observed by Lequeux et al. [1979], metallicity is strongly dependent on galaxy stellar mass, such that more massive galaxies are more metal rich. Using large datasets from optical surveys such as SDSS, more recent analyses have studied the luminosity-metallicity and mass-metallicity correlations [e.g. Pilyugin and Ferrini, 2000, Tremonti et al., 2004]. Tremonti and collaborators found that, for galaxies of $M_{\rm cross} < M_\star < 10^{12}$ M$_\odot$, $Z \propto M_\star^{0.5}$, while for 10^8 M$_\odot < M_\star < M_{\rm cross}$ the correlation disappears, since Z becomes constant in the entire low-mass range. The observed relation show a significant scatter, with only half of the spread due to measurement errors: analysing the correlations between the scatter and other galaxy properties, they point out a potential connection with stellar surface mass density $\mu_\star$, such that galaxies with higher surface densities are more metal rich relative to galaxies of similar stellar mass.

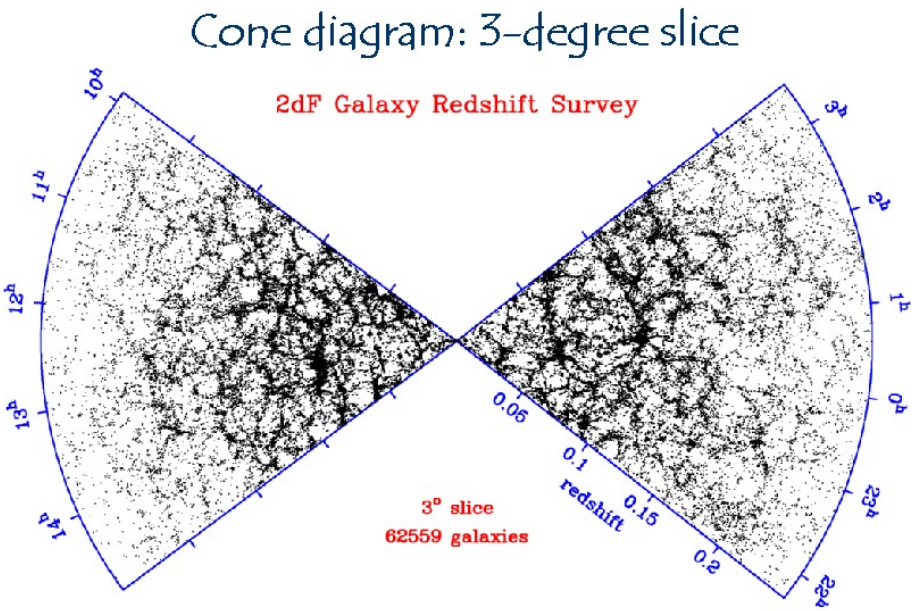

Figure 1.15: Large scale structure of the Universe in the 2dFGRS survey data.

1.1.5 Environment

Galaxies are not distributed uniformly across the Universe, but belong to structures deeply different for density, shape, photometric and dynamic properties: from the enormous voids in which the number density of galaxies is greatly depleted, to the field where galaxies are relatively isolated, to rich and complex hierarchies of structures like the clusters, the densest regions of the universe, where 100-1000 galaxies are bound together by gravitational forces in a region of $\sim 3-6$ Mpc in diameter. The differences between clusters and the field refers not only to the galaxy density, but also in how the galaxies are distributed. Indeed, in clusters, galaxies are distributed in a non homogeneous way being strongly concentrated towards the centre and with a number density decreasing toward the outer regions. Recent large surveys, such as the 2-degree Field Galaxy Redshift Survey (2dFGRS), the Sloan Digital Sky Survey (SDSS), and the COSMOS survey have shown, using statistically significant samples, that galaxies are distributed on filamentary-type structures (see Fig. 1.15) and super-clusters (aggregation of clusters of galaxies), joined by filaments and walls of galaxies creating a foam-like structure of matter and gravitational potential. Voids within this foam can be as large as 50 Mpc across.

In the local universe the fraction of galaxies with elliptical and lenticular

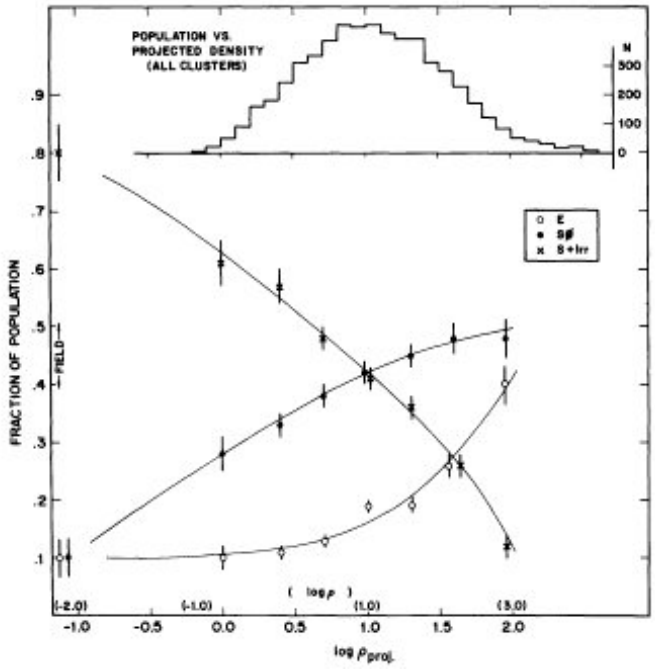

Figure 1.16: The fraction of E, S0 and S+I galaxies as function of the projected density, in Mpc^{-3}. The upper histogram shows the number distribution of the galaxies over bins of projected density [Dressler, 1980].

(i.e., early-type) morphologies is higher in clusters of galaxies than in less dense environments [Hubble, 1926, Oemler, 1974, Melnick and Sargent, 1977, Dressler, 1980]. To first order, this morphology-density relation appears to be a universal characteristic of galaxy populations [e.g. Postman and Geller, 1984, Helsdon and Ponman, 2003]. In quantitative terms, morphological fractions correlate over 3 orders of magnitude in projected galaxy density (Σ), thereby linking the properties of cluster galaxies ($\Sigma \sim 1000\,\mathrm{Mpc}^{-2}$) with those of the field galaxy population ($\Sigma \lesssim 10\,\mathrm{Mpc}^{-2}$).

Early-type galaxies are the dominant population of clusters and are mostly in the centre following overall density distribution, while late-type galaxies form less than 20% of the total cluster population and are principally found in the outer regions. From these results, Dressler [1980] inferred that the distribution of the different morphological galaxy types in clusters is strictly correlated to density (Fig. 1.16).

The morphological segregation of galaxies is a generic prediction of cold dark matter simulations of large-scale structure formation [Frenk et al., 1985, 1988] and more recent semi-analytic galaxy formation models [e.g. Kauffmann, 1995, Springel et al., 2001]. In that context, the observed morphology-density relation is interpreted as the combination of

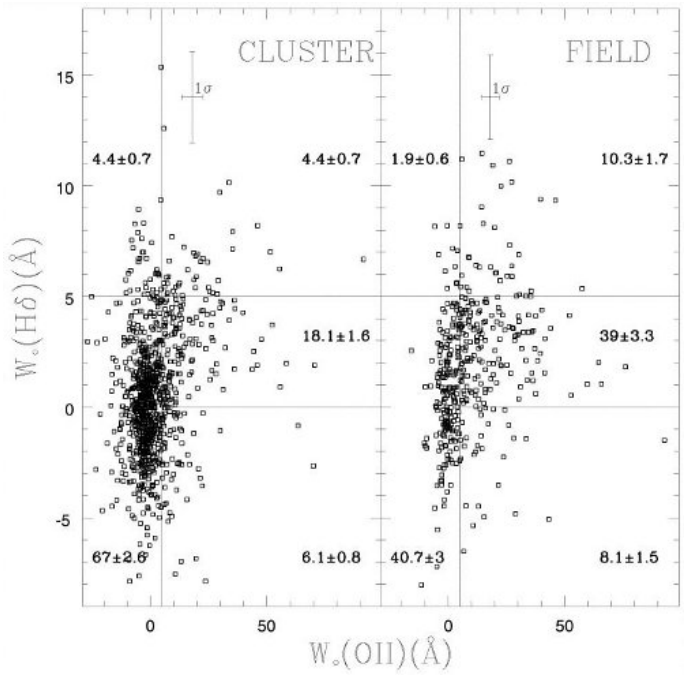

Figure 1.17: Cluster and field data presented separately in the [O II]-Hδ equivalent widths (W_0) plane. Positive values of W_0[O II] and negative values of W_0(Hδ) represent emission in these indexes. The sample error bars represent the mean 1 *sigma* error, and the number in each region represents the weighted percentage of galaxies in that region. The fraction of galaxies undergoing some type of star formation is 57% in the field and only 29% in the clusters [Balogh et al., 1999].

two mechanisms. First, the local density of galaxies and dark matter is a proxy for the epoch of initial collapse of a given structure; the most massive structures at any epoch represent the earliest that collapsed. Second, interactions between galaxies, dark matter, and the intra-cluster medium (i.e., environmental processes) are likely to transform infalling field galaxies from gas-rich spirals to gas-poor lenticular galaxies.

An important element of investigating the physics of morphological transformation is to trace the cosmic evolution of the morphology-density relation over the full range of projected density available locally [Smith et al., 2005]. The time-scales on which the relation evolves in different density regimes will hold important clues to the physical processes responsible. Pioneering observations of the high blue fractions seen in intermediate-redshift clusters by Butcher and Oemler [1978] also raises the possibility of evolution in the morphological mix with look-back time. To that end, Dressler et al. [1997] used high-resolution imaging with the Hubble Space Telescope (HST) to measure the morphology-density relation in the core regions of a

sample of rich clusters at $z \sim 0.5$. Dressler and collaborators found that the fraction of lenticular galaxies in clusters declined by a factor of $2-3$ between $z = 0$ and $z = 0.5$, and this evolution was accompanied by a corresponding increase in the fraction of star-forming spirals [see for instance Andreon, 1998, Treu et al., 2003]. At higher redshifts, the distinction between elliptical and lenticular morphologies becomes increasingly difficult to draw [Smail et al., 1997]. Nevertheless, several authors have measured the total early-type fraction in individual clusters at $z \sim 1$ to be ~ 0.5 [e.g. van Dokkum et al., 2000, van Dokkum and Franx, 2001, Lubin et al., 2002], a smaller fraction than that found in the densest environments at $z = 0$.

The star-formation properties of galaxies in rich clusters is significantly different from those of field galaxies [e.g. Osterbrock, 1960, Koopmann and Kenney, 2004]. In the field, the level of the star-formation in galaxies is several times higher than in systems of similar luminosity in the core of clusters. This is partly due to the morphology-density relation since elliptical and S0 galaxies, principally passive systems, are more abundant in clusters, but there is evidence that even later type galaxies in clusters form stars at lower rates than in the fields [Balogh et al., 2000]. For example, Balogh et al. [1999] show that the [O II] equivalent widths, on average, are much larger for field galaxies then their counterparts in rich cluster with the same bulge-to-disk ratios and luminosities (Fig. 1.17). One of the difficulties in inferring the star-formation rate from the [O II] emission is that it can be influenced by dust [Poggianti and Wu, 2000]. This limit can be overcome using the Hα index, which is less sensitive to dust effects [Kennicutt, 1998]. From the analysis of a Hα survey of galaxies in three clusters at $z \sim 0.3$, Couch et al. [2001] found that in one cluster the star-formation is strongly and uniformly suppressed, while, in general only 10% of galaxies show Hα emission, with an overall star-formation rate of $\sim 4\ \mathrm{M_{\odot}yr^{-1}}$.

The distribution in colour depends strongly on the galaxy density on ~ 1 Mpc scales [Dekel and Birnboim, 2006]: blue and red sequence galaxies tend to populate the low- and high-density environments respectively [e.g. Kauffmann et al., 2004, Blanton et al., 2005].

Blanton et al. [2005] in the SDSS ($\sim 114\,000$ galaxies), analysing the distribution of $g-r$ colour, mean surface brightness, Sérsic index and luminosity, found that galaxy colour is the most predictive property of local environment (see Fig. 1.18). Even if the dependence on luminosity appears more impressive, this dependence only affects a small fraction of the total number density of galaxies in this sample, and the dominant horizontal contours in the lower-right panel demonstrate that colour is in general more

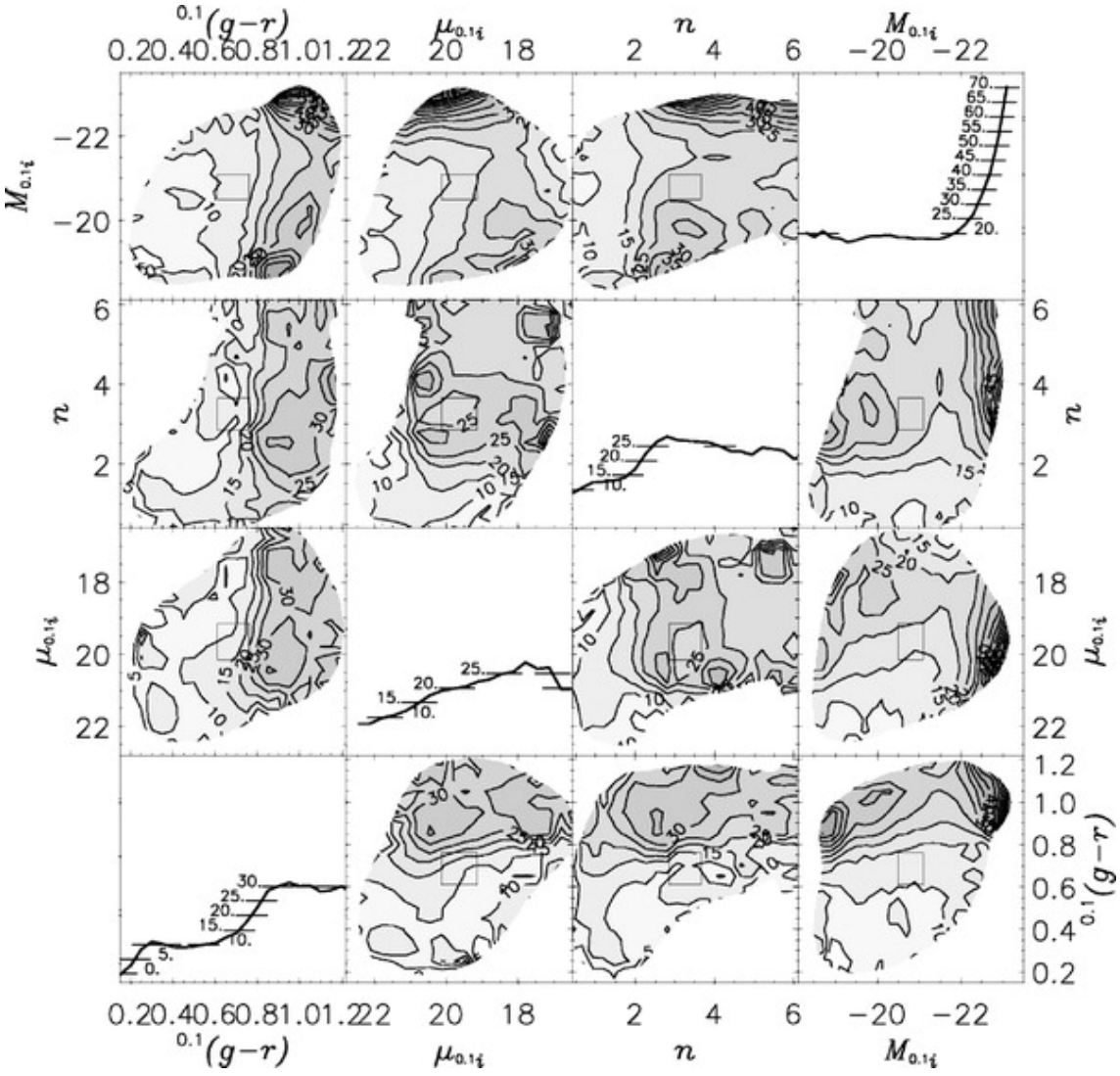

Figure 1.18: Mean local overdensity as a function of pairs of galaxy properties. Off-diagonals show the mean overdensity as a colour-coded contour plot in which darker areas indicate galaxies in denser environments. For example, in the lower right corner, the blue, low luminosity galaxies are on average in the least dense environments and red, high luminosity galaxies are on average in the most dense environments. Plots along the diagonal show the mean overdensity as a function of each property on a linear scale. Labeled cross bars indicate where the mean crosses various thresholds. [Blanton et al., 2005].

predictive than luminosity. For this reason, the pair colour and luminosity taken together can be considered the most predictive properties of local overdensities. At fixed colour and luminosity, density is not closely related to measures of galaxy structure-surface brightness of Sérsic index, implying that the morphology-density relation is driven by the more fundamental colour-density relation.

SECTION 1.2

Galaxy formation

Considering the bimodal distribution of many galaxy properties, it is of great interest and of paramount importance to characterize the mechanisms that allow galaxies to take shape and evolve, to understand the origin of their diversity and scaling relations and why are they clustered in space following a sponge-like structure; finally, which are the physical processes that quench the star-formation and affect the structure of a galaxy, and are responsible of the sharp transition at $M_{\rm cross}$ between galaxies with $M_\star > M_{\rm cross}$ being preferentially red spheroids with old stellar population in cluster environments, and galaxies with $M_\star < M_{\rm cross}$ being mostly blue coloured discs, and in the field. To answer one or all of these questions is of fundamental importance to understanding the origin and evolution of galaxies.

The origin of cosmic structures, including galaxies of all types, is currently described through the dissipation-less gravitational collapse in a Universe dominated by DM. Models have to take as their initial conditions the tiny fluctuations (1 part in 10^5) in the cosmic microwave background which grow via gravitational instability, firstly in the linear regime, and later non-linearly, forming by the present epoch the massive haloes we see as galaxies and clusters, as well as the large-scale structure in which they are embedded. Within these DM haloes, the baryonic component must also evolve to form the observed stars, galaxies and ICM.

The nature of DM is still a debated problem. Different composition of DM derive strongly different cosmologies. In fact, the typical mass of density fluctuations is strictly dependent on the mass of DM particle: the smaller the particle is, the larger are the masses of the density fluctuations. This dependence has led cosmologists to classify hypothetical DM candidates into three broad categories [Silk, 1980]:

- hot DM (HDM) made of low-mass particles like neutrinos in which

massive ($M_{\rm halo} \sim 10^{15}$ M$_\odot$) haloes collapse first;

- warm DM (WDM) where the mass of a typical halo is $\sim 10^{11}$ M$_\odot$;
- cold DM (CDM) where the collisionless particles are so massive (10^2 GeV) that fluctuations of all scales survive ($M_{\rm halo} \sim 10^{-5}$ M$_\odot$).

From this picture it emerges that cosmology provides the theoretical framework for the initial and boundary conditions of the cosmic structure formation model and consequently for galaxy formation.

Starting from the pre-existing DM model it is possible to construct a model for populating haloes of different mass with galaxies using simulations which take into account the dynamics of the DM and gas, star-formation, radiative cooling, and gas loss from galactic winds. Two main families of models may be recognized:

the monolithic scenario developed since the early work by Eggen et al. [1962] and Larson [1975], within which galaxies formed during a single event at very high redshift ($z > 3$) through the gravitational collapse of proto-galactic gas clouds. For early-type galaxies, star formation ceases shortly after the collapse and the subsequent evolution of the galaxies is dominated by passive dimming of the stellar light. In this scenario, the massive galaxies are already in place very early, and hence are the oldest structures of the universe;

the hierarchical scenario [White and Rees, 1978, Cole et al., 1994b] where massive galaxies have formed from smaller units through merging events. Less massive galaxies were the first objects to form at high redshift, while massive ellipticals and S0s have been slowly built up through many generations of mergers. This scenario predicts that the number of massive galaxies is larger at lower redshifts, as merging events form bigger and bigger objects.

The monolithic collapse hypothesis was able to produce the observed tightness of many scaling relations, such as the colour-magnitude relation and the fundamental plane, as well as the evolution of these relations with redshift [Kodama et al., 1998, van Dokkum and Stanford, 2003]. Moreover it well justifies the finding of galaxy objects at higher redshifts ($z > 2$) with high star-formation rates (SFRs) such as Lyman break galaxies (LBG, star-bursting galaxies with SFRs of $10 - 1000$ M$_\odot$yr^{-1} and masses of $10^9 - 10^{10}$ M$_\odot$), sub-millimetre (SCUBA) galaxies (strongly star-bursting galaxies with SFRs of ~ 1000 M$_\odot$yr^{-1} obscured by dust), Lyman α emitters (galaxies with strong

Lyman α lines which imply phases of rapid star-formation or strong cooling) and quasars.

The monolithic collapse model for the formation of elliptical galaxies naturally produces the effect known as "cosmic downsizing" whereby the major epoch of star-formation occurs earlier and over a shorter period in the most massive galaxies and progressively later and over more extended time-scales towards lower mass galaxies. This has been confirmed observationally both in terms of the global decline of star-formation rates in galaxies since $z \sim 1$ [Noeske et al., 2007a,b] and in the fossil records of low-redshift galaxy spectra [Heavens et al., 2004, Panter et al., 2007].

Analysing the absorption lines of local quiescent galaxies, the most massive galaxies are found to have higher mean stellar ages and abundance ratios than their lower mass counterparts, indicating that they formed stars earlier and over shorter time-scales [Nelan et al., 2005]. In this scenario, the mass-scale at which a galaxy becomes quiescent should decrease with time, with the most massive galaxies becoming quiescent earliest, resulting in the red sequence of passively-evolving galaxies being built up earliest at the bright end [Tanaka et al., 2005]. It was previously thought that these effects could be considered the direct consequence of the deeper potential wells of giant galaxies, which accelerates the collapse of gas into stars.

However, in the last decades, some problems have arisen with this scenario: the ubiquitous presence of fine structure such shells, ripples, tidal plumes, nuclear light excesses, and kinematic subsystems in ellipticals [e.g. Schweizer and Seitzer, 1992, Schweizer, 1996] are interpreted as clear signatures of merger events. Moreover, considerable observational evidence indicates that the most massive starbursts, ultra-luminous galaxies (ULIRGs), are always associated with mergers [e.g. Sanders and Mirabel, 1996, Lotz et al., 2004], with dense gas in their centres providing material to feed black hole growth [Hopkins et al., 2008a,b]; in the same way sub-millimetre galaxies and quasars are found to be triggered by merger events [for reviews see Barnes and Hernquist, 1992, Jogee, 2006]. However the strongest evidence in favour of the hierarchical scenario comes from the development of numerical simulations during the last 20 years.

Numerical simulations [e.g. Di Matteo et al., 2005] have shown that major mergers of two gas-rich disk galaxies can produce elliptical galaxies: tidal torques developed during a merger lead gas to fall into the centres of galaxies [Hernquist, 1989, Barnes and Hernquist, 1991, 1996] triggering starbursts and feeding central black hole growth [Mihos and Hernquist, 1994, 1996]. Starbursts consume a great part of the gas in the galaxy and the

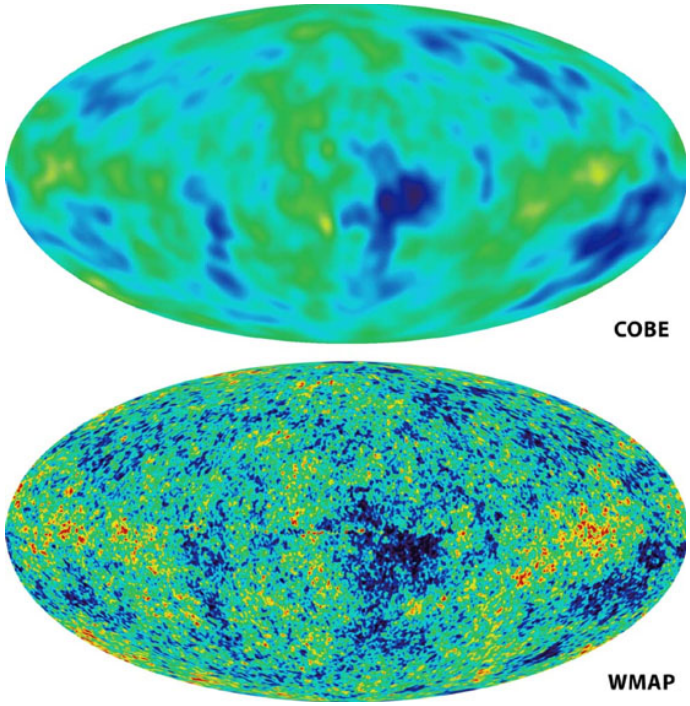

Figure 1.19: Anisotropy of the CMB: all-sky maps, made by COBE (upper) and by WMAP (lower); range of color scale is $\pm 200\,\mu$K [Freedman and Turner, 2003].

remaining part is expelled through galactic winds and feedback from the black hole, producing red and dead elliptical galaxies. However it is necessary to highlight some restrictions of this model: a major merger with masses ratio below 3:1 is required in order for the tidal torques to induce such a strong central inflow of gas that is able to modify the morphology. The great quantity of higher mass-ratio mergers (e.g. 10:1) show that gas inflows can be induced under some circumstances [e.g Hernquist and Mihos, 1995, Bournaud et al., 2005], but detailed studies indicate that this is limited to specific orbital geometries [Younger et al., 2008], and that the efficiency decreases with the increasing mass ratio. The results of these higher mass-ratio mergers could be a galaxy made by a central component like a spheroid surrounded by a surviving disk structure. However, it has to be emphasized that only mergers can reproduce the observed kinematic properties of elliptical galaxies and classical bulges [among others Naab and Burkert, 2003, Bournaud et al., 2005, Jesseit et al., 2007]. Other processes such as harassment (see 1.4.3) may be able to produce spheroid component, but the analysis of these structures show that are characterized by different kinematics and properties from those observed for elliptical galaxies. An open debate in the merger scenario is the further disk formation around the elliptical through the subsequent accretion

and cooling of gas as their host DM haloes grow. Are elliptical galaxies able to quench their star-formation definitively by themselves or other external processes are needed to halt this mechanism?

The monolithic and hierarchical scenarios of formation of galaxies are well collocated into two "contradictory" cosmological models. The top-down monolithic scenario is consistent with a HDM model where massive haloes, in which elliptical galaxies form, develop first, while the hierarchical scenario is better reconciled with a CDM model where small objects would form first in the low-mass haloes predicted in this cosmology, non-linearly interact, and merge to form larger haloes which can then host massive galaxies [de Freitas Pacheco et al., 2003]. The confrontation of the model predictions with astronomical observations have become the most powerful testbed for cosmology. In the last years, the CDM model plus a dark energy field (indicated by Λ), i.e. the well known ΛCDM model is the most accredited cosmological model since, among the others, nicely integrates i) cosmological theories (Big Bang and Inflation), ii) the cosmic microwave background (Fig. 1.19), iii) the large-scale structure of the Universe [Springel et al., 2005b, see Fig. 1.20]. The results of these simulations with observational evidence, seem to suggest the hierarchical scenario as the most plausible for galaxy formation. In this scenario galaxy disks are envisioned to form as the result of gas accreted smoothly from the intergalactic medium [Katz and Gunn, 1991], while the merger of disks is the process responsible for the formation, both of elliptical galaxies and the bulge components of spiral galaxies

At first sight, one of the most major problems with the hierarchical scenario seems to be the observed downsizing. If massive galaxies are formed later, they should be also the youngest systems of the Universe. Chiosi and Carraro [2002], by means of N-body-tree-SPH simulations incorporating cooling, star-formation, energy feedback and chemical evolution studied the SFR as a function of time for different masses as shown in Fig. 1.21. Massive galaxies are characterized by a single episode of star-formation very early in the past, while dwarf galaxies show irregular and intermittent star-formation which is prolonged over wide time intervals. Similar results were found by De Lucia et al. [2006], from the analysis of the Millennium simulation: they find that massive galaxies are systematically older than less massive systems and convert gas into stars at higher level of efficiency. Fig. 1.22 shows the average star-formation rate for elliptical galaxies in the Millennium simulation both in "cluster" environment (top panel) and "field" environments (bottom panel). The different colours represent ellipticals galaxies with different masses: the most massive elliptical galaxies have star-formation rates that peak at higher

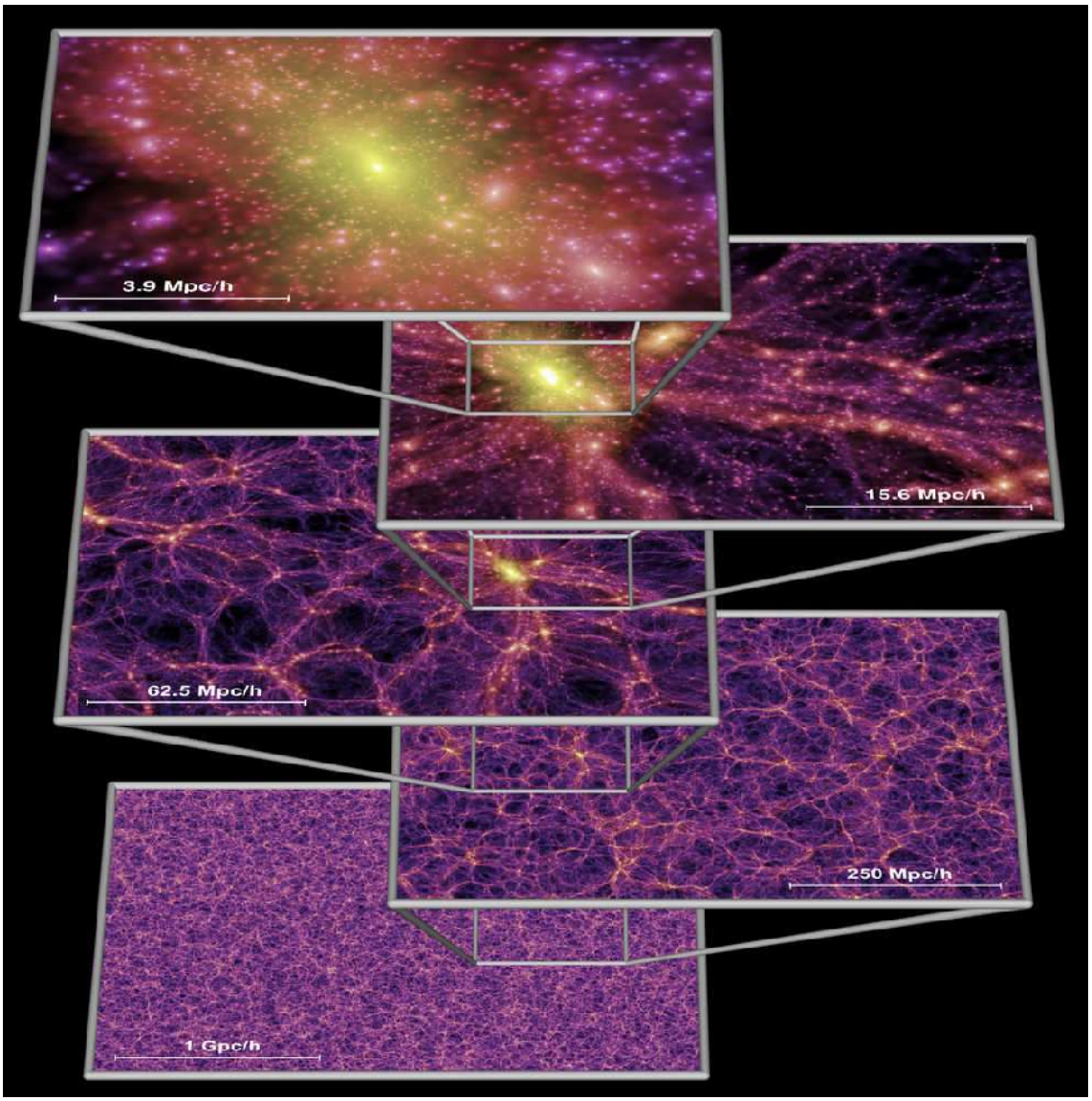

Figure 1.20: The DM density field on various scales from the Millennium simulation, the largest high-resolution simulation of cosmic structure growth ever carried out. Each individual image shows the projected DM density field in a slab of thickness $15h^{-1}$ Mpc, colour-coded by density of the DM distribution [Springel et al., 2005b].

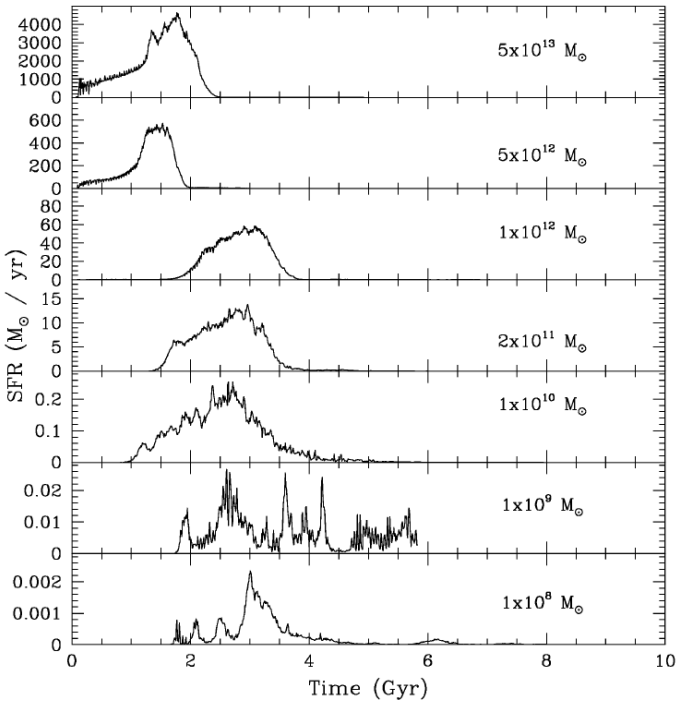

Figure 1.21: Star-formation histories for massive galaxies (top) down to dwarf galaxies (bottom) [Chiosi and Carraro, 2002].

redshift ($z \sim 5$) and are characterized by higher levels of star-formation. The result is visible both in clusters and field, even if, due to the deeper potential wells, in clusters the star-formation rates are higher on average, and the time-scales over which the processes to form stars act, are shorter. Although downsizing appears at first sight to be at odds with the standard hierarchical model for the formation and evolution of galaxies, Merlin and Chiosi [2006] were able to reproduce the same downsizing as seen in the earlier "monolithic" models in a hierarchical cosmological context, resulting in what they describe as a revised monolithic scheme whereby the merging of substructures occurs early in the galaxy life ($z > 2$).

To understand this apparent contradiction, it is important to distinguish between the epoch in which most of galaxy stars are formed, and the age in which galaxy spheroid acquired its dynamical properties through mergers. For the monolithic scenario these two epochs are coincident. Instead in the hierarchical scenario, a galaxy can be assembled recently, and so resulting in a young system when referred to its assembling history, yet the merging could involve galaxies with already old stars, and hence appearing old when referred to their stellar populations. De Lucia et al. [2006] showed that for galaxies more massive than 10^{11} $M_{\odot}$ the median redshift when half of the

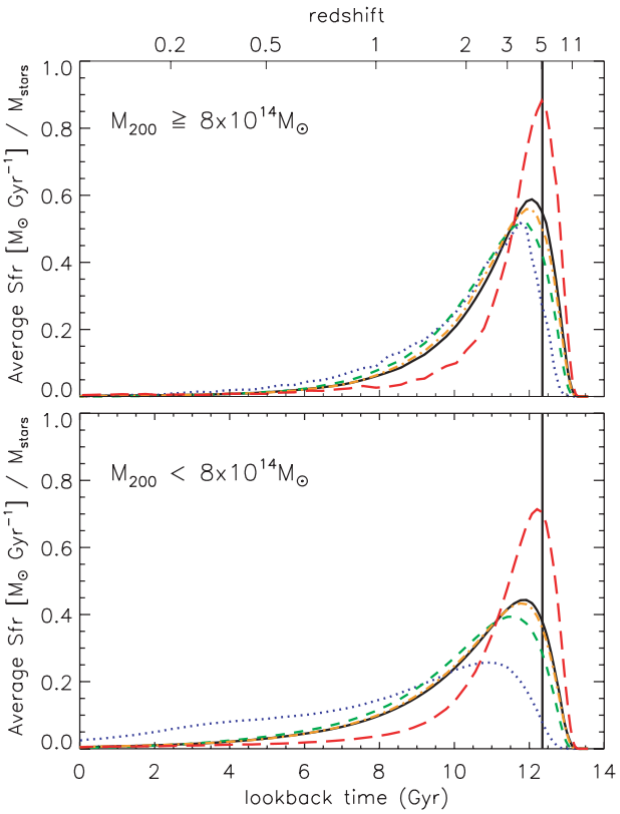

Figure 1.22: The average star-formation rate for elliptical galaxies in Millennium simulation both in "cluster" (top panel) and "field" environments (bottom panel). The different colours represent elliptical galaxies with different masses (red, yellow, green, and blue lines correspond to stellar masses of 10^{12}, 10^{11}, 10^{10} and 10^{9} $M_\odot$ respectively) [De Lucia et al., 2006].

stars were formed is ~ 2.5, while for the same sample, the median redshift in which half of the stars were assembled in a single object is ~ 0.8.

Despite all of this observative evidence in favour of the hierarchical scenario, intriguing questions remain still open, such as the well known problem of the galaxy luminosity function [Benson et al., 2003]. If no feedback processes are included in the formation and evolution of galaxies, the halo mass function deviates from the observed galaxy luminosity function at both ends. Why we do not find so many dwarf galaxies as predicted by the cosmology?, and why, on the other side, are there not massive galaxies greater than a certain mass? Different mechanisms have been proposed: at the faint-end the absence of dwarf galaxies is thought to be due to the energy injection from supernovae and stellar winds, and to the photo-ionization of pre-galactic gas at high redshifts, which make galaxy formation inefficient in small haloes [Benson et al., 2003]. However, this justification enlarges the

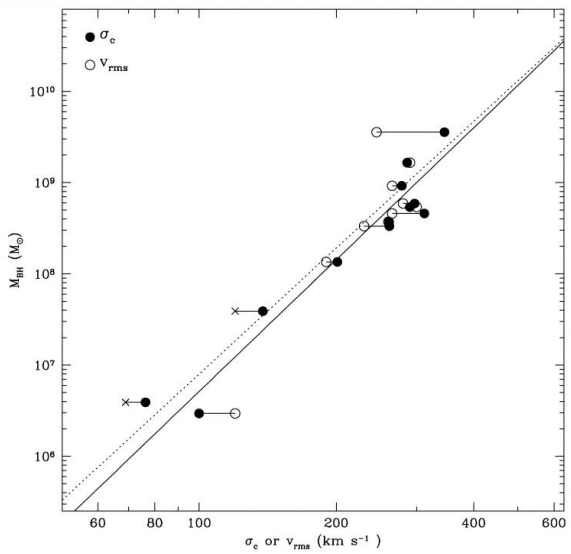

Figure 1.23: BH mass vs. the central velocity dispersion σ_c of the host elliptical galaxy or bulge (filled circles) or the rms velocity $v_{\rm rms}$ measured at one-fourth of the effective radius (open circles). The solid and dashed lines are the best linear fits using σ_c and $v_{\rm rms}$, respectively [Ferrarese and Merritt, 2000].

problem at the massive end, since the heated gas that has not condensed onto dwarf galaxies can eventually cool onto massive haloes giving rise to an excess of bright galaxies that is not observed. In this case the proposed scenario can be summarized as the presence of a heating conduction at the centre of massive haloes and/or to superwinds. Unfortunately, no one of these scenarios is totally satisfactory since the heating source should have an implausibly high efficiency, while the supernovae explosions are not so powerful to prevent the cooling of gas. One of the recent scenario which receiving consent is the injection of energy from the central AGN. The underlying idea is based on the relation between $M_{\rm BH}$ and $M_{\rm bulge}$ whereby $M_{\rm BH} \propto M_{\rm bulge}$ [e.g. Ferrarese and Merritt, 2000, Fig. 1.23]. The black hole mass is seen to grow until it reaches a limiting luminosity: the Eddington limit. At this luminosity, the accretion disk of the central black hole reaches a temperature of $\sim 10^{10}$ K: at this value the pressure of the disk photons is so high that they can escape from the disk forming a strong "wind" which, not only prevents further feeding of the central black hole, but also expels all the remaining gas in the galaxy, stopping the star-formation and the further accretion of mass onto the black hole.

The above picture, if on one side sheds light on the mechanisms that have led the formation of galaxies and their spatial distribution, on the other clearly shows that the existence of galaxies as they appear is a complex mix both of the initial cosmological conditions, but also of a great variety of

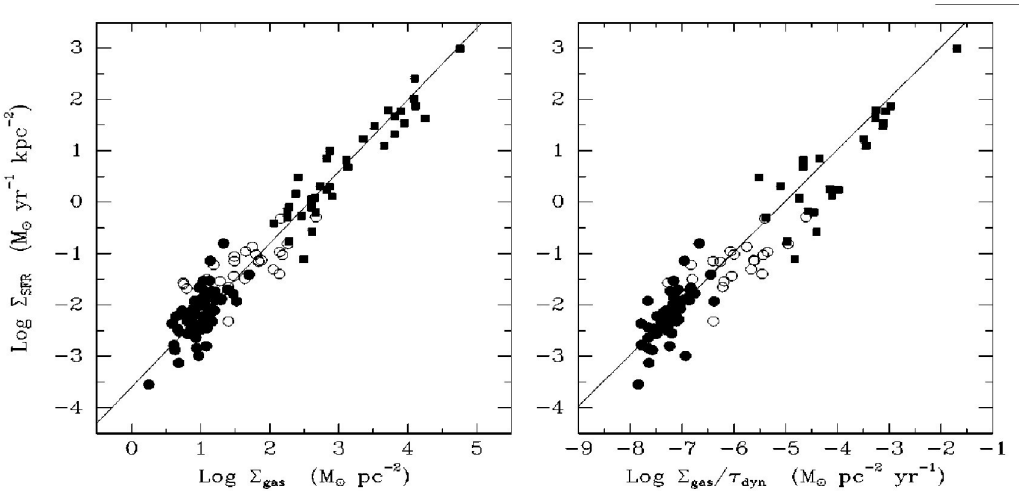

Figure 1.24: *Left*: The global Schmidt law in galaxies. Solid points denote the normal spirals, squares denote the circumnuclear starbursts. The open circles show the SFRs and gas densities of the central regions of the normal disks. *Right*: The same SFR data but plotted against the ratio of the gas density to the average orbital time in the disk [Kennicutt, 1998].

processes that by quenching the star-formation and modifying the morphology are able to convert blue-disk galaxies in the field into red spheroidal galaxies in cluster.

SECTION 1.3

Mechanisms of galaxy transformation

In this section we present the different physical mechanisms that are likely to be important for determining the star-formation histories of galaxies both internal to the galaxy (e.g. gas consumption, AGN feedback and merging) and as the result of direct interactions between the galaxy and its local environment (e.g. ram-pressure stripping and galaxy harassment).

1.3.1 Star-formation

Star-formation in disk galaxies is regulated by a variety of processes (neglecting here AGN feedback, bar instabilities, and galaxy interactions), gravitational instability and turbulence of the gas disk, supernovae feedback, and the inflow and cooling of gas from the halo. The most important parameter for determining the star-formation efficiency appears to be the local gas surface density Σ_{gas}: Schmidt [1959] showed that the observed

surface densities of gas and star-formation in galaxies were related by a simple power law, $\Sigma_{\rm SFR} \propto \Sigma_{\rm gas}^{N}$, where $N = 1.40 \pm 0.15$ over several orders of magnitude in gas density [Kennicutt, 1998, Fig. 1.24]. Moreover, there appears a critical gas density below which star-formation does not occur [Martin and Kennicutt, 2001]. The empirical Kennicutt-Schmidt law is close to that predicted for a self-gravitating disk, where the star-formation rate scales as the ratio of the gas density to the free-fall time-scale ($\tau_{\rm ff} \propto \Sigma_{\rm gas}^{-0.5}$), and implies that star-formation efficiency (SFR/$\Sigma_{\rm gas}$) increases with gas surface density, resulting in star-formation being most inefficient in low-surface brightness dwarf galaxies.

1.3.2 Supernovae feedback

Supernova feedback has also been proposed as a mechanism that could explain the inefficiency of star-formation in dwarf galaxies, as well as their tight correlations between their internal velocities, metallicities, surface brightnesses and stellar masses [e.g. Dekel and Woo, 2003], although Tassis et al. [2008] argue that these scaling relations can be obtained without supernovae feedback, and are simply the result of the Kennicutt-Schmidt law with a critical density threshold. In these models, energy released by the supernovae triggers metal-enriched winds which can drive enriched gas from the disk into the halo and beyond, causing mass loss and self-regulating the star-formation activity, resulting in a quasi-periodic, bursty star-formation rate in low-mass galaxies. However, using hydrodynamic simulations, Mac Low and Ferrara [1999] and Marcolini et al. [2006] find instead that in quite low mass dwarfs with gas masses $M_{\rm gas} \sim 10^7$ M$_\odot$ galactic winds due to supernovae do not form, even during quite large starbursts, despite the energy released by the supernovae being greater than the binding energy of the galaxy. Supernova feedback is likely to further reduce the star-formation efficiency in dwarf galaxies by reheating the surrounding cold gas clouds and blowing it out of the disk (if not from the galaxy entirely), at least for a while [Scannapieco et al., 2006], contributing to the gas depletion time-scales of the order ~ 20 Gyr observed for isolated dwarf irregular galaxies [van Zee, 2001]. The effects of supernova feedback are expected to reduce with increasing galaxy mass, as the deeper gravitational potential wells and larger gas masses make it more difficult for supernovae to drive outflows [Dekel and Silk, 1986].

1.3.3 Gas consumption

In typical spiral galaxies star-formation occurs very efficiently due to their high gas surface densities, resulting in gas consumption time-scales (calculated by comparing their star formation rates and HI contents) of just ~ 3 Gyr. This implies that if no gas replenishment were to occur, most spiral galaxies would consume all their gas in much less than a Hubble time, and this led Larson et al. [1980] to propose that their gas is continuously replenished from their extended halos, allowing them to continue forming stars to the present day.

Hydrodynamical simulations following this accretion and cooling of gas from the halo onto the disk have shown there are two processes by which this occurs, the relative importance of these modes depending strongly on galaxy mass [Kereš et al., 2005, Dekel and Birnboim, 2006]. In high-mass galaxies, the infalling gas follows the track expected in the conventional picture of galaxy formation, being shock-heated to roughly the virial temperature of the galaxy potential well ($T_{\rm vir} \sim 10^6$ K), forming a stable diffuse atmosphere in quasi-hydrostatic equilibrium with the DM, before being accreted in a quasi-spherical manner through radiative cooling, condensing onto the disk and forming stars. In low-mass galaxies, or at high-redshifts, gas is accreted onto the disk along filamentary structures, and cools too rapidly for stable virial shocks to occur, allowing for a more rapid and efficient cooling, condensation and formation of stars. Although the approaches of Dekel and Birnboim [2006] and Kereš et al. [2005] are radically different, both obtain characteristic transition masses of $M_{\rm vir} \sim 6 \times 10^{11}$ M$_\odot$ (corresponding to a stellar mass of $\sim 3 \times 10^{10}$ M$_\odot$) between the "hot" and "cold" accretion modes, which appear in good agreement with the observed characteristic stellar mass at which there is a sharp transition in the global properties of galaxies from low-mass, star-forming disks to high-mass, passively-evolving spheroids [Kauffmann et al., 2003a].

1.3.4 Suffocation

What would happen to galaxies if this accretion of fresh gas from the halo (through either hot or cold modes) were to be permanently shut off? Larson et al. [1980] proposed that when a galaxy enters a more massive halo, such as a group or cluster, its reservoir of halo gas is lost to that of its host halo, either through tidal effects or ram-pressure stripping. The remaining gas in the disk is slowly consumed by star-formation over a period of few Gyrs, leaving a passively-evolving galaxy. This physical process, described as "suffocation"

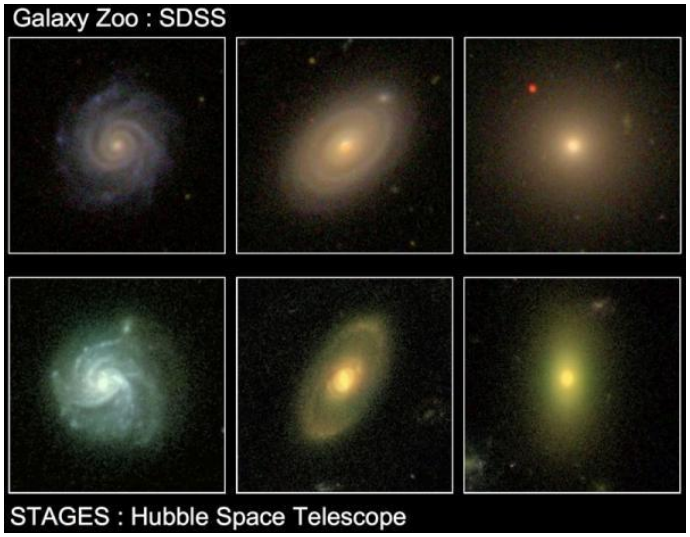

Figure 1.25: Three galaxies from the Galaxy Zoo (top) and STAGES surveys (bottom). At left, examples of normal spiral galaxies; on the right are examples of elliptical galaxies. In the centre are examples of the strangled (or suffocated) galaxies: most of the gas has been removed by tidal interaction and the remnant is a "red" spiral galaxy

(also starvation or strangulation, Fig. 1.25), was proposed by Larson et al. [1980] as a mechanism that would strip away the halo gas reservoirs and exhaust the remaining gas of spiral galaxies, and transform them into passive S0s over a period of ~ 3 Gyr.

The numerical and hydrodynamical simulations of Bekki et al. [2001, 2002] following the evolution of the extended halo gas of spiral galaxies in cluster or group environments, show that even if the spiral is orbiting the cluster ($M_{\rm cl} = 5 \times 10^{14}$ M$_\odot$) with pericentre distances of the order 500 kpc (well outside the cluster core), a combination of the hydrodynamic interaction with the ICM and the effects of the global tidal field of the cluster are able to effectively strip 80% or more of the halo gas within a few Gyr, and prevent further accretion of gas onto the galaxy. They found that in group environments ($M_{\rm grp} = 10^{13}$ M$_\odot$) halo gas stripping is only effective on orbits that pass through the core of the group.

Suffocation acts to globally remove gas from a galaxy, and hence the radial profiles of the remaining gas and star-formation should only be mildly affected [Boselli et al., 2006]. The process should act to slowly dim the disk, without affecting its morphology or radial profile, and has been favoured as a mechanism to produce the anaemic spirals seen in present day clusters [van den Bergh, 1976].

Figure 1.26: The famous Antenna Galaxies are a pair of galaxies undergoing a violent collision some 90 million light years away toward the constellation Corvus. This image shows the innermost regions of the galaxies, at the very heart of the collision. The nuclei of the two galaxies are visible in the image as the yellow and orange concentrations of light. Most galaxies probably undergo at least one significant collision in their lifetimes.

1.3.5 Galaxy Merging

Toomre [1977] was the first to suggest that merging (Fig. 1.26) could have a profound impact on galaxy evolution, proposing that the elliptical galaxy population could result from the merging of disk galaxies. Subsequently the hierarchical merging scenario was developed to describe the growth of structure and the evolution of massive galaxies [e.g. White and Rees, 1978, Lacey and Cole, 1993].

Hydrodynamical simulations following the mergers of gas-rich disk galaxies showed that gas inflows induced by gravitational torques channel large amounts of gas onto the central nucleus, fuelling powerful star-bursts (often after the initial encounter, but before the galaxies coalesce) that use up significant fractions $(65-85\%)$ of the gas content from the original disk [Mihos and Hernquist, 1996], leaving bulge-dominated remnants possessing the $r^{1/4}$ surface brightness profiles typical of early-type galaxies [Barnes and Hernquist, 1992]. More recent hydrodynamical simulations incorporating black hole growth [Springel et al., 2005a] show that the gas inflows fuel also rapid growth of the central supermassive black hole, which may become sufficiently massive to power quasar winds which entirely expel the remaining gas, effectively terminating star-formation in the merger remnant

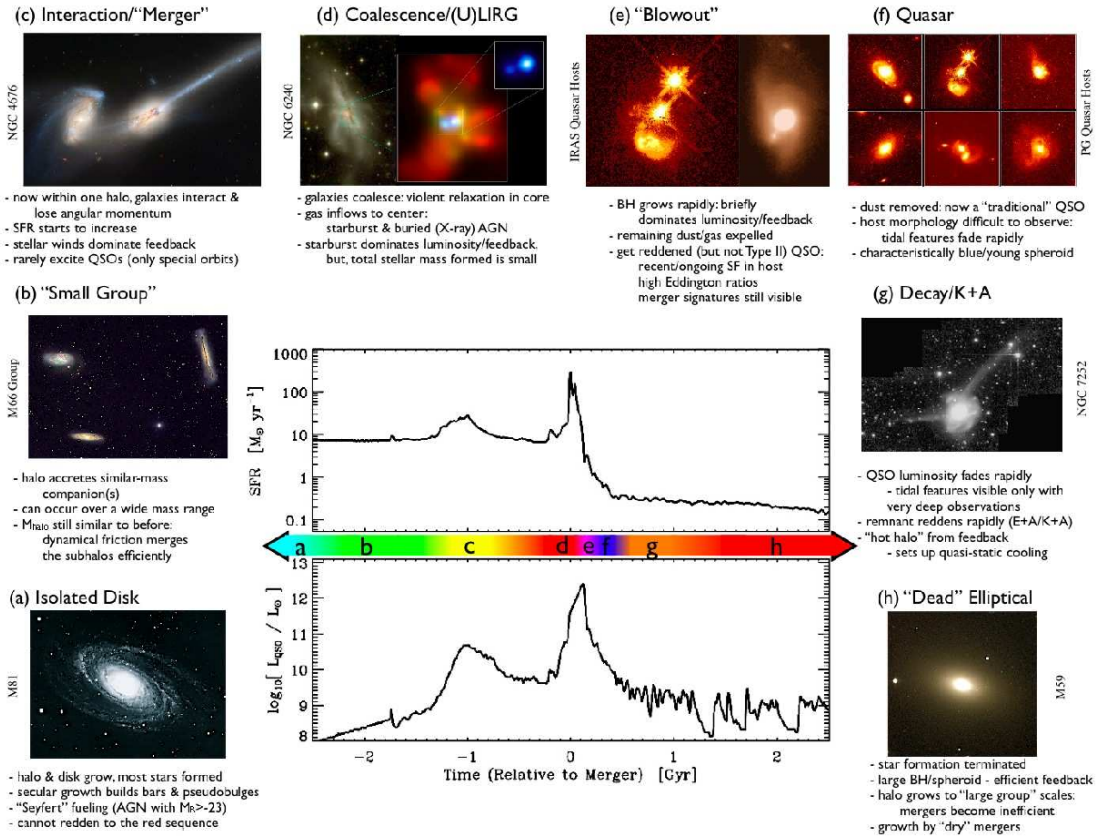

Figure 1.27: The famous Antenna Galaxies are a pair of galaxies undergoing a violent collision some 90 million light years away toward the constellation Corvus. This image shows the innermost regions of the galaxies, at the very heart of the collision. The nuclei of the two galaxies are visible in the image as the yellow and orange concentrations of light. Most galaxies probably undergo at least one significant collision in their lifetimes.

[Di Matteo et al., 2005].

Fig. 1.27 [taken from Hopkins et al., 2008b] shows a schematic outline of current theoretical model for the main phases of the formation of a passive elliptical via a major merger of gas-rich disk galaxies. In panel (c) the two galaxies start to merge: the interaction has distorted the discs and a strong shock occurs in the impact region [Di Matteo et al., 2005]. Gas ha begun to fall into the central region accreting mass onto the central black hole, but no significant episode of star-formation occurs. In panel (d) the galaxies coalesce, and massive inflows of gas trigger starbursts (often heavily obscured by dust) with strengths similar to those inferred for ULIRGs and sub-mm galaxies, and a great part of the gas is converted into stars via central nuclear starbursts. The high gas densities feed rapid black hole growth, but the black holes are obscured at optical wavelengths by gas and dust. Most of the nuclear

gas is consumed by the starburst, and eventually feedback from supernovae and the black hole begins to disperse the gas (panel e). The remaining gas is then heated by the feedback energy provided by the accretion and is partly expelled in a powerful wind. During this short phase the object could appear as a bright quasar (panel f). The expulsion of the gas by the wind imply a sudden quenching of the star-formation and of the accretion of the black hole itself, terminating the quasar phase (g), and leaving as a result a "dead" elliptical whose stellar population quickly evolves from blue to red. The central panel of Fig 1.27 shows the star-formation rate during the merger event: it shows the star-burst triggered during the coalescence/ULIRG phase (d) and the subsequent quenching of the star-formation as the gas is expelled from the galaxies by the quasar winds.

Galaxy mergers at the present epoch are relatively rare, with just $\sim 0.5\%$ in close physical pairs. For interacting galaxies to be able to merge their encounter velocity must be less than or comparable to their velocity dispersions and as a result mergers should be most frequent in groups with high galaxy densities but low velocity dispersions. In contrast in rich clusters the encounter velocities are too high, meaning that while interactions are frequent, mergers are extremely rare [Ghigna et al., 1998].

While mergers may be rare now, in the much denser and active early universe they were much more frequent. Conselice [2006] shows that galaxies undergo a phase of rapid growth through merging at high redshifts $z > 1$, but at later epochs the merger rate drops exponentially to a current rate that is only a hundredth of that at $1 < z < 3$. During this early and rapid merging, the stellar masses of an average galaxy increases by a factor $10 - 100$, undergoing ~ 4 major mergers at $z > 1$. The epoch at which galaxies grow and merge is also dependent on environment. Haloes that are in local clusters have built up their mass through mergers and accretion earlier than isolated haloes of the same mass [Maulbetsch et al., 2007]. Additionally, during this epoch of rapid growth through mergers ($1 < z < 4$), progenitors of cluster and group halos have $3 - 5$ times higher merger rates than isolated halos [Gottlöber et al., 2001].

1.3.6 Ram-pressure stripping

Gunn and Gott [1972] first proposed that the ISM of cluster galaxies could be removed through ram-pressure stripping as they move at high velocities ($\sim 1\,000\,\mathrm{km\,s^{-1}}$) through the dense ($\sim 10^{-3}\,\mathrm{cm^{-3}}$), hot ($\sim 10^{7}\,\mathrm{K}$) ICM. As a galaxy orbits through the cluster, it experiences a wind because of its motion relative to the diffuse gaseous ICM. Although the ICM is tenuous, the rapid motion of

the galaxy causes a large pressure front to build up to in front of the galaxy. Depending on the binding energy of the galaxy's own ISM, the ICM will either be forced to flow around the galaxy or will blow through the galaxy, removing some or all of the diffuse ISM.

Hydrodynamic simulations of ram-pressure stripping confirm that gas should be stripped from cluster spirals from the outside in, and that the radius to which the gas is stripped depends on the relation of the ram-pressure to the restoring force [e.g Abadi et al., 1999].

Before stripping a galaxy, ram-pressure compresses the gas ahead of the galaxy and in the case of edge-on interactions the central gas density may increase by a factor two, due to capture of the outer HII gas, resulting in a temporary ($\sim 10^8$ yr) increase in star-formation [Fujita and Nagashima, 1999, Vollmer et al., 2001].

Ram-pressure stripping should be more efficient for lower mass, low-surface-brightness galaxies, for those galaxies on radial orbits that take them through the densest parts of the ICM at the highest speeds, and for galaxies in the richest clusters. Using hydrodynamical simulations Roediger and Hensler [2005] find that the gas disks in massive spirals are heavily truncated or even completely stripped in cluster cores, while even in lower density environments such as the cluster outskirts or in poor groups, they are partially stripped. In the same group environments Marcolini et al. [2003] find that dwarf galaxies can be completely stripped of their gas. The dense ICM is built-up over time (mainly at $z < 1$) through the gradual loss of gas from cluster galaxies through ram-pressure stripping, galaxy winds and interactions, and so ram-pressure stripping should be most effective at late epochs ($z < 0.5$). However, Kapferer et al. [2007] also show that gas loss from ram-pressure stripping is also important during the cluster formation epoch at $1 < z < 2$ when galaxies in sub-clusters enter the main cluster at high velocities. Such cluster-cluster mergers can create shocks in the ICM, triggering starburst in galaxies over large scales, before rapidly stripping them [Roettiger et al., 1996].

1.3.7 Harassment

Moore et al. [1996] proposed that cluster spirals could be disrupted by "galaxy harassment", whereby repeated close (< 50 kpc) high-velocity ($> 1\,000$ km s^{-1}) encounters with massive galaxies and the cluster's tidal field cause impulsive gravitational shocks that damage the fragile disks of late-type disks, transforming them over a period of few Gyrs into spheroids. High-surface brightness spirals are relatively stable to the effects of harassment, suffering little or no mass loss, although their disks may thicken and their

spiral structures weaken [Moore et al., 1999]. Low surface brightness dwarf spirals with their shallower potentials may suffer significant mass losses (up to 90%) of both their stellar and DM components during harassment. These low-mass galaxies undergo significant morphological transformations, even at the outskirts of the cluster, the remnants resembling dwarf ellipticals, although the disks are never completely destroyed [Mastropietro et al., 2005].

1.3.8 Tidal interactions

Dwarf spiral/irregular galaxies orbiting as satellites to massive galaxies may also be transformed into passively-evolving dEs through tidal interactions with the primary galaxy and ram-pressure stripping as they pass through its gaseous halo. Mayer et al. [2001] show that high-surface brightness dwarf spirals orbiting a Milky Way type galaxy on eccentric orbits taking them within 50 kpc of the primary experience tidal shocks during their pericentre passages, that can cause significant mass loss (mostly of the outer gaseous halo and DM, but also of the stellar disk), formation of bar instabilities that channel gas inflows triggering nuclear star-bursts, and loss of angular momentum, resulting in their transformation over a period of ~ 5 Gyr into an early-type dwarf. Mayer et al. [2006] indicate that while tidal stirring of disky dwarf galaxies can transform them into remnants that resemble dEs after a few orbits, ram-pressure stripping is required to entirely remove their gas component. The tides may aid ram-pressure stripping by diminishing the overall potential of the dwarf, but the channelling of gas inwards to form a concentrated remnant makes subsequent stripping more difficult. The mutual efficiency of these processes which act on different mass scales and environments could give rise to the sharp transition observed at $M_{\rm cross}$.

CHAPTER 2

The Classification Cube

In this chapter we will first outline a description of the zCOSMOS survey, which is the general framework this Thesis is set in, then we will present the galaxy classification method called *classification cube*, adapted from Mignoli et al. [2009, hereafter M09] and extended in this work, describing the methods we used for galaxy classification and the results.

SECTION 2.1

Description of zCOSMOS

zCOSMOS [Lilly et al., 2007, 2009] is a large redshift survey which has been carried out using VIMOS spectrograph [Le Fèvre et al., 2005] installed at the 8 m UT3 "Melipal" of the European Southern Observatory's Very Large Telescope at Cerro Paranal. The main goal of the survey is to trace the large scale structure of the universe up to $z \sim 3$ and to characterize galaxy groups and clusters.

In order to exploit more efficiently the resources of the VIMOS spectrograph, the zCOSMOS survey has been split in two distinct parts:

- zCOSMOS-bright, a magnitude-limited ($I_{\mathrm{AB}} < 22.5$) survey that consists of $\sim 20\,000$ galaxies in a redshift range of $0.1 < z < 1.2$. This part of the survey has been undertaken on the 1.7 deg^2 COSMOS field fully covered by the ACS camera of the Hubble Space Telescope;
- zCOSMOS-deep, a survey whose $\sim 10\,000$ galaxies are selected through various colour criteria, with a redshift range of $1.4 < z < 3.0$, concentrated in the central 1 deg^2 of the COSMOS field.

The bright part of the survey (zCOSMOS-bright) makes use of a medium resolution grism ($R \sim 600$) in order to achieve the desired velocity accuracy of ~ 100 km s^{-1}; to reach the 90% success rate the observations are carried out with 1 hour integration time, divided into 5 exposures of 720 s each. The exposures are taken with a seeing better than 1.2 arcsec. The specifications of the bright part of the survey include a very high success rate in redshift determination ($\sim 90\%$), a uniform sampling rate across the whole field, and very high velocity accuracy (~ 100 km s^{-1}) with the possibility to define the dynamical environment of the galaxies.

Redshifts are given a confidence class, indicated by a flag, representing the quality of the spectra and the reliance in the redshift determination. The possible values of the flag are:

- 4, very secure redshift (spectroscopic verification $> 99.5\%$);
- 3, secure redshift (spectroscopic verification $> 99.5\%$);
- 2, likely redshift (spectroscopic verification $\sim 92\%$);
- 1, possible redshift (spectroscopic verification $\sim 70\%$);
- 9, redshift based on a single strong emission line (spectroscopic verification $> 95\%$);
- 0, no redshift determination.

Spectroscopic verification is computed exploiting the repeated observation of some spectra. Assuming that the chance of getting the same redshift (within 2000 km s^{-1}) when both redshifts are wrong is negligible, the probability that any pair of independent redshift measurements with confidence classes i and j agree is just the product of the two probabilites $p_i \cdot p_j$. By examining all pairs of measurements of common objects, two triangular matrices N and F can be constructed, for which the elements N_{ij} (with $i \geq j$) contain the number of "trials" where one confidence class was i and the other j, and F_{ij} gives the fraction of these trials where the two redshifts were actually in agreement. For a given set of p_i, the probabilities of observing F_{ij} with N_{ij} trials, P_{ij}, is evaluated using standard binomial statistics and the preferred set of p_i selected through a maximum likelihood approach by maximizing the product $\prod_{i,j \geq i} P_{ij}$ [see discussion in Lilly et al., 2007].

In addition, photometric redshifts [Ilbert et al., 2006, 2009] are compared to the spectroscopic ones to check for consistency. A decimal flag is therefore added to the confidence class flag: if the photometric redshift is consistent with the spectroscopic one within $0.08 \cdot (1 + z_{\rm spec})$ then a ".5" flag is appended to the confidence class; if not, a ".1" flag is appended instead.

2.1.1 The data sample

The data release this paper is based upon, called *10k sample*, is made up of 10 642 galaxies from the zCOSMOS-bright part of the survey, regardless of the spectral quality. Our first work sample is composed by 4 874 galaxies between $0.48 < z < 1.28$: this will be referred to as *high redshift whole sample*. This choice is due to the fact that given the spectral range of the observations (5550-9650 Å), the spectral features around rest-frame 4000 Å that we use in this work (the continuum break at ~ 4000 Å – from now on $D4000$ – and the O II emission line) can be detected only in the that redshift range. The *high redshift high quality sample*, instead, is composed by all the galaxies with spectroscopic flag 4, 3 and 2.5, i.e. galaxies with secure redshifts, or likely redshifts confirmed by the photometric one. Galaxies with spectroscopic flag=1 are excluded because of their poor-defined spectral features, while flag=9 are excluded because of the absence of other spectral features beside the single strong emission line; this high quality subset is composed by 3 720 objects (76% of the whole sample).

The subsequent extension of the work to lower redshifts, achieved by substituting $D4000$ and EW_0[O II] with the rest-frame equivalent width of Hα (EW_0(Hα)), builds up a different dataset composed by 3 402 galaxies (*low redshift whole sample*); the corresponding *low redshift high quality sample* is made up by 3 005 galaxies (88% of the whole sample). It has to be noted that, throughout the analysis, the informations on the errors associated with the parameters were not included, since many parameters (like the morphological ones) were not given an error. Furthermore, spectroscopical stars and broad-line active galactic nuclei have been excluded from both samples.

SECTION 2.2

The classification cube method

We extended the classification method developed by M09, applied to the first release of the zCOSMOS-bright catalogue (the so-called *1k sample*, composed by $\sim 1\,000$ galaxies) to the larger dataset provided by the 10k sample. This classification is based on three independent datasets (spectroscopic, photometric, morphological) which exploits the bimodality shown by galaxies in many features.

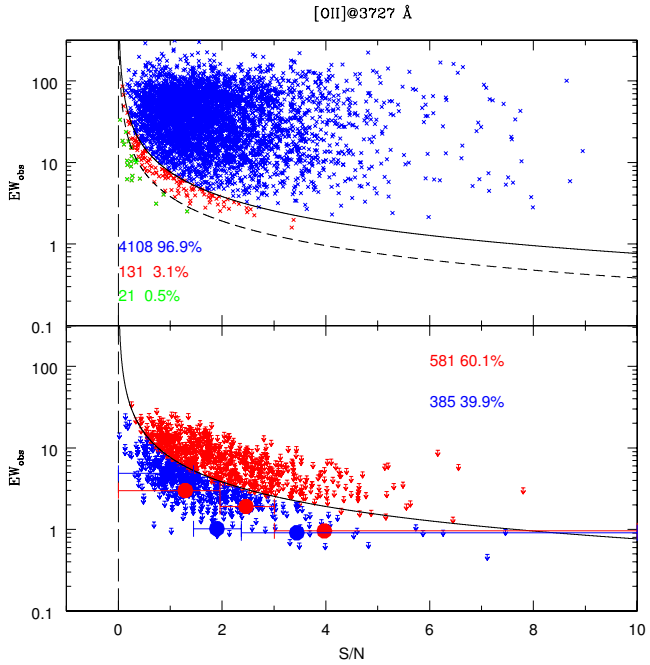

Figure 2.1: *Top*: EW_0[O II] versus $S/N_{\rm cont}$. The solid and dashed lines represent Eq. 2.1 for $SL = 3$ and $SL = 1.5$ respectively. *Bottom*: upper limits of EW_0[O II] versus $S/N_{\rm cont}$. The solid line represents Eq. 2.1 with $SL = 3$, while the red and blue large dots represent the recomputed upper limit values (in bins of $S/N_{\rm cont}$) for, respectively, objects above and below the envelope line.

2.2.1 Spectral classification

Spectral measurements of the 10k sample were carried out by the automatic computer code `PlateFit` [Lamareille et al., 2006]. The program analyses the galaxy spectra and performs measurements of equivalent width and flux for the most important spectral features.

We classified galaxies in the sample using the diagram $D4000$ vs. rest-frame equivalent width of [O II] (from now on EW_0[O II]) developed by Cimatti et al. [2002] and extensively used in many works, e.g. Kauffmann et al. [2004], Mignoli et al. [2005], Franzetti et al. [2007]. $D4000$ is a tracer of cumulative star forming: galaxies with stronger 4000 Å breaks had a longer history of forming stars [Bruzual, 1983, Marcillac et al., 2006]; on the other hand, the presence of [O II] in emission is an effective signature of ongoing star formation [Kewley et al., 2004, Kennicutt, 1998]. Upper limits of the observed equivalent widths of [O II] emission lines have been computed using the empirical relation proposed by Mignoli et al. [2005], and compared to the values of the upper limits produced by `PlateFit`. The empirical envelope

relation is:

$$EW_{\rm lim} = \frac{SL \cdot \Delta}{S/N_{\rm cont}} \tag{2.1}$$

where SL is the significance level of each line computed on the continuum noise, Δ is the spectrum resolution (in Å) and $S/N_{\rm cont}$ is the signal-to-noise ratio of the spectrum calculated in the proximity of the line.

In the upper panel of Fig. 2.1 we plotted $EW_{\rm obs}[{\rm O\,II}]$ versus signal-to-noise ratios of the continuum near the line for all galaxies as measured by `PlateFit`. The vast majority (97%) of the measurements lie above our envelope function (solid line in Eq. 2.1 with $SL = 3$). It seemed not advisable to delete the 3% of measurements below the envelope, so we tried other values of SL. The dashed line represents Eq. 2.1 where $SL = 1.5$. We decided to keep this envelope as a threshold for the measurements and reject the 21 objects whose lines lie below it.

In the lower panel we put the objects for which `PlateFit` gives just and estimate of upper limits for $EW_{\rm obs}[{\rm O\,II}]$. As it can be easily seen, `PlateFit` upper limits are not constrained below the envelope lines as we would expect but are split in two roughly equal subsamples by the envelope itself. We decided to remeasure the average $EW_{\rm obs}[{\rm O\,II}]$ of these two subsamples, in order to compare directly our results and those of `PlateFit`. We divided each subsample in three bins of equal cumulative $S/N_{\rm cont}$: bins at low $S/N_{\rm cont}$ contained a larger number of objects than those at high $S/N_{\rm cont}$. For each bin we computed an average spectrum from source spectra, performed our measurements of local $S/N_{\rm cont}$ and of line equivalent width using IRAF `splot` task. We detected and measured the [O II] line in all of our composite spectra and used Eq. 2.1 to calculate its corresponding $EW_{\rm obs}[{\rm O\,II}]$ upper limit.

Errorbars in $S/N_{\rm cont}$ represent the bin width, while (almost invisible) errorbars in $EW_{\rm obs}[{\rm O\,II}]$ depend on the redshift range of the objects in the bin: since $EW_{\rm obs}[{\rm O\,II}]$ measured from spectra are rest-frame, we had to correct them for redshift. We therefore used the average redshift $\bar{z}$ for plotting the point ($EW_{\rm obs}[{\rm O\,II}] = EW_0[{\rm O\,II}] \cdot (1+\bar{z})$), and lowest and highest values of the redshift bin for errorbars in equivalent width.

We show that our measurements of $EW_{\rm obs}[{\rm O\,II}]$ upper limits for objects above and below the the envelope line are comparable, differing at most for a factor 2, while `PlateFit` values are a factor 10 higher and much dispersed. Moreover, all our measurements lie below the $SL = 3$ envelope line, showing that this estimate of upper limits is robust; we therefore substituted `PlateFit` upper limits below the envelope with the values provided by our

Eq. 2.1.

In Fig. 2.2 the $D4000$-$EW_0[\mathrm{O\,II}]$ plane is shown. The horizontal dashed line represents the cut at 5 Å in $EW_0[\mathrm{O\,II}]$ used to separate strong and weak line emitters, adopted by M09. We used an iterative σ-clipping least squares algorithm to constrain the regions of highest density obtaining the following boundaries:

$$1.64 \leq D4000 + 0.36 \log(EW_0[\mathrm{O\,II}]) \leq 2.14 \tag{2.2}$$

This is somewhat narrower with respect to Eq. (2) in M09, especially toward the left side of the diagram – low $D4000$ values – probably due both to a lower σ rejection in the algorithm and to the larger sample that tends to concentrate the objects in the region.

We defined *star-forming* galaxies the 66% of the spectroscopic high quality galaxies with low values of $D4000$ and high values of $EW_0[\mathrm{O\,II}]$, and *quiescent* galaxies (21%) those with low values of $EW_0[\mathrm{O\,II}]$ and high values of $D4000$. The remaining fraction of galaxies populating the upper-right part of the diagram is defined as *red emitters*, featuring a quiescent-like continuum but with strong emission lines.

The left part of the diagram is mainly populated by low quality spectra objects (crosses in the diagram); high quality objects (which are 4% of the total high quality sample) reside mostly near the boundary. These objects are left out of the classification.

Considering the high quality sample only, we noted that nearly 88% of the galaxies are classified in one of the two main classes. Relaxing the constraints on the requested confidence on the spectral features, the fraction of galaxies in each area of the $D4000$-$EW_0[\mathrm{O\,II}]$ plane is mostly unchanged.

2.2.2 Photometric classification

We expect a rather tight correlation between some spectral property (e.g. $D4000$) of the galaxies and their colours. As the colours of galaxies reflect their star population, we would expect our star-forming galaxies to be bluer than the quiescent ones, because of the well known colour-age relation.

We introduce another classification based on the photometric properties of the galaxies. In the lower panel of Fig. 2.3 the colour $B-\mathrm{z}$ of the galaxies [Capak et al., 2007] is shown as a function of their redshift. We used $B-\mathrm{z}$ colour because of its effectiveness in separating the two galaxy classes [M09]. Spectroscopic star-forming galaxies (blue triangles) have lower $B-\mathrm{z}$ and thus are bluer than both quiescent galaxies and red emitters (respectively red

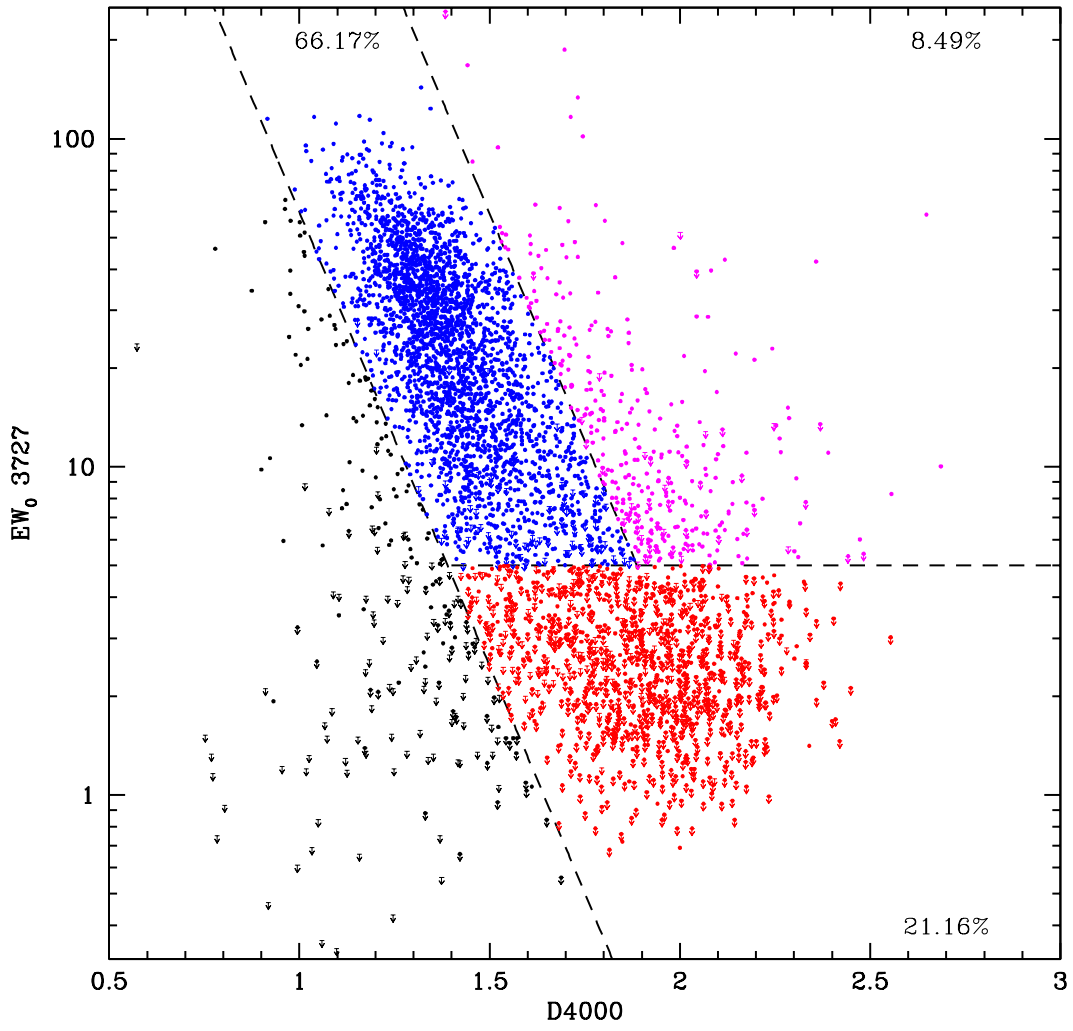

Figure 2.2: Spectral classification diagram for the 10k high quality zCOSMOS sample. In red are *passive galaxies*, in blue *star forming galaxies* and in magenta *red emitters*. Small arrows mark object for which we have only upper limits in EW_0[O II]. Numbers represent the fraction of objects belonging to each class.

$B-z$	Quiescent	Star-forming	Total
Red	983 (1167)	227 (318)	1210 (1485)
Blue	208 (320)	2431 (3081)	2639 (3401)
Total	1191 (1487)	2658 (3399)	3849 (4886)

Table 2.1: Summary of the number of high spectral quality galaxies in spectroscopic and photometric classifications. Between parentheses are figures from the whole sample.

squares and yellow dots). As a way of discriminating the two populations, we used the colour track of a Sab galaxy template, from the set provided by Coleman et al. [1980, see discussion in M09].

Galaxies classified as red emitters, on the basis of their spectral properties, are distributed in the same region as the quiescent ones; this can be seen in the upper panel, where is plotted the distribution of the distances between measured colours and the colour of the template at the redshift of the galaxy:

$$\Delta(B-z) = (B-z)_{\rm obs} - (B-z)_{\rm templ} \tag{2.3}$$

where $(B-z)_{\rm obs}$ are the observed colours of the galaxies and $(B-z)_{\rm templ}$ is the Sab evolutionary track colour at the redshift of each object.

We use the quantity $\Delta(B-z)$ to segregate photometrically the galaxies: if $\Delta(B-z) > 0$ galaxies are considered "red", while when $\Delta(B-z) < 0$ galaxies are assigned to the "blue" class. Since, as we said, red emitters seem to share colours with the quiescent galaxies, we decided to merge these spectroscopic classes into one general "quiescent" category.

In Tab. 2.1 the 2×2 contingency table for spectral and photometric classifications is shown: almost 90% of the high quality sample shows a full agreement between the spectral and photometric classifications (87% for the whole sample). The Cohen's kappa coefficient for inter-rater agreement is 0.74, confirming that the classifications are statistically consistent.

2.2.3 Morphological classification

Morphology data are provided by Scarlata et al. [2007], who built their *Zurich Estimator of Structural Types* (ZEST) performing a Principal Component Analysis (PCA) on 5 parameters derived directly from HST/ACS images of the COSMOS survey. The PCA – performed on asymmetry (A), concentration (C), ellipticity (ε), second order moment of the brightest 20% pixels (M_{20}) and Gini coefficient (G) – produced a five-dimensional principal component space, of which just three are used for subsequent analysis; those first

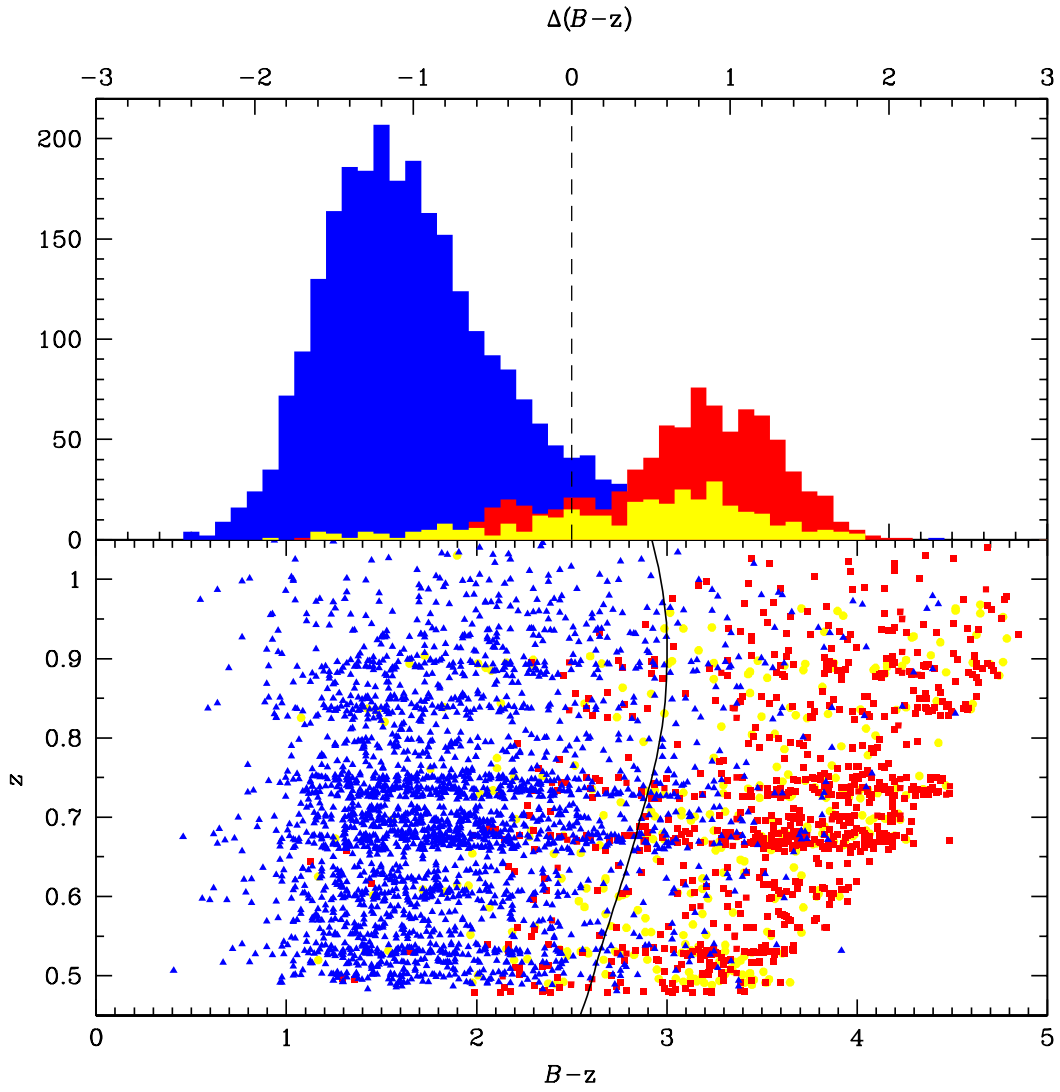

Figure 2.3: Photometric classification of the 10k zCOSMOS-bright high quality sample. In the lower panel colour $B-z$ versus redshift z is shown: blue triangles are star-forming, red squares are quiescent, yellow are dots are red emitters. Solid line represents the evolutionary $B-z$ track of a template Sab galaxy from Coleman et al. [1980] [Sawicki et al., 1997]. In the upper panel the distributions of $\Delta(B-z)$, as defined in Eq. (2.3), for star-forming galaxies (blue histogram), quiescent galaxies (red histogram) and red emitters (yellow histogram) are plotted. The dashed line represents $\Delta(B-z)$ of the Sab galaxy evolutionary track used as separator.

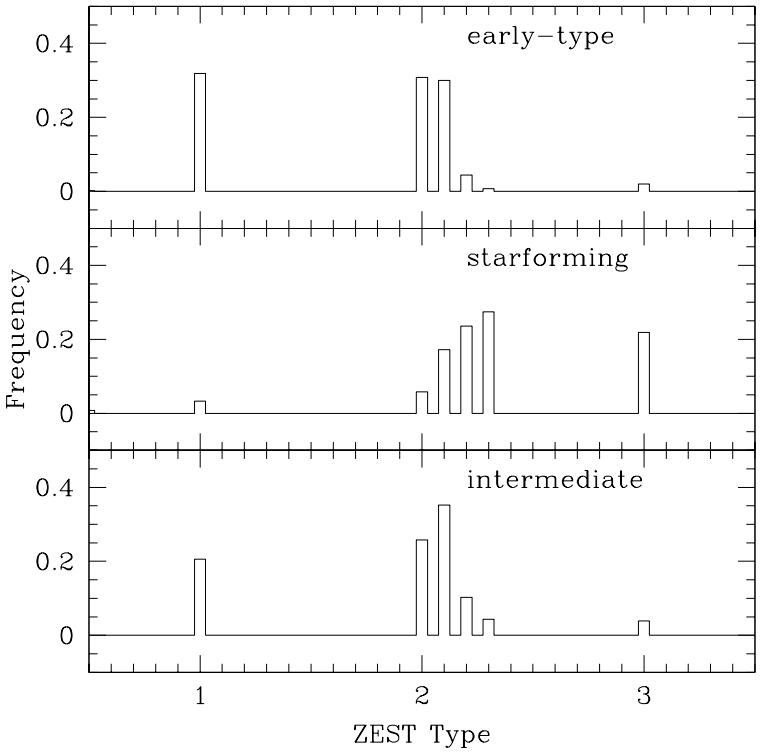

Figure 2.4: Distribution of ZEST indexes for the three spectral types. Spectral quiescent galaxies are represented in the upper panel, star-forming in the middle one and red emitters (here labeled "intermediate") in the bottom panel.

three components sum up to 92% of the original total variance. This three-dimensional space is subdivided into equally spaced regions, and a dominant morphological class is assigned to galaxies in each region.

The ZEST classification scheme adopt a main morphological index, which can be 1 (for elliptical galaxies), 2 (for spirals) or 3 (for irregulars), plus an integrative bulgeness parameter (only for galaxies with main index of 2), calculated from galaxy Sérsic indexes. In this way spiral galaxies are further divided into four subclasses: 2.0, 2.1, 2.2, 2.3 going from bulge dominated spirals to disk dominated, largely following Hubble classification of spiral galaxies from S0 through Sc types.

In Fig. 2.4 is plotted the distribution of ZEST types for our spectral classes. Looking at the upper and middle panels a clear dichotomy can be seen, as quiescent galaxies prefer lower ZEST types, while star-forming galaxies tend to have higher indexes. Red emitters' distribution is very similar to those of early types, confirming our choice to consider from now on these objects and the quiescent galaxies in the same spectral category.

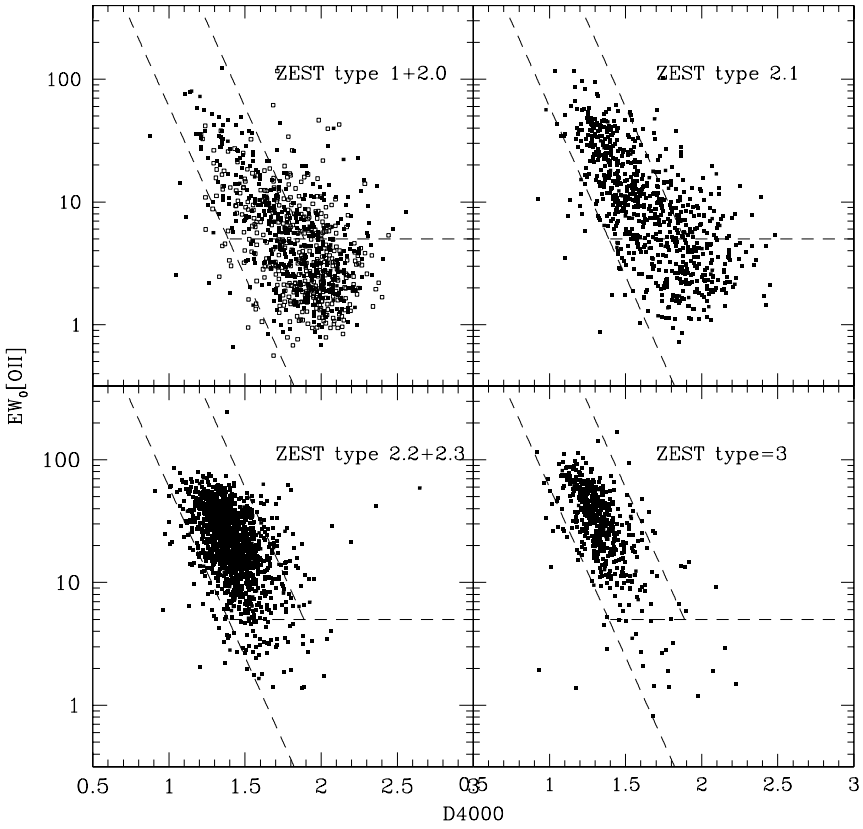

Figure 2.5: The $D4000$-EW_0[O II] plane for different morphological types using the ZEST scheme. Here only galaxies with high quality spectral measurements are shown.

In Fig. 2.5 we show our $D4000$-EW_0[O II] plane for the different ZEST types. At the bottom the spectral plane of ZEST 2.2, 2.3 and 3 types, which are spirals with lowest bulge-to-disk ratio or, in terms of Hubble classification, latest disks, and irregular galaxies, are shown. The vast majority of these three types (combined together, almost 90%) set themselves in the narrow star-forming galaxies region, proving the tight correlation between their spiral-like morphology and the prominence of their emission lines.

We assigned ZEST type 2.2, 2.3 and 3 galaxies to a common morphological category, the *disk-dominated and irregular galaxies*, and ZEST types 1 and 2.0 to another common category, the *ellipsoidal galaxies*. ZEST types 2.1 (spiral galaxies with an intermediate bulge-to-disk ratio) are furtherly divided according to their colour properties: We explored further the properties of ZEST 2.1 type galaxies given their broad properties in terms of spectral and photometric features. In Fig. 2.6, we plotted the histograms of $\Delta(B-z)$ for our

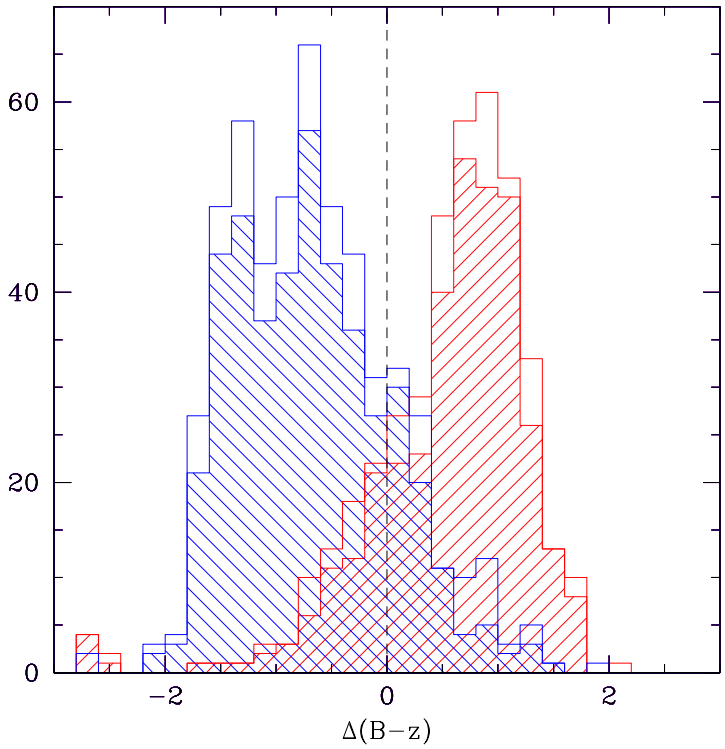

Figure 2.6: Distribution of $\Delta(B-z)$ for ZEST types 2.1. The blue and red histograms represent respectively the distribution of spectroscopic star-forming galaxies and that of the quiescent galaxies for the whole sample; the dashed histograms represent the same distributions for the high spectroscopic quality sample.

ZEST \ spectral	Quiescent	Star-forming	Total
ellipsoidal	607 (717)	236 (292)	843 (1009)
2.1	350 (410)	436 (528)	786 (938)
disk-dominated	141 (232)	1860 (2391)	2001 (2623)
Total	1098 (1359)	2532 (3211)	3630 (4570)

Table 2.2: Summary of the number of high spectral quality galaxies in spectroscopic and photometric classifications. Between parentheses are figures from the whole sample.

morph $+B-z$	Quiescent	Star-forming	Total
Spheroidal	894 (1049)	312 (394)	1206 (1443)
Disk/Irregular	204 (310)	2220 (2817)	2424 (3127)
Total	1098 (1359)	2532 (3211)	3630 (4570)

Table 2.3: Spectral–morphological contingency table. Figures are for the high quality sample (between parentheses are figures for the full sample).

ZEST type 2.1 galaxies for the spectroscopically quiescent galaxies and star-forming galaxies (red and blue histograms: the dashed histograms represent the high quality sample, the open ones are the whole sample). Indeed, most (83%, $360/436$) star-forming galaxies of ZEST type 2.1 have a negative $\Delta(B-z)$, and are therefore classified as "blue", while a similar percentage (82%, $287/350$) of quiescent galaxies have $\Delta(B-z) > 0$ and are classified as "red". Therefore, we included the "red" population of the ZEST 2.1 type in the morphologically ellipsoidal class and and the "blue" population of them in the disk-dominated class (see discussion in M09).

In Table 2.3, we presented the numerical results of our morphological classification. We calculated Cohen's kappa coefficient, which turned out to be ≈ 0.67 for the high quality sample, proving the goodness of our classifications.

2.2.4 The cube

To better analyse the correlations and similarities of our galaxies, we merged the three classifications (spectroscopic, photometric and morphological) into a three-axial framework, a *classification cube*. To simplify the classification we assigned to each galaxy a 3-digit numerical flag which encompasses information from the three categories:

- The first digit represents the spectral classification. The flag 1 and 2 classified a galaxy as a "quiescent" and "star-forming" type, respectively.
- the second digit stands for the colour classification. The flag 1 and 2 classified a galaxy as a "red" and "blue" type, respectively.
- the third digit is the morphological flag. The flag 1 and 2 classified a galaxy as a "spheroidal" and "disk/irregular" type, respectively.

So, for instance, a "212" classificator denotes a star-forming, disk-dominated galaxy with $\Delta(B-z) > 0$, therefore red.

Table 2.4 shows the complete building of the 3D classification cube. Removing from the *high redshift whole sample* objects for which the full set

Cube identifier	High quality sample	Whole sample
111	846 (23.3%)	985 (21.4%)
222	2171 (59.9%)	2743 (59.7%)
121	48 (1.3%)	64 (1.4%)
212	49 (1.3%)	74 (1.6%)
211	168 (4.6%)	255 (5.5%)
122	139 (3.8%)	216 (4.7%)
221	144 (4.0%)	169 (3.7%)
112	65 (1.8%)	94 (2.0%)
Total	3630 (100%)	4600 (100%)

Table 2.4: Complete classification cube. The column "Cube identifier" contains the 3-digit label for the classification adopted in this paper: first, second and third digits represent respectively spectral, photometric and morphological classifications.

of data was not available, the full sample of the cube retains 4 600 sources, while the high quality sub-sample is made up of 80% of them (3 630). Figures change very little between the two samples: almost 60% of the sources show a full concordant "222" classification (star-forming spectra, blue colours, disk-dominated morphologies) and more than 20% of the sample is composed by "111" galaxies (quiescent spectra, red colours, spheroidal morphologies). On the whole, 83% of the galaxies show a full concordant cube classification, very similar to the 85% of concordance shown by the smaller zCOSMOS-bright 1k sample (see M09).

This agreement confirms the goodness of this kind of classification: the vast majority of the galaxies in the sample belong to one of the two larger classes that show concordant behaviour in spectral, photometric and morphological properties. In these three fundamental observational features, bimodality is a major property of the galaxy population, either considering these features one at a time or comparing them in a more organic way.

CHAPTER 3

PCA-Clustering classification method

In this chapter we will present an entirely new method of galaxy classification, which exploits in a natural way the global bimodal properties of the galaxies. We will describe first the Principal Component Analysis and its application to our dataset, then we will present the Unsupervised Fuzzy Partition, that is the cluster analysis algorithm that actually classifies galaxies into early types, late types and intermediate galaxies. Finally we will exploit the large capabilities and flexibility of PCA+UFP method extending the work to a lower redshift sample of galaxies.

SECTION 3.1

The PCA+UFP clustering method

The bimodality is an intrinsic property of galaxies, not only considering specific characteristics like colours, spectral indices, morphologies etc, but also taking those properties as a whole, as we have seen in the previous section. A classification cube stands on its own because of this global bimodality, which tells us that galaxies are well divided in two categories, "early types" and "late types". How those two categories relate to each other is still matter of debate, and the characterisation of transitional galaxies – objects that represent the bridge from one category to another, the so-called *green valley* – is of paramount importance for the definition of the evolutive history of the galaxies and to understand how and why galaxies migrate

between categories.

For these reasons we decided to pursue a more global look to our sample, considering properties of galaxies as a whole. To accomplish this task, we used the Principal Component Analysis on our sample and a Cluster Analysis to identify the loci of *early type* and *late type* galaxies.

3.1.1 Principal Component Analysis

The Principal Component Analysis (PCA) [Pearson, 1901, Hotelling, 1933] is an orthogonal linear transformation useful to reduce multidimensional data sets to lower dimensions, in order to facilitate subsequent analysis. It transforms the data to a new coordinate system such that the greatest variance by any projection of the data comes to lie on the first coordinate (called the first principal component), the second greatest variance on the second coordinate, and so on. For this reason PCA is the ideal tool to study a large number of parameters, allowing us to understand their importance and correlations.

Our PCA run involved 8 major observational properties of the sample: two parameters are derived from spectra (the $D4000$ break and the rest-frame equivalent width of [O II], i.e. $EW_0[\mathrm{O\,II}]$); one is derived from the photometric analysis ($\Delta(B-z)$) and the remaining parameters are morphological: M_{20} (second-order moment of the brightest 20% of galaxy flux), concentration C (ratio between radii including 80% and 20% of galaxy light), Gini coefficient G (uniformity of light distribution), asymmetry A (rotational symmetry of light distribution) and clumpiness S, as taken from ZEST catalogue. We chose these parameters in order to keep our results comparable to the previous classification, the 3D cube, which makes use of the same observables.

The first step required to apply the PCA to a data set is to normalise the involved observables. Thus, we took the logarithm of $EW_0[\mathrm{O\,II}]$, as the variable was distributed as a log-normal distribution. Therefore, from now on we will be referring to $\log(EW_0[\mathrm{O\,II}])$ every time we mention the equivalent width of [O II].

The result of the PCA application to our eight variables is a rotated eight-dimensional space, where every new variable (PCx, where $x \in \mathbb{N}$, $x \leq 8$) is a linear combination of the original ones:

$$PCx = \sum_{i=1}^{8} a(i)_x V_i \tag{3.1}$$

where $a(i)_x$ are the coefficients of the linear transformation and V_i are the original variables.

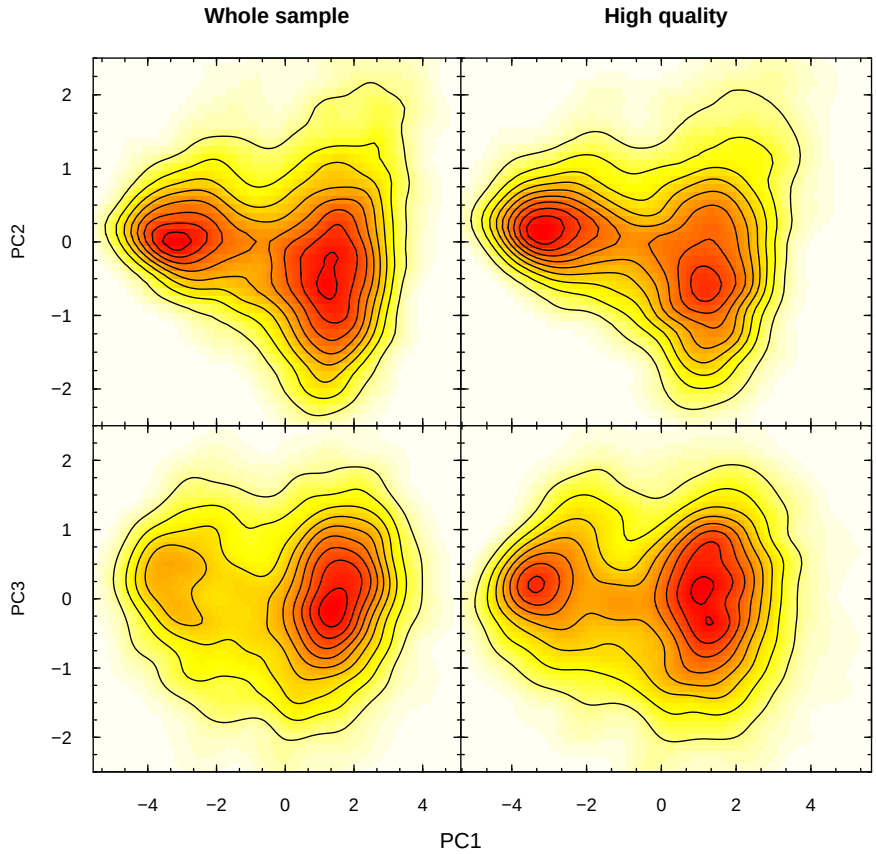

Figure 3.1: 2D density maps of the high redshift galaxies in PC1-PC2 plane (upper panels) and in PC1-PC3 plane (lower panels). Left maps are calculated on the whole sample, while right ones are calculated on the high quality sample only. It is clearly visible the global bimodality of galaxy properties, represented by the two "clumps" in density.

In Tab. 3.1 the coefficients $a(i)_x$ of our PCA are shown. Coefficients show the relative importance of the original variables in each eigenvector PCx: the larger the value of $a(i)_x$, the stronger the importance of the associated variable within the principal component. The two last rows of PCA table show the proportional variance (how much variance is expressed by each single PC) and the cumulative variance (how much variance is expressed by *the sum* of the previous PCs). We decided to never let the cumulative variance be below 80% of the original total one, so we decided to keep only the three first PCs, which express the 84% of the original variance.

Fig. 3.1 shows the density of the data points in the PC1-PC2 and PC1-PC3 planes, achieved via kernel density estimation with an axis-aligned bivariate normal kernel, evaluated on a square grid [Venables and Ripley, 2002]. The plot shows the isodenses of the points, both using lines of equal density and

Parameter	PC1	PC2	PC3	PC4	PC5	PC6	PC7	PC8
$D4000$	-0.368	0.117	0.423	0.062	-0.653	0.329	-0.365	-0.026
$EW_0[\mathrm{O\,II}]$	0.359	-0.056	-0.429	-0.245	-0.733	-0.177	0.233	-0.025
$\Delta(B-\mathrm{z})$	-0.392	0.139	0.388	0.023	-0.114	-0.525	0.621	0.039
G	-0.367	0.304	-0.415	0.031	0.002	-0.571	-0.522	-0.038
M_{20}	0.419	-0.013	0.323	0.131	-0.058	-0.314	-0.261	0.730
C	0.400	0.125	-0.289	-0.447	0.065	0.320	0.160	0.640
A	0.185	0.772	-0.160	0.488	-0.028	0.234	0.215	0.066
S	0.278	0.510	0.318	-0.693	0.124	-0.052	-0.119	-0.222
Prop. Variance	0.586	0.142	0.109	0.063	0.043	0.024	0.022	0.011
Cum. Variance	0.586	0.728	0.838	0.901	0.944	0.968	0.990	1.000

Table 3.1: Results of the Principal Component Analysis applied to eight different properties of the galaxies. Absolute values of the coefficients show the relative importance of the original variables within each Principal Component; a negative coefficient means an anti-correlation.

a colour-coded 2D map: the global bimodal nature of the whole population of galaxies is reflected by the two "clumps" in density, separated by a narrow under-dense "valley", in which transitional objects lie. The global bimodality is much more evident in the high quality sample, due to better measurements of the spectral features involved.

It is interesting to notice that Disney et al. [2008] stated that only one parameter should be sufficient to describe the nature of a galaxy, although they were not able to identify it: our PCA shows that the bimodality unfolds itself in the PC1 direction alone. Although PC1 cannot be that single simple parameter, it is a very interesting fact that the main properties of a galaxy can be described just by looking to its PC1 value.

The so-called biplot is a very useful tool to understand the relationships between the original variables and the PCs [Gabriel, 1971], and in our work it can help explain why do galaxies arrange themselves in this way in the PC space. In the biplot in Fig. 3.2 the arrows represent the axes where each original variable lies, and their length is an index of their "strength", their importance within each PC – in mathematical terms the coefficients $a(i)_x$ shown in Tab. 3.1, also called loadings. Looking at the coefficients of $D4000$, $EW_0[\mathrm{O\,II}]$, $\Delta(B-\mathrm{z})$, G, M_{20} and C within PC1, for instance, one can see that they are roughly the same (in absolute value): this explains why in the biplot the relative arrows have more or less the same length along PC1 axis.

Fig. 3.2 shows that $D4000$ and $\Delta(B-\mathrm{z})$ are strongly correlated, because the arrows point in the same direction and have similar strength. The $EW_0[\mathrm{O\,II}]$ is anti-correlated to them both, and that is somewhat expected since spectral

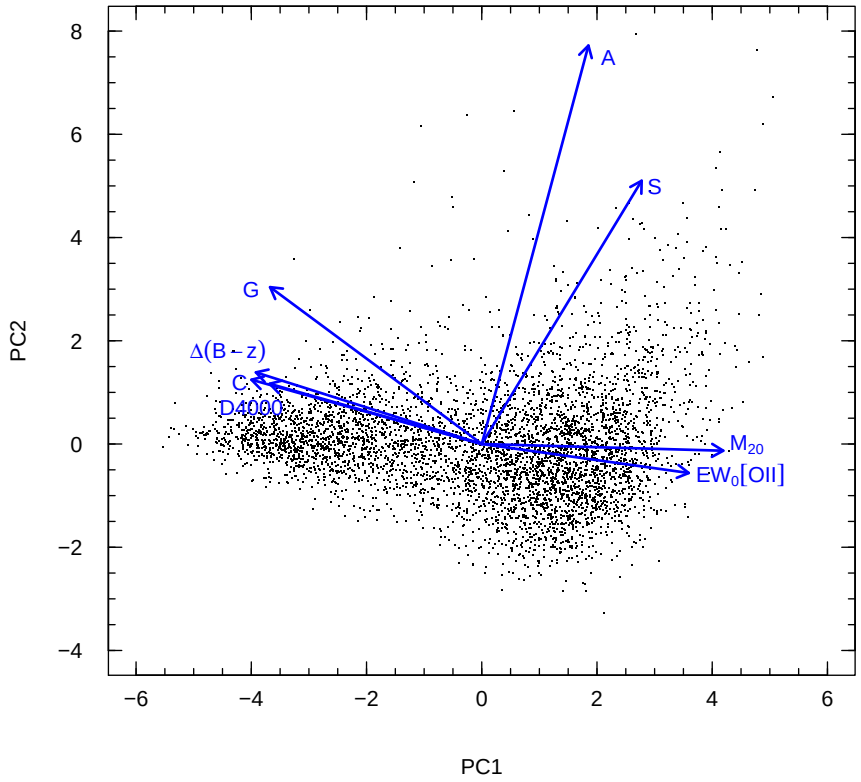

Figure 3.2: Biplot of our PC1-PC2 plane. Black points are the galaxies as expressed in terms of PCs, while blue arrows represent the "direction" in which each original variable tends to scatter the data.

classification shown in Fig. 2.2: most galaxies with high values of $D4000$ have little or no emission lines, and vice-versa. $\Delta(B-\mathrm{z})$ increases with $D4000$, so basically redder galaxies have a larger $D4000$, and that is also expected from Fig. 2.3. We noted also that C and G are strongly correlated: G is a measure of how uniformly the flux is distributed among pixels in the galaxy image, so more concentrated galaxies have a larger value of G, or that the flux is not uniformly distributed. M_{20} is anti-correlated with the two other morphological parameters: since M_{20} is a measure of how many bright off-centred knots of light are present, the greater is the value of M_{20}, the "later" is the galaxy, because disk-dominated galaxies have more bright spots (star formation regions, spiral arms, bars) than spheroidal or elliptical galaxies.

Taking into consideration only PC2 we can see that asymmetry A and clumpiness S are very strongly correlated: the larger the value of PC2 of a galaxy, the more disturbed its morphology is. Objects with low values of PC2

show more regular morphologies, and are separated by their values of the other morphological parameters like C, M_{20} and G.

3.1.2 Cluster analysis

Cluster analysis is based on partitioning a collection of data points into a number of subgroups, where the objects inside a cluster show a certain degree of closeness or similarity. Hard clustering assigns each data point (feature vector) to one and only one of the clusters, with a degree of membership equal to one, assuming well defined boundaries between the clusters. This model often does not reflect the description of real data, where boundaries between subgroups might be fuzzy, and where a more nuanced description of the object's affinity to the specific cluster is required. For this reason we applied a fuzzy clustering method to our PCA-reduced sample in order to segregate galaxies between the two clusters.

Our method makes use of the Unsupervised Fuzzy Partition (UFP) clustering algorithm as introduced and developed by Gath and Geva [1989]. The approach of this method is Bayesian: first it is required to run a partition algorithm to provide first guesses of memberships and cluster centroids. This is achieved via a modification of the fuzzy c-means algorithm [Bezdek, 1973]. These prototypes are then used by the second algorithm (Fuzzy modification of maximum likelihood estimation – FMLE) to achieve optimal fuzzy partition [Geva et al., 2000].

The fuzzy c-means algorithm

The *k-means algorithm* is a hard partitioning method quite simple and popular, though its results are not always reliable and can suffer from numerical problems. This algorithm allocates each data point to one of c clusters to minimize the within-cluster sum of squares:

$$\sum_{i=1}^{c} \sum_{k \in A_i} \| \mathbf{x}_k - \mathbf{v}_i \|_2 \tag{3.2}$$

where A_i is a set of objects (data points) in the i-th cluster and $\mathbf{v}_i$ is the mean for that points over cluster i. In k-means clustering the cluster prototype is a point.

The *fuzzy c-means algorithm* (FCM) can be seen as the fuzzified version of the k-means algorithm and is based on the minimization of an objective function called *c-means functional*:

$$J(\mathbf{X};\mathbf{U},\mathbf{V}) = \sum_{i=1}^{c}\sum_{k=1}^{N}(\mu_{ik})^m \parallel \mathbf{x}_k - \mathbf{v}_i \parallel_{\mathbf{A}}^2 \tag{3.3}$$

where $\mathbf{V} = [\mathbf{v}_1, \mathbf{v}_2, \ldots, \mathbf{v}_c], \mathbf{v}_i \in \mathbb{R}^n$ is a vector of cluster prototypes (centres), which have to be determined, $\parallel \mathbf{x}_k - \mathbf{v}_i \parallel_{\mathbf{A}}^2 = D_{ikA}^2 = (\mathbf{x}_k - \mathbf{v}_i)^{\mathbf{T}}\mathbf{A}(\mathbf{x}_k - \mathbf{v}_i)$ is a squared inner-product distance norm, and $U = [\mu_{ik}]$ is a $N \times c$ matrix representing the fuzzy partitions, where μ_{ik} denotes the membership degree that the i-th data points belongs to the k-th cluster. Its conditions are given by:

$$\mu_{ik} \in [0,1], \forall i,k, \quad \sum_{i=1}^{c}\mu_{ik} = 1, \forall i, \quad 0 < \sum_{i=1}^{N}\mu_{ik} < N, \forall k. \tag{3.4}$$

Statistically, Eq. (3.3) can be seen as a measure of the total variance of $\mathbf{x}_k$ from $\mathbf{v}_i$. The minimization of Eq. (3.3) represents a non-linear optimization problem that can be solved by using a variety of available methods, ranging from grouped coordinate minimization to genetic algorithms. The most popular method, however, is a simple Picard iteration through the first-order conditions for stationary points of Eq. (3.3), known as the fuzzy c-means (FCM) algorithm.

The FMLE clustering algorithm

The *fuzzy maximum likelihood estimates (FMLE) clustering algorithm* employs a distance norm based on the fuzzy maximum likelihood estimates, proposed by Bezdek and Dunn [1975]:

$$D_{ik}(\mathbf{x}_k, \mathbf{v}_i) = \frac{\sqrt{\det(\mathbf{F}_{wi})}}{\alpha_i} \exp\left(\frac{1}{2}\left(\mathbf{x}_k - \mathbf{v}_i^{(l)}\right)^{\mathbf{T}}\mathbf{F}_{wi}^{-1}\left(\mathbf{x}_k - \mathbf{v}_i^{(l)}\right)\right). \tag{3.5}$$

This distance norm involves an exponential term and thus decreases faster than the inner-product norm. $\mathbf{F}_{wi}$ denotes the fuzzy covariance matrix of the i-th cluster, given by:

$$\mathbf{F}_{wi} = \frac{\sum_{k=1}^{N}(\mu_{ik})^w(\mathbf{x}_k - \mathbf{v}_i)(\mathbf{x}_k - \mathbf{v}_i)^{\mathbf{T}}}{\sum_{k=1}^{N}(\mu_{ik})^w}, 1 \leq i \leq c \tag{3.6}$$

where $w = 1$ in the original FMLE algorithm, but we use the $w = 2$ weighting exponent, so that the partition becomes more fuzzy to compensate the exponential term of the distance norm. The α_i is the prior probability of selecting cluster i, given by:

$$\alpha_i = \frac{1}{N}\sum_{k=1}^{N}\mu_{ik}. \tag{3.7}$$

The membership degrees μ_{ik} are interpreted as the posterior probabilities of selecting the i-th cluster given the data point $\mathbf{x}_k$. Gath and Geva [1989] reported that the fuzzy maximum likelihood estimates clustering algorithm is able to detect clusters of varying shapes, sizes and densities. The cluster covariance matrix is used in conjunction with an exponential distance, and the clusters are not constrained in volume. However, this algorithm needs a good initialization, since due to the exponential distance norm, it converges to a near local optimum [Kenesei et al., 2008].

Both these algorithms have been implemented using R statistical package [R Development Core Team, 2009].

3.1.3 Application of the PCA+UFP method

Fig. 3.3 shows 2D projections of the application of the UFP clustering algorithm to our 3D dataset. The global bimodality shown by the PCA application is confirmed and well defined by the UFP algorithm. As already noticed in §3.1.1, the leftmost objects (in red in the plot) are the early type galaxies, while in the rightmost part of the diagram (in blue) are the late type galaxies. Figs. 3.4 are 3D visualizations of the data, trying to show the PC-spatial distribution of the different galaxy populations.

Being a fuzzy partitioning method, objects do not belong just to one cluster: their probability of membership is spread across all the clusters, provided that the sum of memberships for all clusters, for a given data point, is equal to 1. In our work we assign the i-th object to a cluster k only if its probability of membership is $\mu_{ik} > 0.9$. We chose this threshold because, due to the exponential nature of the FMLE distance function, there is a steep rise in the probability function until ~ 0.9, and then there is a general flattening. In Fig. 3.3 red objects are galaxies which belong to the "early type cluster" with a probability more than 90%, while blue objects are galaxies which belong to the "late type cluster" with the same probability. All other galaxies (those which belong to any cluster with a probability $0.5 < \mu_{ik} < 0.9$) are marked in green.

Early type galaxies, defined in this way, represent almost 30% of the entire sample (1413 objects), while late types are 62% (3035) and the other 8% (426) are classified as intermediate objects. The early types' locus here is more populated than the correspondent class in the classification cube (the "111" class), which was composed by the 23% of the total sample (Tab. 2.4).

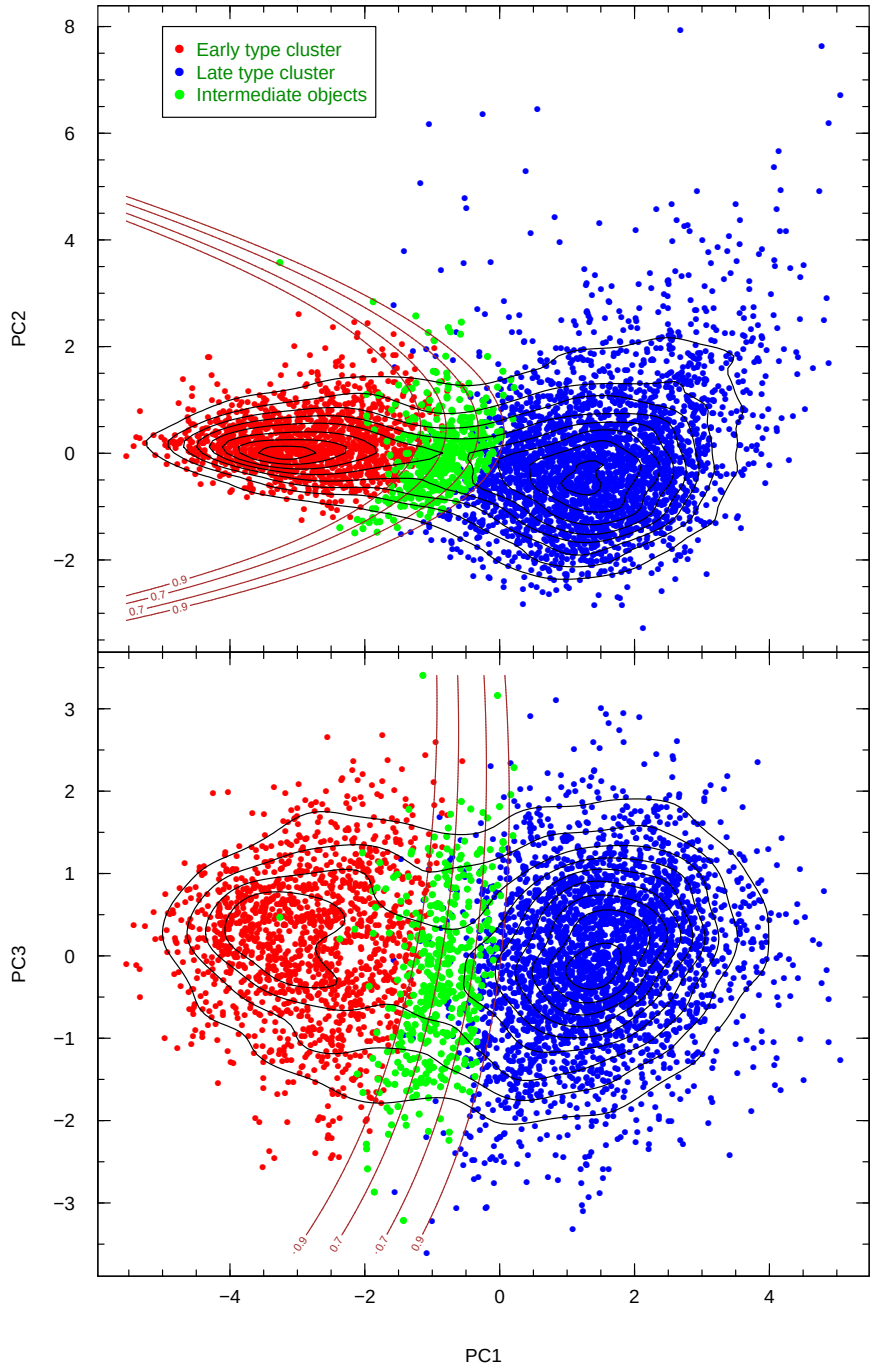

Figure 3.3: Result of the Unsupervised Fuzzy Partition (UFP) clustering algorithm applied to the PCA-reduced whole sample: the upper panel represent the PC1-PC2 plane, while the lower panel represent the PC1-PC3 plane. In red are early type galaxies, in blue late type galaxies, in green our intermediate objects. Brown lines are the interceptions on plane PC1-PC2 of the isoprobability surfaces with probabilities 70% and 90%. Black curves are the isodenses of the points in the planes, computed via Gaussian kernel smoothing.

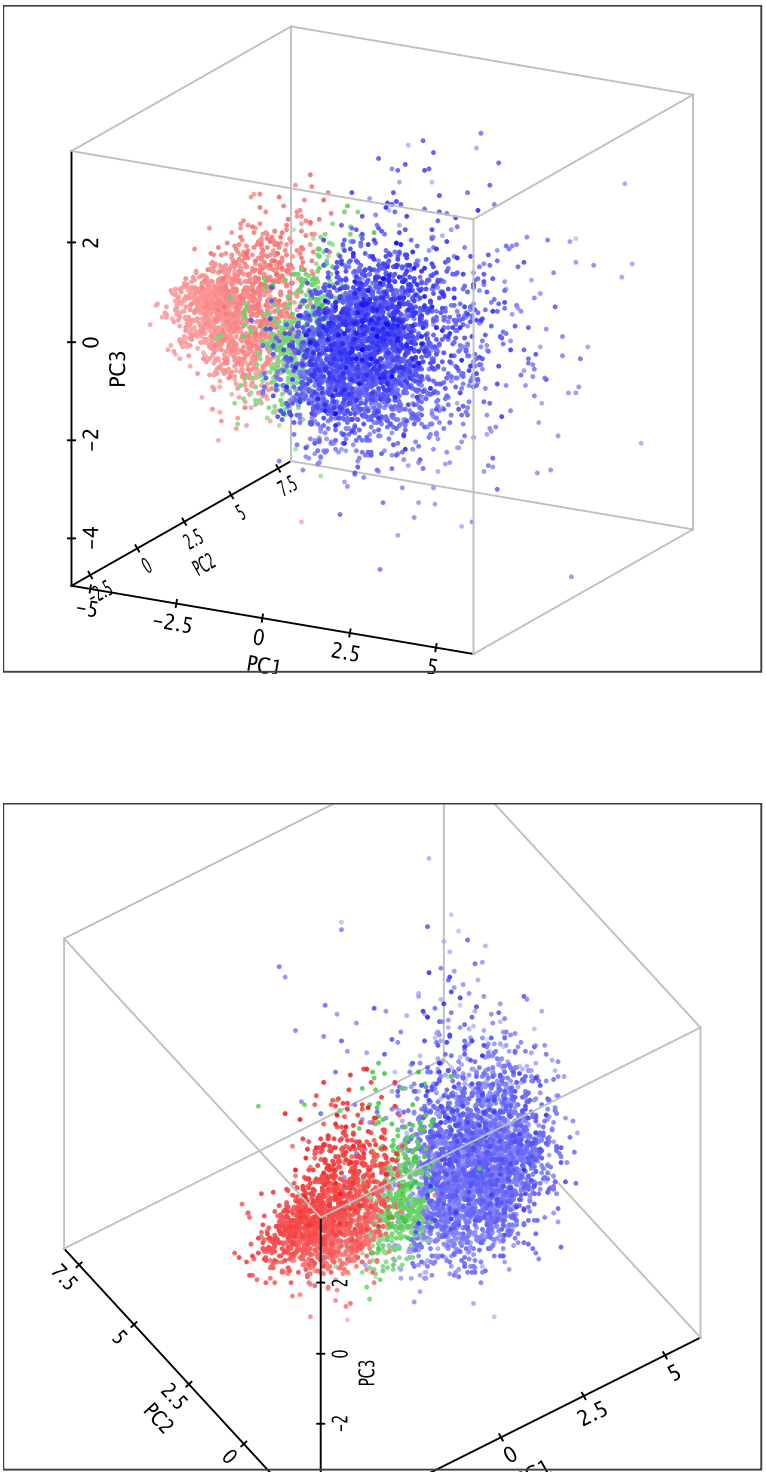

Figure 3.4: Two different three-dimensional visualizations of the PC space. The colours represent the clusters as defined by the UFP cluster analysis in Fig. 3.3. Different intensities of the colours represent the distance of the point from the vantage point, trying to give the idea of the depth of the points distribution.

This is due to several reasons: the 90% membership threshold for the UFP cluster analysis, which seemed a fair choice due to the shape of the probability function, is however more or less arbitrary; choosing a 95% membership threshold, for instance, lowers the percentage of early type objects to $\sim 20\%$. Moreover, the classification cube considers 8 different classes of objects, while PCA+UFP only 3 of them: many of the outliers in the classification cube (all the 121s and the 211s, and a great part of 112s and 221s) are now classified as early types in PCA+UFP. If they were to be classified as fully concordant 111s in classification cube, this class would be made up of nearly the 31% of the whole sample. Finally, one must keep in mind that the "early type cluster", as defined by PCA+UFP, is not intended to be made up of pure passive galaxies; rather, it is composed also by bulge-dominated weakly-starforming objects.

Most of the differences between the two methods could be ascribed to errors and misclassifications due to the "hard partitioning" logic of the cube classification: each of the sub-classifications of the cube are characterized by clear cut boundaries that can produce placement misclassifcations, especially for objects that are in proximity of those boundaries. Another culprit could be the high number of morphological parameters in the PCA+UFP analysis, that might assign greater importance to those to the detriment of other parameters; however, several runs of the PCA+UFP algorithms with lower numbers of morphological parameters do not seem to substantially change the results.

Fig. 3.3 shows also the results of the cluster analysis with respect of the local density evaluation as shown in Fig. 3.1. It can be easily seen that the intermediate objects lie in the "valley" between the two major clumps of data points. This is something expected, since we wanted to point out the relative difference between these objects and the galaxies belonging to the two clusters.

3.1.4 Extension to low redshifts

Due to the parameter choice of this analysis, we were forced to limit the analysis to a sub-sample of the 10k zCOSMOS sample: as we said in §2.1, the spectral features involved in the analysis ($D4000$ and $EW[\mathrm{O\,II}]$) are detectable within zCOSMOS-bright only between $0.48 < z < 1.28$. The higher limit in redshift coincides with the limit of the zCOSMOS-bright survey, but the nearest galaxies (between $0 < z < 0.48$) were left out of the analysis. In order to expand the analysis, to follow the behaviour of galaxies in the entire redshift range of zCOSMOS-bright survey, we decided to exploit the PCA+UFP method to probe the galaxies even at lower redshifts, substituting

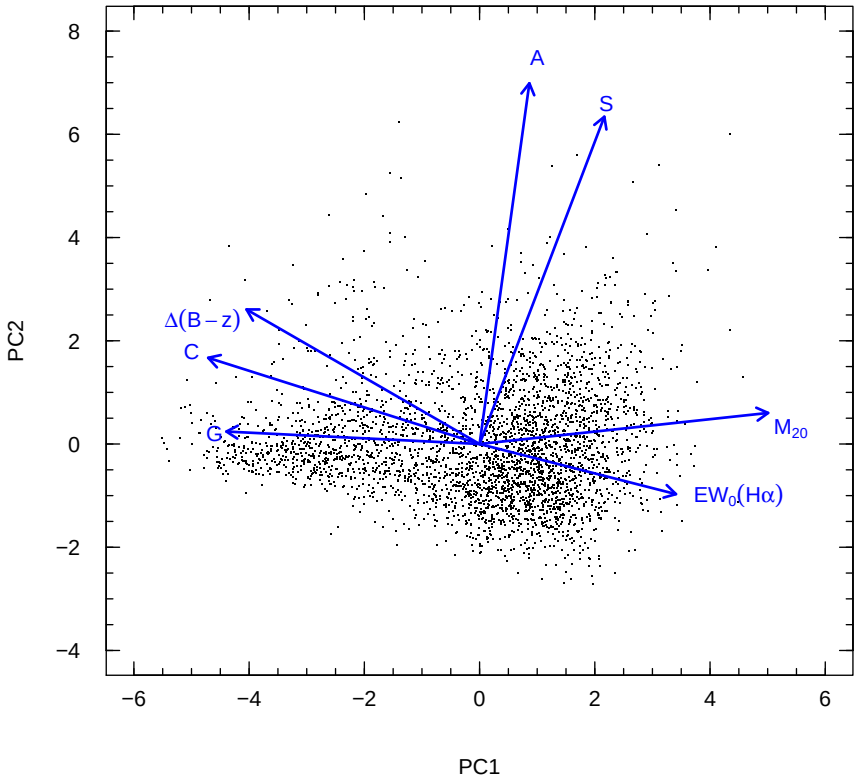

Figure 3.5: Biplot of PC1-PC2 plane for low redshift galaxies.

the spectral features used at high redshifts with one of the best star formation indicators – Hα – which is detectable within zCOSMOS-bright from the local universe to $z \sim 0.48$. This is one of the main reasons behind this work: the PCA+UFP method, not being tied to a particular set of data, is able to use different parameters and probe different redshift ranges and properties of the galaxies.

For the extension at low redshifts we therefore considered 7 observable parameters: $\Delta(B-\mathrm{z})$, M_{20}, concentration C, Gini coefficient G, asymmetry A, clumpiness S and $EW_0(\mathrm{H}\alpha)$ – like in previous analysis with $EW_0[\mathrm{O\,II}]$ we considered the logarithm of the rest-frame equivalent width due to its log-normal distribution, so from now on $EW_0(\mathrm{H}\alpha)$ has to be intended as $\log EW_0(\mathrm{H}\alpha)$. The *low redshift sample* defined in this way is composed by 3402 galaxies. Results of the application of the PCA are shown in Tab. 3.2. As for the analysis at high redshifts we decided to consider those PCs that give a cumulative variance not less than 80%. In this case we took into account the

Parameter	PC1	PC2	PC3	PC4	PC5	PC6	PC7
$EW_0(\mathrm{H}\alpha)$	0.340	-0.097	-0.545	-0.541	-0.529	0.032	-0.042
$\Delta(B-\mathrm{z})$	-0.404	0.260	0.311	0.153	-0.766	0.230	-0.085
G	-0.439	0.024	-0.463	-0.024	0.249	0.717	0.119
M_{20}	0.500	0.060	0.104	0.220	0.060	0.471	-0.678
C	0.216	0.634	0.358	-0.520	0.178	0.217	0.269
A	-0.471	0.167	-0.045	-0.427	0.186	-0.293	-0.666
S	0.086	0.698	-0.499	0.423	-0.007	-0.274	-0.004
Prop. Variance	0.483	0.177	0.126	0.104	0.060	0.035	0.014
Cum. Varariance	0.483	0.660	0.786	0.891	0.950	0.986	1.000

Table 3.2: Results of the Principal Component Analysis applied to the low redshift ($z < 0.48$) galaxies.

first 4 PCs, which account for 89% of the total original variance.

In Fig. 3.5 the biplot of the PCA for low redshift galaxies is shown. By comparing it with Fig. 3.2 one can see the striking resemblance in the cloud's shape and in loadings' directions. The function of $D4000$ and $EW_0[\mathrm{O\,II}]$ – to segregate the galaxies mainly in PC1 direction – is taken over by $EW_0(\mathrm{H}\alpha)$, while the other parameters' relations remain largely unchanged. With respect to Fig. 3.2, galaxies in the early-type cluster spread more in PC2 (which is mainly morphology driven): this is probably due to ACS being progressively abler to recognise features, even in spheroidal galaxies, with decreasing redshift, due to the larger size of the galaxies themselves. So spheroidal galaxies with streams due to encounters with companions, interacting galaxies or just objects with companions nearby, have larger values of asymmetry A and clumpiness S with respect to galaxies with similar features but at higher redshifts (angular dimensions of those galaxies will be smaller and their features will most likely be too small to be appreciated with an automatic analysis). This is evident in Fig. 3.6, where ACS snapshots of the galaxies in early types' cluster with the highest values of the second principal component ($\mathrm{PC2} > 2$) are shown.

Fig. 3.7 shows the result of the UFP clustering algorithm application. As in previous analysis for high redshift analysis, we used a threshold of 90% membership to distinguish between objects belonging to the "early-type" cluster, to the "late-type" one or object not belonging to any cluster – our "green valley" galaxies. Green valley objects lie in the saddle between the two main clusters, as it can be seen in the plot represented by isodenses, calculated by Gaussian square kernel smoothing of the PC1-PC2 and PC1-PC3 planes, in a way similar to that of the high redshift galaxies (Fig. 3.3).

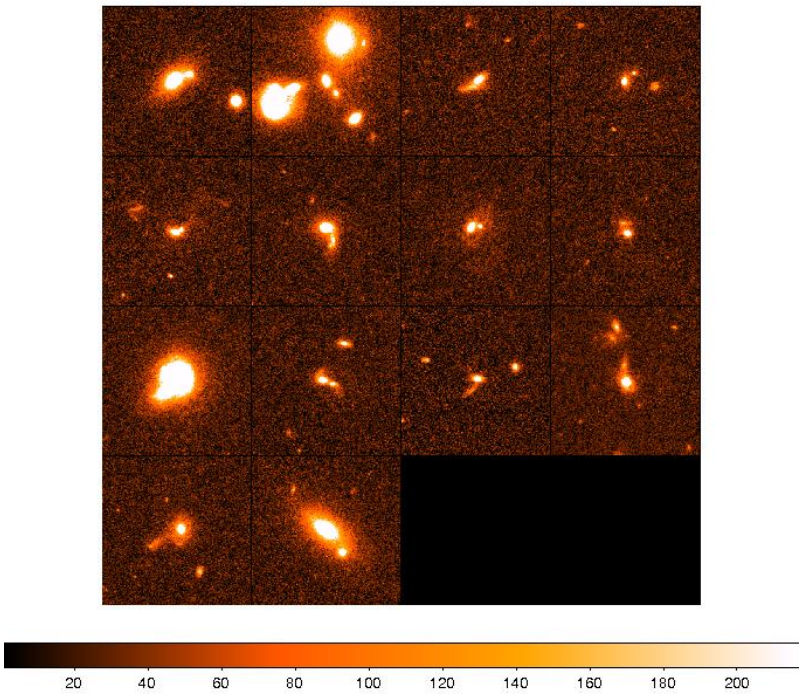

Figure 3.6: Composite image of high redshift early type galaxies with the highest values of PC2. Their morphologies are quite complex, suggesting tidal interactions and recent merging.

With respect to high redshift galaxies, clusters of low redshift galaxies appear less centred and defined: green dots, for instance, appear well beyond the boundaries of 90% isoprobability that define them. This is due to the isoprobability curves being merely 2D projections of 4D hypersurfaces, since as we said we considered the first 4 PCs for the cluster analysis.

Out of the 3402 objects the low redshift sample is made up of, early type galaxies represent 20.6% (704 objects), while late type galaxies are 70.5% (2401), and the green valley galaxies are 8.9% (297). With respect to the high redshift sample, green valley objects represent more or less the same percentage of objects, while there is significant shift of populations between the two main clusters: late type galaxies are $\sim 10\%$ more with respect to the high quality sample, while conversely early types are 10% less. This can be due to a selection effect (at low redshift we are sampling galaxies with lower luminosities and lower masses, which are on average "later" at all redshifts), therefore not a real evolutive feature. In the next chapter we well explore in more details the evolution of the galaxy populations with redshift.

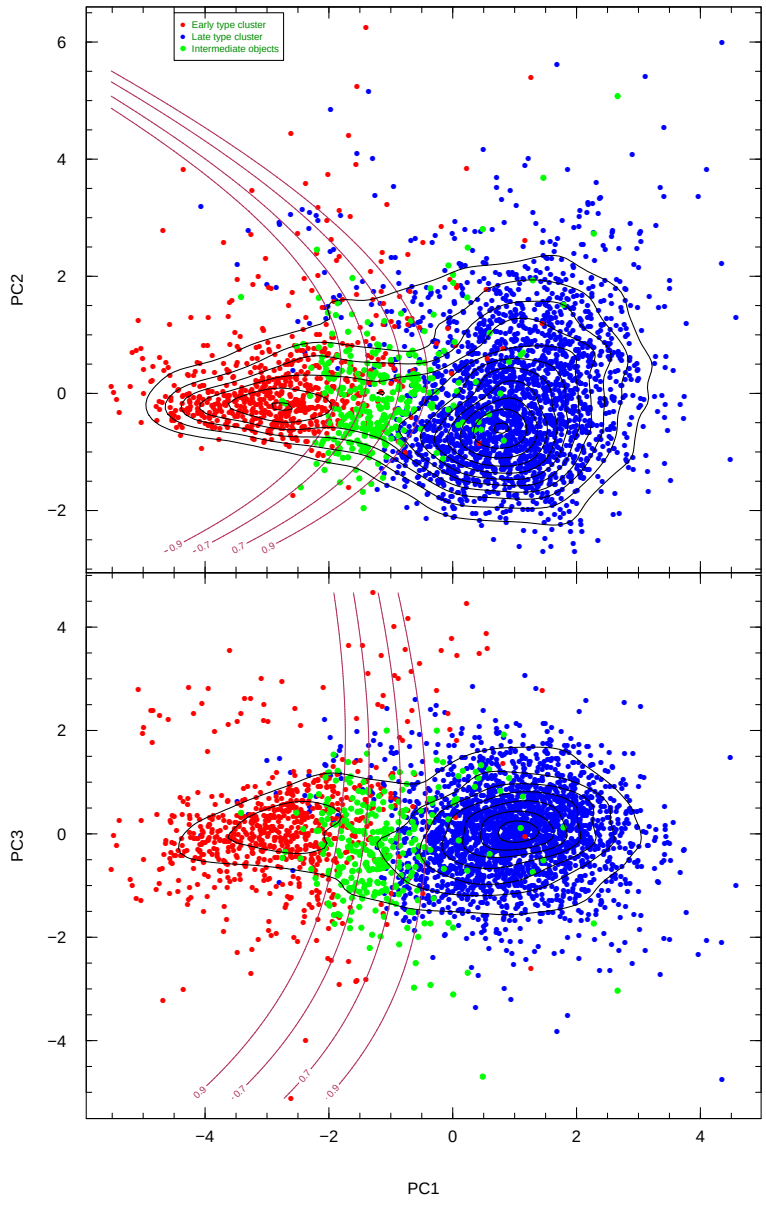

Figure 3.7: Cluster analysis results for low redshift galaxies. Superimposed to the points, as in Fig. 3.3, are the isodenses of the points calculated via kernel smoothing in PC1-PC2 and PC1-PC3 planes. The curved lines represent the projected isoprobability curves. Clusters and green valley objects appear more scattered across the planes because of projection issues from four-dimensional PCA to the 2 dimensions of the plot.

CHAPTER 4

Results

This chapter offers a view on the evolution patterns of the different populations defined by the PCA+UFP clustering method. We will focus on the evolution with z of the galaxies at different masses, giving the opportunity to define the mass M_{cross} at which the transition from the blue cloud to the red sequence is more evident. We define an interesting population of galaxies that show many of the properties of the green valley galaxies, and we will compare this population with a definition of green valley from literature. Finally, we will provide analysis of some interesting subpopulations like AGNs, red spiral and blue elliptical galaxies.

SECTION 4.1

Results

The analysis presented in this work offers many improvements with respect to the previous methods of classification like the classification cube. One of the greatest advantages of such an approach is given by its self-consistency and its global approach to the parameters: as we stated in §3.1.2, the classification cube is more subject to wrong assignments of one or more of its sub-classification methods because they are "hard partition" ones. Since the fact that every parameter is treated separately from the others, it is easier to have one of them misclassified due to internal errors or closeness of the value to the boundaries.

The PCA+UFP method avoids this kind of errors because its parameters are treated simultaneously: using the PCA on a multidimensional space we

are "averaging out" outlying values in a small number of parameters. This can be intuitively understood by looking at biplots (Figs. 3.2 and 3.5): an outlying value in M_{20}, for instance, can be compensated by "normal" values in spectral emission lines, $D4000$ and C. On the other side the PCA+UFP method is probably less sensitive to emphasise objects with discordant behaviour of only one of its parameters.

Another powerful feature of the PCA+UFP analysis is its flexibility: while the classification cube is strongly bound to its defining parameters – and for this reason has been applied to the high redshift sample only – the PCA+UFP analysis is not restricted to a particular dataset or a particular set of parameters. We therefore can extend the work to low redshifts just by substituting the two spectral parameters with a different one. The choice of Hα has been made in order to keep the possibility to compare the results of high and low redshift samples, and have a comprehensive look to the whole 10k dataset. Actually, the PCA+UFP method can successfully be applied also to completely different datasets (star formation rates, masses, luminosities) of this or other galaxy surveys, and that is possibly its most important achievement.

In the next subsections we will show some of the properties of the whole 10k population, and of interesting subsamples, in PCA+UFP analysis.

SECTION 4.2

Combined high and low redshift sample

Fig. 4.1 shows the evolution of the different populations of galaxies, within the whole 10k sample, with redshift and with stellar mass[1]. Masses have been computed by Bolzonella et al. [2009], using Bruzual and Charlot [2003] population synthesis models, by means of the `Hyperzmass` code, a modified version of the photo-z code `Hyperz` [Bolzonella et al., 2000].

In Fig. 4.1 we show the positions of the zCOSMOS 10k galaxies in the PC1-PC2 planes as function of redshift and mass.

Low mass galaxies ($\log M/M_{\odot} < 9.9$, first column) are almost exclusively part of the late-type cluster, while high mass galaxies ($\log M/M_{\odot} > 10.7$, last column) mainly belong to the early-type cluster. The transition can be mostly seen in the intermediate mass bins: at $9.9 < \log M/M_{\odot} < 10.3$, galaxies at high redshift ($z > 0.80$) are still forming stars actively, and are therefore

[1] Hereinafter we will refer to stellar masses as simply "masses".

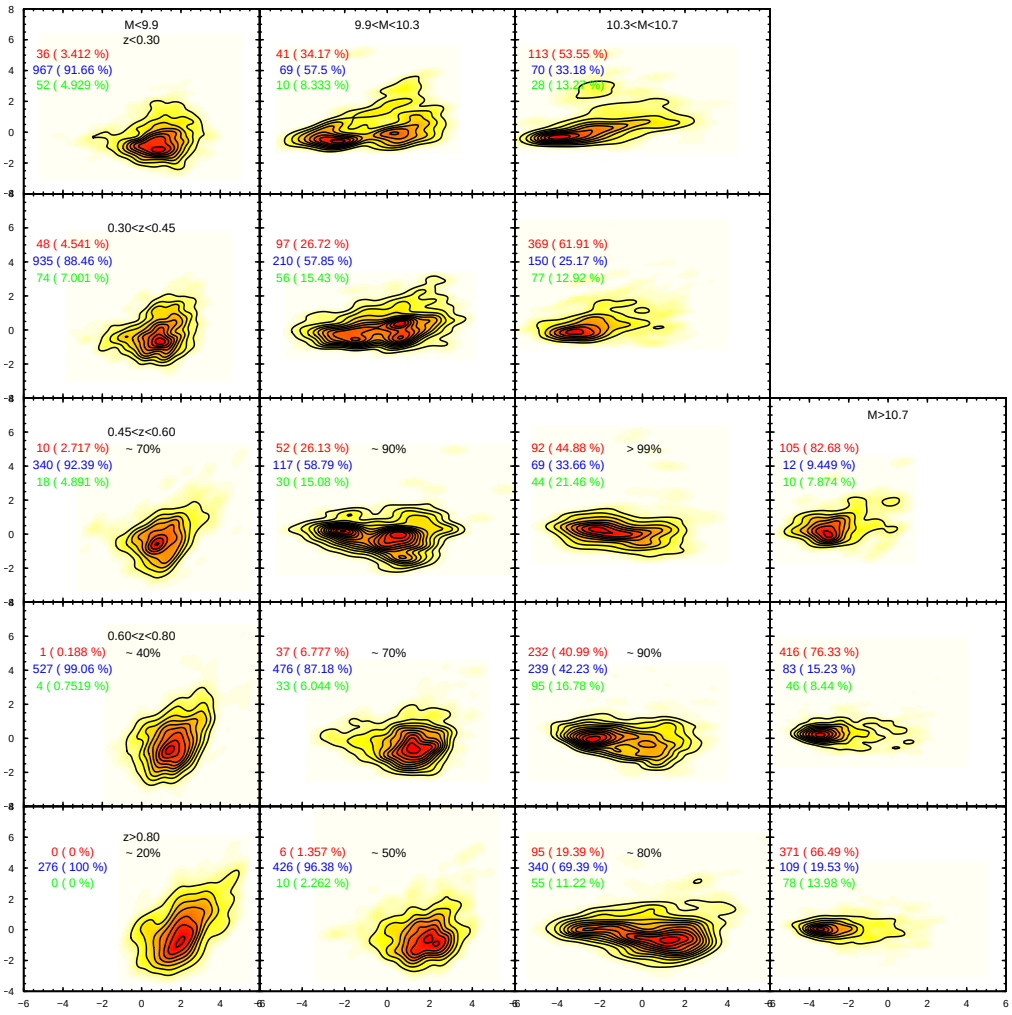

Figure 4.1: PC1-PC2 diagrams for low redshift (upper two rows) and high redshift (lower three rows) samples, kernel smoothed with the usual technique. Columns represent bins of mass (growing from left to right, in units of $\log M/M_{\odot}$ – specified inside first row boxes) while rows represent bins of redshift (growing from top to bottom – written inside first column boxes). Inside each panel are also shown the absolute numbers and fractions of galaxies in each cluster (early-type, late-type and green valley), in red, blue and green respectively. Inside some of the high redshift panels are shown the mass completenesses [as computed by Pozzetti et al., 2009]; where there are no percentages the sample has to be intended as mass-complete.

concentrated in the late-type cluster; the "migration" towards the early type cluster seems to begin at moderately lower redshifts ($0.60 < z < 0.80$), slowing down from $z \sim 0.50$ and being still ongoing also in the local Universe.

At slightly larger masses ($10.3 < \log M/M_{\odot} < 10.7$) this transition seems to be completed at earlier epochs: at $0.60 < z < 0.8$ early-type and late-type galaxies are numerically comparable, and the transition appears almost complete at $0.30 < z < 0.45$. This delay in the star formation quenching for the lower mass galaxies, in opposition to the larger ones, can be regarded as one manifestation of the *downsizing* effect: the main reasons behind this effect are still unclear, even if some mechanisms have been suggested [Bower et al., 2006, Hopkins et al., 2006, Dekel and Birnboim, 2006]. Some numerical simulations [Schweizer, 2000] show that the transition in colours should be very fast (of the order of ~ 500 Myr), and other observative studies seem to suggest that this is the case if the star formation is quenched efficiently. Our work seem to suggest that the transition from our "late type" locus to the "early type" takes longer to be achieved (at least some Gyrs). Part of this is could be due to the changes in colours and morphologies taking place with different timescales; Balogh et al. [2004], however, showed that an exponentially decaying star formation can lengthen the transition phase to some Gyrs.

Looking at the Fig. 4.1 by rows it is possible to appreciate the mass distribution of the galaxy population at fixed redshifts. At low redshifts the zCOSMOS survey cannot sample the high mass galaxies ($\log M/M_{\odot} > 10.7$) due to the small sampled volume and the bright magnitude cut, so the corresponding boxes are empty; conversely, more than half of the objects are low-mass star-forming galaxies. At higher redshifts mass incompleteness prevents us to directly compare the numbers of galaxies in each mass bin (as it can be seen in the plot, at $z > 0.80$ the mass completeness of the sample with $\log M/M_{\odot} < 9.9$ is of the order of 20%). However, this is not a sever issue when dealing with fractions within each mass and redshift bin; we can assume that within the bin the mass distribution is rather flat.

We translated these considerations in Fig. 4.2, where each of the first five panels represents a row of Fig. 4.1, i.e. a bin of redshift in which we divided our sample. For every given redshift bin the fraction of early type, late type and intermediate objects for each mass bin are plotted. Low mass early type galaxies are very few (up to $\sim 4\%$) in every redshift bin, late types being by far most frequent at $\log M/M_{\odot} < 9.9$, as it can be seen also in the first column of Fig. 4.1. This is in good agreement with determinations of Kovač et al. [2010] for the same zCOSMOS sample, who found a similar behaviour in different

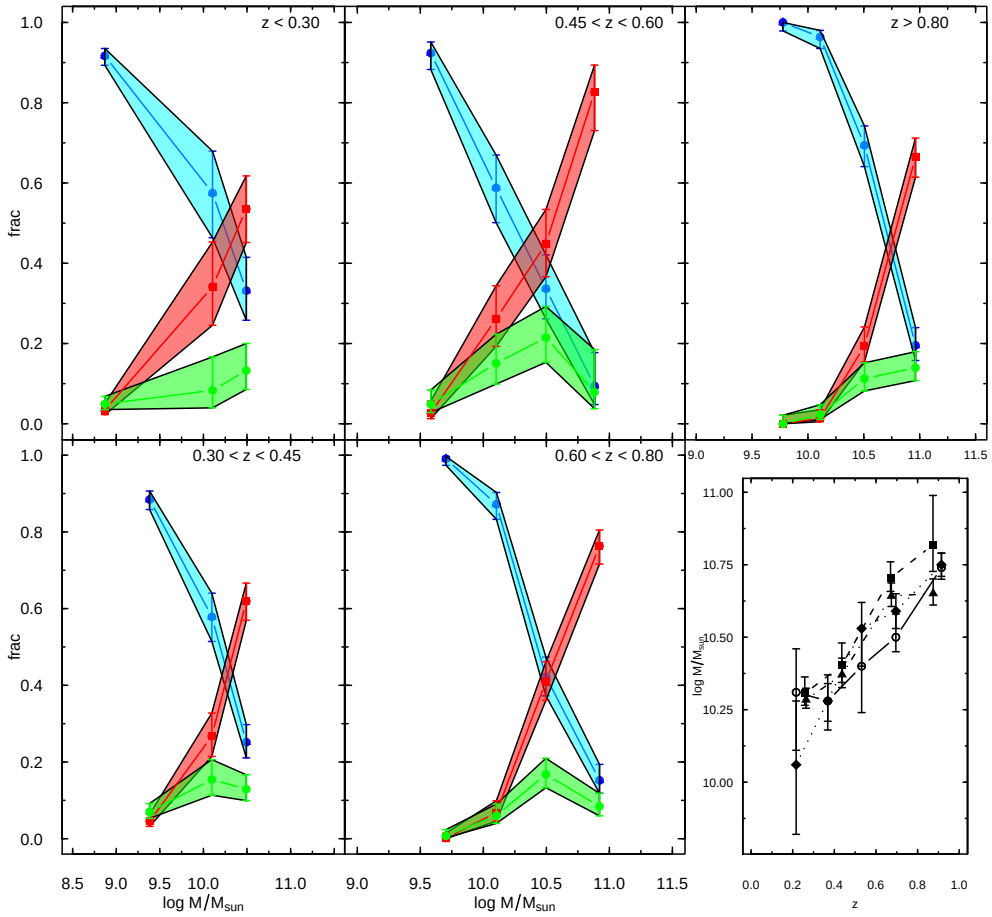

Figure 4.2: Evolution with redshift of the fractions of different galaxy populations in mass. Each panel shows the fraction of galaxies in each mass bin that belong to each PCA+UFP cluster (in cyan are late-type galaxies, in red the early-type ones, in green the green valley ones), in a specific redshift bin. Errors are 95% confidence intervals for multinomial populations [Miller, 1966]. The last panel represent the evolution in z of the transition mass ($M_{\rm cross}$), defined as the point where red line and cyan line meet (solid line). Errors associated are given by the width of the region where the two strips meet. Dashed and dot-dashed lines represent the transition masses as calculated in Pozzetti et al. [2009], respectively using Marseille morphologies and SED colours photometric classifications. The dotted line represents the transition masses as calculated using Balogh et al. [2004] definition of green valley applied to our combined sample (see §4.2.1).

environments for galaxies of different morphological type.

Intermediate objects seem to be numerically important around $\log M/M_{\odot} \sim 10.5$ at high redshifts, constituting up to $\sim 20\%$ of the sample at $z \sim 0.5$. This suggests that the evolutive transition from the blue cloud towards the red sequence may be most important at intermediate redshifts and intermediate masses (central quadrants in Fig. 4.1).

From Fig. 4.2 the masses at which early-type and late-type galaxies are numerically the same at different redshifts ($M_{\rm cross}$), can also be derived. This transition mass $M_{\rm cross}$ is plotted in the lower right panel of Fig. 4.2 as a function of redshift. Transition masses computed in this work (solid line in the plot) are in fair agreement with those calculated by Pozzetti et al. [2009] using Marseille morphologies [Cassata et al., 2007, 2008, Tasca et al., 2009] as separators of different galaxy types – dashed line in figure – and using a photometric classification [Zucca et al., 2009] – dot-dashed line. A Cramér-von Mises test [Anderson, 1962] confirms the consistency of the three estimates of $M_{\rm cross}$ (p-values above 0.73). It must be kept in mind, though, that determinations of $M_{\rm cross}$ in this work are made within a three-cluster framework (early type, late type and intermediate galaxies), while other determinations are made taking into account only the two main galaxy populations. Splitting our intermediate galaxy sample between the other two clusters, using a 50% threshold as membership values, the evolution with redshift of $M_{\rm cross}$ steepens, and especially at high redshifts transition masses are more in agreement. Considering the different techniques of calculation, however, the agreement among these determinations is quite remarkable.

4.2.1 Green valley galaxies

Green valley galaxies have been defined in a number of different ways, usually exploiting their natural bimodal distribution using colour indicators like $u-r$ [Strateva et al., 2001, Baldry et al., 2004], $U-V$ [Brown et al., 2007, Silverman et al., 2008], $U-B$ [Vergani et al., 2010], $B-i$ [Caputi et al., 2009]. In this subsection we will analyse the $U-V$ rest-frame colour distribution (from now on $(U-V)_0$) of our PCA+UFP clustered galaxies.

The $(U-V)_0$ distribution of the combined high+low redshift samples (Fig. 4.3) shows a clear bimodality, that reflects the global one we discussed throughout the paper. The separation between the two families in colour happens at $(U-V)_0 \sim 1.6$; the colour distribution of our late type galaxies peaks at $(U-V)_0 \sim 1$, while the distribution of the early types is peaked at $(U-V)_0 \sim 1.9$. All of these are in fair agreement with other determinations from literature [Silverman et al., 2008, Brammer et al., 2009]. The green

valley objects' distribution is peaked at $(U-V)_0 \sim 1.5$, near the saddle of the total distribution.

We can compare the $(U-V)_0$ distribution of our green valley galaxies with Balogh et al. [2004] definition of green valley, which is defined as the 0.2 mag dip between the two observed Gaussian distribution for early- and late-type galaxies. Applying the above definition, in the combined sample 760 objects out of 8 256 (9.2%) would be defined as "green valley" objects; this number is very close to the number of green valley galaxies in our classification (721, the 8.7%); more than 25% of our green valley objects are so also in the Balogh et al. [2004] definition, while the rest of the objects within those boundaries are almost equally divided by PCA+UFP between the two main clusters. The largest part of our intermediate galaxies lies to the left of the colour-defined green valley, i.e. in the region of the blue galaxies, but makes up only the 6.5% of all the objects in that region; conversely, PCA+UFP intermediate galaxies constitute the 8.4% of all the objects in the red galaxies region.

Being based on overall properties of the galaxies, our classification method gives somewhat different results compared to classical colour definitions of green valley: the cores of the early-type and late-type clusters are correctly reproduced, but our classification suggests that relying on a single colour might not be sufficient to correctly recover those galaxies which are really in transition between the late-types and the early-types clusters.

The transition masses $M_{\rm cross}$ of the sample divided using Balogh et al. definition of green valley were also calculated (dotted line in Fig. 4.2); the agreement between the determinations is very high, even considering the uncertainties in the first redshift bin due to the low number of objects. Using a mass and/or redshift dependent colour definition of the green valley [e.g. Brand et al., 2009] results are very similar.

4.2.2 Red spirals

We checked the PCA+UFP clustering properties of some of the outliers in the classification cube. Obviously this has been possible only with galaxies from the high redshift sample, because the classification cube has been defined using $D4000$ and $EW_0[\mathrm{O\,II}]$, which were available only at $z > 0.48$ (see §2.2.1). *Red spirals*, for instance, are often identified with edge-on spiral galaxies, reddened by a strong dust lane [Zucca et al., 2009, Tasca et al., 2009], while face-on galaxies are thought to be the very oldest spirals which used up their gas reservoirs, probably aided by strangulation and bar instabilities [Masters et al., 2009]. In our classification cube, red spirals may be identified by the three-digit codes "112" and "212", both representing morphological late-type

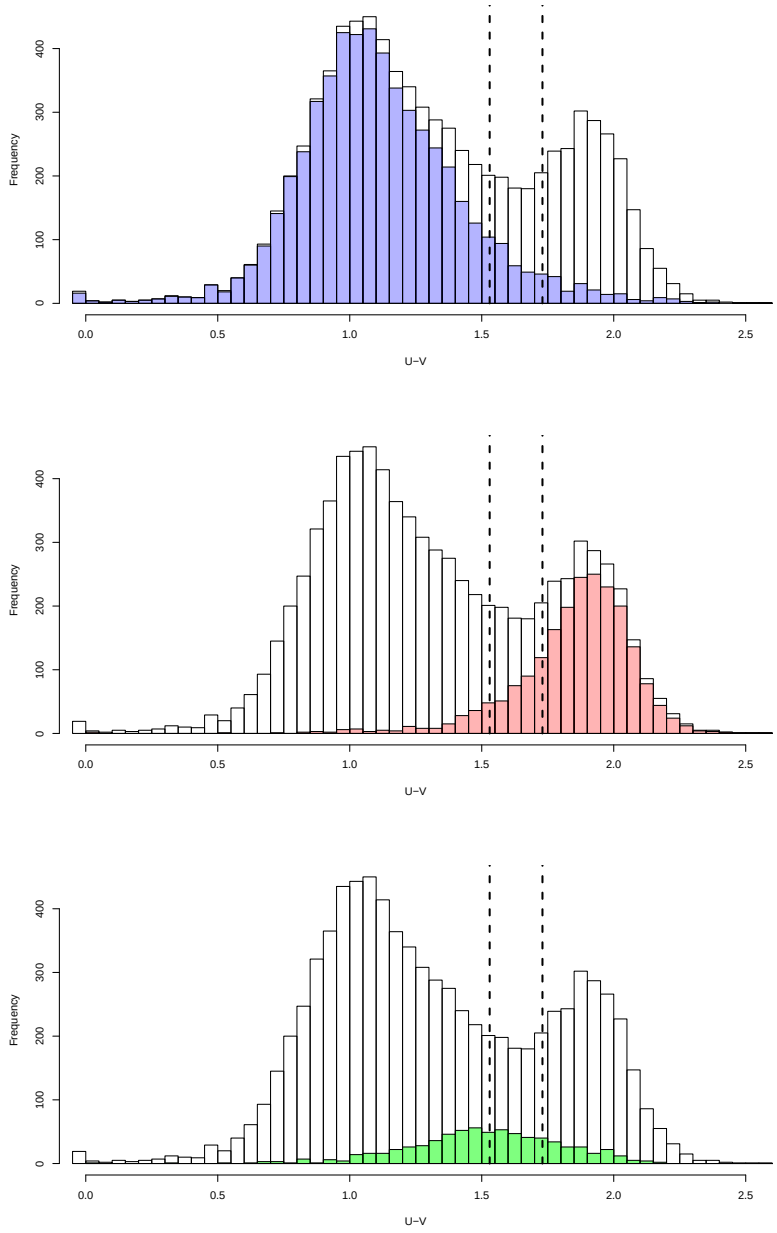

Figure 4.3: Rest frame $U-V$ distributions of the galaxies in the combined sample (high+low redshift). Open histograms represent the distribution of the total sample; blue, red and green histograms represent the distribution of PCA+UPF late types, early types and intermediate galaxies, respectively. Dashed lines represent green valley boundaries as defined by Balogh et al. [2004] for comparative purposes.

galaxies (third digit "2"), the first one representing spectrally passive red objects and the latter one referring to red star-forming galaxies.

Galaxies with classification cube code "112" are 93: of those, 24 (25.8%) are classified by PCA+UFP in the green valley group; 27 (29%) are in the late type cluster; 43 (46.2%) are in the early type cluster. A fairly high number of them (14) possess unusually high values of PC2: at a visual inspection those objects revealed very disturbed morphologies, dominated by merging and tidal streams (Fig. 3.6), in agreement with determinations from Conselice et al. [2000a] who found that very large values of A (reflecting in our work in large values of PC2) are a good indication of ongoing major merging. At least for these objects, automatic morphological classification methods apparently fail to identify correctly them as merging spheroidals: their asymmetric characteristics are instead intepreted as late type morphologies.

Galaxies with classification cube code "212" are 74: 25 of them (33.8%) are classified in the green valley group, 43 (58.1%) are in the late type cluster and only 6 (8.1%) are classified in the early type cluster. Their range in PC1 and PC2 is quite narrow, making those object a rather homogeneous sample, located in the middle of the PC1-PC2 diagram, in or very near the low density saddle between the clusters. Those galaxies, showing spiral morphologies, low star formation rates (indicated by PC1 ~ 0) and reddish colors are the best candidates of the old spirals population mentioned by Masters et al. [2009].

We also checked the position of "red spiral" galaxies according to their classification based on the Marseille morphologies and on photometric type ($\mathcal{PT}$) calculated with the SED templates provided by Ilbert et al. [2006]. We defined red spiral galaxies as those objects classified as "morphologically late type" (Marseille type 2) and having red SEDs ($\mathcal{PT} < 13$). With these specifications red spiral galaxies in the whole sample are 420: 289 (69%) are in the PCA+UFP early type cluster, 79 (19%) are in the late type cluster, 52 (12%) in the intermediate region. Our technique places these red spirals mainly in the early types' cluster; this is probably due to the fact that in our classification the very early spirals (Sa) are included in the red cluster, but it also seems to imply that for these objects the spectrophotometric properties are more important than the morphological ones.

4.2.3 Blue ellipticals

In our classification cube, blue ellipticals are identified by the three-digit codes "121" and "221", the first one representing spectrally passive objects and the latter one referring to active star-forming galaxies, both bulge-dominated.

Classification cube code "121" galaxies are almost exclusively assigned to

the early type galaxies cluster by the PCA+UFP algorithm (60/64), while code "221" show a somewhat diverse behaviour, being equally divided among the groups: 56 out of 169 (33.1%) belong to the green valley group, 52 (30.8%) to the late type cluster and 61 (36.1%) to the early type cluster. In PCA terms, objects in the latter group are characterised by positive values of PC2 and generally negative values of PC1: while code "121" galaxies are most probably the result of a color misclassification in the classification cube, and therefore are "normal" early type galaxies — confirmed by their $\Delta(B-z)$ very close to the divider in Fig. 2.3 — code "221" objects seem to be more complex. Late type "221"s have large values of PC2, while the PC2 value of early type "221"s is around 0. This may imply a misclassification in $\Delta(B-z)$, too, but it is not sufficient to explain all their features. Most probably many of these objects, especially at higher values of PC1, present complex morphologies and are the result of tidal interactions.

As for the red spiral galaxies, we checked the PCA+UFP properties of the "blue ellipticals" using the morphological informations from Marseille catalogue and the photometric ones from the spectral energy distributions; blue ellipticals are those objects with Marseille type 1 and with $\mathcal{PT} > 13$. Out of 848 objects with these characteristics in the whole sample, 205 (24%) are classified by PCA+UFP as green valley objects, while the rest is almost equally divided between the the late type and the early type clusters.

These results seem to imply that for these objects the spectrophotometric properties are given more importance than the morphological ones by PCA+UFP algorithm. In fact, as we said, a spiral morphology classifier – especially when using wide classifiers and automatic recognition systems – is more subject to errors due to the asymmetries of merging objects.

4.2.4 Active Galactic Nuclei

We also investigated the positions, in the PCA spaces, of known AGN in the zCOSMOS sample. Type-1 AGN, which are easily recognisable by their broad emission lines, are given a particular confidence class since the determination of their redshifts (10 + normal confidence class – see §2.1) and have been excluded from the subsamples; type-2 AGN, on the other hand, are included in the sample since they are more difficult to identify, because their emission lines are very similar to those of regular star-forming galaxies. We used the diagnostic diagram selection of Bongiorno et al. [2009] to identify Seyfert 2 galaxies and LINERs and investigate their positions in PCA planes. Two different diagnostic diagrams have been exploited to select type-2 AGN, at low redshift using the line ratio [N III]/Hα and [O III]/Hβ whereas at high

redhift the line ratios [O III]/Hβ and [O II]/Hβ have been used. Due to the different ionization properties of Seyfert 2 and LINERs galaxies, only at low redhift the diagnostic diagrams are able to separate the two active nuclei populations. For this reason we will discuss the properties of the whole type-2 AGN population (which includes both the active galaxy classes) in the two redshift ranges, separating the LINERs and Seyfert 2 galaxies only for $z \lesssim 0.5$ [for a more detailed analysis see Bongiorno et al., 2009].

The sample is composed by 79 type-2 AGN in the high redshift sample and 125 type-2 AGN (95 of which are LINERs, while the other 30 are Seyfert 2 galaxies) in the low redshift sample. Considering both the high redshift and the low redshift samples, 204 galaxies are classified as Narrow Line AGN: 126 of them (62%) are placed by PCA+UPF algorithms in the late type galaxies cluster, while 47 (23%) are in the early types cluster and 31 (15%) are in the green valley region. If we restrict our analysis to the low redshift sample, 95 active galaxies are classified as LINERs: 54 of them (57%) are in the late types cluster, 22 (23%) are in the early types one and 19 (20%) are in the green valley. Conversely, the 30 pure Seyfert 2 galaxies are placed by our PCA+UPF algorithms as follows: 15 of them (50%) in the late types cluster, 11 (37%) in the early types region and only 4 (13%) in the green valley. Though we are facing small number statistics, it is clear that the majority of the analysed type-2 AGN are hosted by galaxies which belong to the blue, late-type cluster. This is quite expected, since our active galaxies span the low luminosity regime, as indicated by the [O III] at 5007 Å line luminosity $10^{5.5} L_{\odot} < L[\mathrm{O\,III}] < 10^{9.1} L_{\odot}$[Bongiorno et al., 2009].

Maybe more interesting is esploring whether the selected active nuclei preferentially reside in the intermediate cluster as defined by the PCA+UPF method. While the fraction of type-2 AGN in each main cluster is around 2%, this class of objects consitutes up to 4% of the galaxies in the PCA+UFP green valley region. At low redshifts, LINERs represent 2% of the objects in the late type cluster and 3% of galaxies in the early type one, but they make up to 6% of the green valley galaxies. This picture suggests a certain concentration of type-2 AGN in the green valley region. Since LINERs tend to be associated mostly with earlier morphological type galaxies [ellipticals, lenticulars and early spirals – Ho et al., 1997] we were not surprised to see that the percentage of LINERs in the early type cluster is larger than that of the whole population of type-2 AGN: however, since figures are small – and therefore errors are large – this might not be statistically significant. In fact, fractions from these subclasses are still compatible with being flat sub-samples extracted purely random from the parent sample.

CHAPTER 5

Summary and conclusions

The classification cube method [Mignoli et al., 2009] has been extendend and applied to the high redshift sample of the zCOSMOS-bright 10k release, exploiting bimodalites in spectral ($D4000$ and O II equivalent width, photometric ($B-z$ colour) and morphologic (ZEST classification scheme) properties of the galaxies. In order to overcome some of its limitations (rigidity of the scheme due to its "hard partitioning" nature and emergence of misclassifications, reliance on a particular set of data and the impossibility to adopt different variables, a certain degree of arbitrariety in the boundary definitions for the subclassifications) in this work we set up a different classification method based on statistical approaches like the Principal Component Analysis and the Unsupervised Fuzzy Partition (PCA+UFP), that exploits the bimodal nature of galaxy properties in a more organic and rigorous way.

The PCA+UFP analysis is a very powerful and robust tool to probe the nature and the evolution of galaxies in a survey. It allows to define with less uncertainties the classification of galaxies, adding the flexibility to be adapted to different parameters: being a fuzzy classification it avoids the problems due to a hard classification, such as the classification cube presented in the first part of the article. The PCA+UFP method can be easily applied to different datasets: it does not rely on the nature of the data and for this reason it can be successfully employed with others observables (magnitudes, colours) or derived properties (masses, luminosities, SFRs, etc.).

The agreement between the two classification cluster definitions is very high. "Early" and "late" type galaxies are well defined by the spectral, photometric and morphological properties, both considering them in a separate way and then combining the classifications (classification cube) and treating them as a whole (PCA+UFP cluster analysis). Differences arise in the

definition of outliers: the classification cube is much more sensitive to single measurement errors or misclassifications in one property than the PCA+UFP cluster analysis, in which errors are "averaged out" during the process.

The PCA+UFP analysis has been extended to the low redshift sample, substituting $D4000$ and $EW_0[\mathrm{O\,II}]$ with $EW_0(\mathrm{H}\alpha)$: PCA+UFP analyses, for the high and the low redshift samples, allowed us to behold the *downsizing* effect taking place in the PC spaces: the migration between the blue cloud towards the red clump happens at higher redshifts for galaxies of larger mass. The determination of M_{cross} the transition mass is in significant agreement with others values in literature.

The green valley objects, as defined with the PCA+UFP cluster analysis, represent also a more strict and coherent sample with respect to classical colour definitions, having the same overall physical properties. Subsequent X and radio analysis could help unveil more the nature of these transitional objects.

Bibliography

M. G. Abadi, B. Moore, and R. G. Bower. Ram pressure stripping of spiral galaxies in clusters. *MNRAS*, 308:947–954, October 1999. doi: 10.1046/j.1365-8711.1999.02715.x.

R. G. Abraham, F. Valdes, H. K. C. Yee, and S. van den Bergh. The morphologies of distant galaxies. 1: an automated classification system. *ApJ*, 432:75–90, September 1994. doi: 10.1086/174550.

R. G. Abraham, N. R. Tanvir, B. X. Santiago, R. S. Ellis, K. Glazebrook, and S. van den Bergh. Galaxy morphology to $I = 25$ mag in the Hubble Deep Field. *MNRAS*, 279:L47–L52, April 1996a.

R. G. Abraham, S. van den Bergh, K. Glazebrook, R. S. Ellis, B. X. Santiago, P. Surma, and R. E. Griffiths. The Morphologies of Distant Galaxies. II. Classifications from the Hubble Space Telescope Medium Deep Survey. *ApJS*, 107:1–+, November 1996b. doi: 10.1086/192352.

T. W. Anderson. On the distribution of the two-sample cramér-von mises criterion. *The Annals of Mathematical Statistics*, 33(3):1148–1159, 1962. ISSN 00034851. URL `http://www.jstor.org/stable/2237885`.

S. Andreon. Is There a Deficit of S0 Galaxies at Intermediate Redshift? *ApJ*, 501:533–+, July 1998. doi: 10.1086/305853.

I. K. Baldry, K. Glazebrook, J. Brinkmann, Ž. Ivezić, R. H. Lupton, R. C. Nichol, and A. S. Szalay. Quantifying the Bimodal Color-Magnitude Distribution of Galaxies. *ApJ*, 600:681–694, January 2004. doi: 10.1086/380092.

N. M. Ball, J. Loveday, R. J. Brunner, I. K. Baldry, and J. Brinkmann. Bivariate galaxy luminosity functions in the Sloan Digital Sky Survey. *MNRAS*, 373:845–868, December 2006. doi: 10.1111/j.1365-2966.2006.11082.x.

M. Balogh, V. Eke, C. Miller, I. Lewis, R. Bower, W. Couch, R. Nichol, J. Bland-Hawthorn, I. K. Baldry, C. Baugh, T. Bridges, R. Cannon, S. Cole, M. Colless, C. Collins, N. Cross, G. Dalton, R. de Propris, S. P. Driver, G. Efstathiou, R. S. Ellis, C. S. Frenk, K. Glazebrook, P. Gomez, A. Gray, E. Hawkins, C. Jackson, O. Lahav, S. Lumsden, S. Maddox, D. Madgwick, P. Norberg, J. A. Peacock, W. Percival, B. A. Peterson, W. Sutherland, and K. Taylor. Galaxy ecology: groups and low-density environments in the SDSS and 2dFGRS. *MNRAS*, 348:1355–1372, March 2004. doi: 10.1111/j.1365-2966.2004.07453.x.

M. L. Balogh, S. L. Morris, H. K. C. Yee, R. G. Carlberg, and E. Ellingson. Differential Galaxy Evolution in Cluster and Field Galaxies at $z \sim 0.3$. *ApJ*, 527:54–79, December 1999. doi: 10.1086/308056.

M. L. Balogh, J. F. Navarro, and S. L. Morris. The Origin of Star Formation Gradients in Rich Galaxy Clusters. *ApJ*, 540:113–121, September 2000. doi: 10.1086/309323.

J. E. Barnes and L. Hernquist. Dynamics of interacting galaxies. *ARA&A*, 30: 705–742, 1992. doi: 10.1146/annurev.aa.30.090192.003421.

J. E. Barnes and L. Hernquist. Transformations of Galaxies. II. Gasdynamics in Merging Disk Galaxies. *ApJ*, 471:115–+, November 1996. doi: 10.1086/177957.

J. E. Barnes and L. E. Hernquist. Fueling starburst galaxies with gas-rich mergers. *ApJ*, 370:L65–L68, April 1991. doi: 10.1086/185978.

C. M. Baugh, S. Cole, and C. S. Frenk. Evolution of the Hubble sequence in hierarchical models for galaxy formation. *MNRAS*, 283:1361–1378, December 1996.

K. Bekki, W. J. Couch, and Y. Shioya. Tidal Truncation of Gas Replenishment and Global Suppression of Galactic Star Formation in Distant Clusters. *PASJ*, 53:395–400, June 2001.

K. Bekki, W. J. Couch, and Y. Shioya. Passive Spiral Formation from Halo Gas Starvation: Gradual Transformation into S0s. *ApJ*, 577:651–657, October 2002. doi: 10.1086/342221.

E. F. Bell, C. Wolf, K. Meisenheimer, H.-W. Rix, A. Borch, S. Dye, M. Kleinheinrich, L. Wisotzki, and D. H. McIntosh. Nearly 5000 Distant Early-Type Galaxies in COMBO-17: A Red Sequence and Its Evolution since $z \sim 1$. *ApJ*, 608:752–767, June 2004. doi: 10.1086/420778.

A. J. Benson, R. G. Bower, C. S. Frenk, C. G. Lacey, C. M. Baugh, and S. Cole. What Shapes the Luminosity Function of Galaxies? *ApJ*, 599: 38–49, December 2003. doi: 10.1086/379160.

J. C. Bezdek. *Fuzzy Mathematics in Pattern Classification*. PhD thesis, Applied Math. Center, Cornell University, Ithaca, 1973.

J. C. Bezdek and J. C. Dunn. Optimal Fuzzy Partitions: A Heuristic for Estimating the Parameters in a Mixture of Normal Distributions. *IEEE Trans. Computers*, 24(8):835–838, 1975.

M. R. Blanton, D. W. Hogg, N. A. Bahcall, I. K. Baldry, J. Brinkmann, I. Csabai, D. Eisenstein, M. Fukugita, J. E. Gunn, Ž. Ivezić, D. Q. Lamb, R. H. Lupton, J. Loveday, J. A. Munn, R. C. Nichol, S. Okamura, D. J. Schlegel, K. Shimasaku, M. A. Strauss, M. S. Vogeley, and D. H. Weinberg. The Broadband Optical Properties of Galaxies with Redshifts $0.02 < z < 0.22$. *ApJ*, 594:186–207, September 2003. doi: 10.1086/375528.

M. R. Blanton, D. Eisenstein, D. W. Hogg, D. J. Schlegel, and J. Brinkmann. Relationship between Environment and the Broadband Optical Properties of Galaxies in the Sloan Digital Sky Survey. *ApJ*, 629:143–157, August 2005. doi: 10.1086/422897.

M. Bolzonella, J.-M. Miralles, and R. Pelló. Photometric redshifts based on standard SED fitting procedures. *A&A*, 363:476–492, November 2000.

M. Bolzonella, K. Kovac, L. Pozzetti, E. Zucca, O. Cucciati, S. J. Lilly, Y. Peng, A. Iovino, G. Zamorani, D. Vergani, L. A. M. Tasca, F. Lamareille, P. Oesch, K. Caputi, P. Kampczyk, S. Bardelli, C. Maier, U. Abbas, C. Knobel, M. Scodeggio, C. M. Carollo, T. Contini, J. -. Kneib, O. Le Fevre, V. Mainieri, A. Renzini, A. Bongiorno, G. Coppa, S. de la Torre, L. de Ravel, P. Franzetti, B. Garilli, J. -. Le Borgne, V. Le Brun, M. Mignoli, R. Pello, E. Perez-Montero, E. Ricciardelli, J. D. Silverman, M. Tanaka, L. Tresse, D. Bottini, A. Cappi, P. Cassata, A. Cimatti, L. Guzzo, A. M. Koekemoer, A. Leauthaud, D. Maccagni, C. Marinoni, H. J. McCracken, P. Memeo, B. Meneux, C. Porciani, R. Scaramella, H. Aussel, P. Capak, O. Ilbert, J. Kartaltepe, M. Salvato, D. Sanders, C. Scarlata, N. Scoville, Y. Taniguchi, and D. Thompson. Tracking the impact of environment on the Galaxy Stellar Mass Function up to $z \sim 1$ in the 10k zCOSMOS sample. *ArXiv e-prints*, June 2009.

A. Bongiorno, M. Mignoli, G. Zamorani, F. Lamareille, G. Lanzuisi, T. Miyaji, M. Bolzonella, C. M. Carollo, T. Contini, J. P. Kneib, O. Le Fevre, S. J.

Lilly, V. Mainieri, A. Renzini, M. Scodeggio, S. Bardelli, M. Brusa, K. Caputi, F. Civano, G. Coppa, O. Cucciati, S. de la Torre, L. de Ravel, P. Franzetti, B. Garilli, C. Halliday, G. Hasinger, A. M. Koekemoer, A. Iovino, P. Kampczyk, C. Knobel, K. Kovac, J. -. Le Borgne, V. Le Brun, C. Maier, A. Merloni, P. Nair, R. Pello, Y. Peng, E. Perez Montero, E. Ricciardelli, M. Salvato, J. Silverman, M. Tanaka, L. Tasca, L. Tresse, D. Vergani, E. Zucca, U. Abbas, D. Bottini, A. Cappi, P. Cassata, A. Cimatti, L. Guzzo, A. Leauthaud, D. Maccagni, C. Marinoni, H. J. McCracken, P. Memeo, B. Meneux, P. Oesch, C. Porciani, L. Pozzetti, and R. Scaramella. The [OIII] emission line luminosity function of optically selected type-2 AGN from zCOSMOS. *ArXiv e-prints*, November 2009.

A. Boselli, S. Boissier, L. Cortese, A. Gil de Paz, M. Seibert, B. F. Madore, V. Buat, and D. C. Martin. The Fate of Spiral Galaxies in Clusters: The Star Formation History of the Anemic Virgo Cluster Galaxy NGC 4569. *ApJ*, 651:811–821, November 2006. doi: 10.1086/507766.

F. Bournaud, C. J. Jog, and F. Combes. Galaxy mergers with various mass ratios: Properties of remnants. *A&A*, 437:69–85, July 2005. doi: 10.1051/0004-6361:20042036.

R. G. Bower, A. J. Benson, R. Malbon, J. C. Helly, C. S. Frenk, C. M. Baugh, S. Cole, and C. G. Lacey. Breaking the hierarchy of galaxy formation. *MNRAS*, 370:645–655, August 2006. doi: 10.1111/j.1365-2966.2006.10519.x.

G. B. Brammer, K. E. Whitaker, P. G. van Dokkum, D. Marchesini, I. Labbé, M. Franx, M. Kriek, R. F. Quadri, G. Illingworth, K.-S. Lee, A. Muzzin, and G. Rudnick. The Dead Sequence: A Clear Bimodality in Galaxy Colors from z = 0 to z = 2.5. *ApJ*, 706:L173–L177, November 2009. doi: 10.1088/0004-637X/706/1/L173.

K. Brand, J. Moustakas, L. Armus, R. J. Assef, M. J. I. Brown, R. R. Cool, V. Desai, A. Dey, E. LeFloc'h, B. T. Jannuzi, C. S. Kochanek, J. Melbourne, C. J. Papovich, and B. T. Soifer. The Origin of the 24 μm Excess in Red Galaxies. *ApJ*, 693:340–346, March 2009. doi: 10.1088/0004-637X/693/1/340.

M. J. I. Brown, A. Dey, B. T. Jannuzi, K. Brand, A. J. Benson, M. Brodwin, D. J. Croton, and P. R. Eisenhardt. The Evolving Luminosity Function of Red Galaxies. *ApJ*, 654:858–877, January 2007. doi: 10.1086/509652.

A. G. Bruzual. Spectral evolution of galaxies. I - Early-type systems. *ApJ*, 273:105–127, October 1983. doi: 10.1086/161352.

G. Bruzual and S. Charlot. Stellar population synthesis at the resolution of 2003. *MNRAS*, 344:1000–1028, October 2003. doi: 10.1046/j.1365-8711.2003.06897.x.

K. Bundy, A. Georgakakis, K. Nandra, R. S. Ellis, C. J. Conselice, E. Laird, A. Coil, M. C. Cooper, S. M. Faber, J. A. Newman, C. M. Pierce, J. R. Primack, and R. Yan. AEGIS: New Evidence Linking Active Galactic Nuclei to the Quenching of Star Formation. *ApJ*, 681:931–943, July 2008. doi: 10.1086/588719.

H. Butcher and A. Oemler, Jr. The evolution of galaxies in clusters. I - ISIT photometry of C1 0024+1654 and 3C 295. *ApJ*, 219:18–30, January 1978. doi: 10.1086/155751.

P. Capak, H. Aussel, M. Ajiki, H. J. McCracken, B. Mobasher, N. Scoville, P. Shopbell, Y. Taniguchi, D. Thompson, S. Tribiano, S. Sasaki, A. W. Blain, M. Brusa, C. Carilli, A. Comastri, C. M. Carollo, P. Cassata, J. Colbert, R. S. Ellis, M. Elvis, M. Giavalisco, W. Green, L. Guzzo, G. Hasinger, O. Ilbert, C. Impey, K. Jahnke, J. Kartaltepe, J.-P. Kneib, J. Koda, A. Koekemoer, Y. Komiyama, A. Leauthaud, O. Lefevre, S. Lilly, C. Liu, R. Massey, S. Miyazaki, T. Murayama, T. Nagao, J. A. Peacock, A. Pickles, C. Porciani, A. Renzini, J. Rhodes, M. Rich, M. Salvato, D. B. Sanders, C. Scarlata, D. Schiminovich, E. Schinnerer, M. Scodeggio, K. Sheth, Y. Shioya, L. A. M. Tasca, J. E. Taylor, L. Yan, and G. Zamorani. The First Release COSMOS Optical and Near-IR Data and Catalog. *ApJS*, 172:99–116, September 2007. doi: 10.1086/519081.

K. I. Caputi, S. J. Lilly, H. Aussel, E. Le Floc'h, D. Sanders, C. Maier, D. Frayer, C. M. Carollo, T. Contini, J.-P. Kneib, O. Le Fèvre, V. Mainieri, A. Renzini, M. Scodeggio, N. Scoville, G. Zamorani, S. Bardelli, M. Bolzonella, A. Bongiorno, G. Coppa, O. Cucciati, S. de la Torre, L. de Ravel, P. Franzetti, B. Garilli, O. Ilbert, A. Iovino, P. Kampczyk, J. Kartaltepe, C. Knobel, K. Kovač, F. Lamareille, J.-F. Le Borgne, V. Le Brun, M. Mignoli, Y. Peng, E. Pérez-Montero, E. Ricciardelli, M. Salvato, J. Silverman, J. Surace, M. Tanaka, L. Tasca, L. Tresse, D. Vergani, E. Zucca, U. Abbas, D. Bottini, P. Capak, A. Cappi, P. Cassata, A. Cimatti, M. Elvis, G. Hasinger, A. M. Koekemoer, A. Leauthaud, D. Maccagni, C. Marinoni, H. McCracken, P. Memeo, B. Meneux, P. Oesch, R. Pellò, C. Porciani, L. Pozzetti, R. Scaramella, C. Scarlata, D. Schiminovich,

Y. Taniguchi, and M. Zamojski. The Optical Spectra of Spitzer 24 μm Galaxies in the Cosmic Evolution Survey Field. II. Faint Infrared Sources in the zCOSMOS-Bright 10k Catalog. *ApJ*, 707:1387–1403, December 2009. doi: 10.1088/0004-637X/707/2/1387.

P. Cassata, L. Guzzo, A. Franceschini, N. Scoville, P. Capak, R. S. Ellis, A. Koekemoer, H. J. McCracken, B. Mobasher, A. Renzini, E. Ricciardelli, M. Scodeggio, Y. Taniguchi, and D. Thompson. The Cosmic Evolution Survey (COSMOS): The Morphological Content and Environmental Dependence of the Galaxy Color-Magnitude Relation at $z \sim 0.7$. *ApJS*, 172:270–283, September 2007. doi: 10.1086/516591.

P. Cassata, A. Cimatti, J. Kurk, G. Rodighiero, L. Pozzetti, M. Bolzonella, E. Daddi, M. Mignoli, S. Berta, M. Dickinson, A. Franceschini, C. Halliday, A. Renzini, P. Rosati, and G. Zamorani. GMASS ultradeep spectroscopy of galaxies at $z \sim 2$. III. The emergence of the color bimodality at $z \sim 2$. *A&A*, 483:L39–L42, June 2008. doi: 10.1051/0004-6361:200809881.

C. Chiosi and G. Carraro. Formation and evolution of elliptical galaxies. *MNRAS*, 335:335–357, September 2002. doi: 10.1046/j.1365-8711.2002.05590.x.

A. Cimatti, M. Mignoli, E. Daddi, L. Pozzetti, A. Fontana, P. Saracco, F. Poli, A. Renzini, G. Zamorani, T. Broadhurst, S. Cristiani, S. D'Odorico, E. Giallongo, R. Gilmozzi, and N. Menci. The K20 survey. III. Photometric and spectroscopic properties of the sample. *A&A*, 392:395–406, September 2002. doi: 10.1051/0004-6361:20020861.

S. Cole, A. Aragon-Salamanca, C. S. Frenk, J. F. Navarro, and S. E. Zepf. A Recipe for Galaxy Formation. *MNRAS*, 271:781–+, December 1994a.

S. Cole, A. Aragon-Salamanca, C. S. Frenk, J. F. Navarro, and S. E. Zepf. A Recipe for Galaxy Formation. *MNRAS*, 271:781–+, December 1994b.

G. D. Coleman, C.-C. Wu, and D. W. Weedman. Colors and magnitudes predicted for high redshift galaxies. *ApJS*, 43:393–416, July 1980. doi: 10.1086/190674.

C. J. Conselice. The fundamental properties of galaxies and a new galaxy classification system. *MNRAS*, 373:1389–1408, December 2006. doi: 10.1111/j.1365-2966.2006.11114.x.

C. J. Conselice. The Symmetry, Color, and Morphology of Galaxies. *PASP*, 109:1251–1255, November 1997. doi: 10.1086/134004.

C. J. Conselice. The Relationship between Stellar Light Distributions of Galaxies and Their Formation Histories. *ApJS*, 147:1–28, July 2003. doi: 10.1086/375001.

C. J. Conselice, M. A. Bershady, and J. S. Gallagher, III. Physical morphology and triggers of starburst galaxies. *A&A*, 354:L21–L24, February 2000a.

C. J. Conselice, M. A. Bershady, and A. Jangren. The Asymmetry of Galaxies: Physical Morphology for Nearby and High-Redshift Galaxies. *ApJ*, 529: 886–910, February 2000b. doi: 10.1086/308300.

W. J. Couch, M. L. Balogh, R. G. Bower, I. Smail, K. Glazebrook, and M. Taylor. A Low Global Star Formation Rate in the Rich Galaxy Cluster AC 114 at $z = 0.32$. *ApJ*, 549:820–831, March 2001. doi: 10.1086/319459.

J. A. de Freitas Pacheco, R. Michard, and R. Mohayaee. Formation and Cosmic Evolution of Elliptical Galaxies. *ArXiv Astrophysics e-prints*, January 2003.

G. De Lucia, V. Springel, S. D. M. White, D. Croton, and G. Kauffmann. The formation history of elliptical galaxies. *MNRAS*, 366:499–509, February 2006. doi: 10.1111/j.1365-2966.2005.09879.x.

G. de Vaucouleurs. Classification and Morphology of External Galaxies. *Handbuch der Physik*, 53:275–+, 1959.

A. Dekel and Y. Birnboim. Galaxy bimodality due to cold flows and shock heating. *MNRAS*, 368:2–20, May 2006. doi: 10.1111/j.1365-2966.2006.10145.x.

A. Dekel and J. Silk. The origin of dwarf galaxies, cold dark matter, and biased galaxy formation. *ApJ*, 303:39–55, April 1986. doi: 10.1086/164050.

A. Dekel and J. Woo. Feedback and the fundamental line of low-luminosity low-surface-brightness/dwarf galaxies. *MNRAS*, 344:1131–1144, October 2003. doi: 10.1046/j.1365-8711.2003.06923.x.

T. Di Matteo, V. Springel, and L. Hernquist. Energy input from quasars regulates the growth and activity of black holes and their host galaxies. *Nat*, 433:604–607, February 2005. doi: 10.1038/nature03335.

M. J. Disney, J. D. Romano, D. A. Garcia-Appadoo, A. A. West, J. J. Dalcanton, and L. Cortese. Galaxies appear simpler than expected. *Nat*, 455:1082–1084, October 2008. doi: 10.1038/nature07366.

A. Dressler. Galaxy morphology in rich clusters - Implications for the formation and evolution of galaxies. *ApJ*, 236:351–365, March 1980. doi: 10.1086/157753.

A. Dressler, A. Oemler, Jr., W. J. Couch, I. Smail, R. S. Ellis, A. Barger, H. Butcher, B. M. Poggianti, and R. M. Sharples. Evolution since $z = 0.5$ of the Morphology-Density Relation for Clusters of Galaxies. *ApJ*, 490:577–+, December 1997. doi: 10.1086/304890.

S. P. Driver, P. D. Allen, A. W. Graham, E. Cameron, J. Liske, S. C. Ellis, N. J. G. Cross, R. De Propris, S. Phillipps, and W. J. Couch. The Millennium Galaxy Catalogue: morphological classification and bimodality in the colour-concentration plane. *MNRAS*, 368:414–434, May 2006. doi: 10.1111/j.1365-2966.2006.10126.x.

O. J. Eggen, D. Lynden-Bell, and A. R. Sandage. Evidence from the motions of old stars that the Galaxy collapsed. *ApJ*, 136:748–+, November 1962. doi: 10.1086/147433.

S. C. Ellis, S. P. Driver, P. D. Allen, J. Liske, J. Bland-Hawthorn, and R. De Propris. The Millennium Galaxy Catalogue: on the natural subdivision of galaxies. *MNRAS*, 363:1257–1271, November 2005. doi: 10.1111/j.1365-2966.2005.09521.x.

S. M. Faber, C. N. A. Willmer, C. Wolf, D. C. Koo, B. J. Weiner, J. A. Newman, M. Im, A. L. Coil, C. Conroy, M. C. Cooper, M. Davis, D. P. Finkbeiner, B. F. Gerke, K. Gebhardt, E. J. Groth, P. Guhathakurta, J. Harker, N. Kaiser, S. Kassin, M. Kleinheinrich, N. P. Konidaris, R. G. Kron, L. Lin, G. Luppino, D. S. Madgwick, K. Meisenheimer, K. G. Noeske, A. C. Phillips, V. L. Sarajedini, R. P. Schiavon, L. Simard, A. S. Szalay, N. P. Vogt, and R. Yan. Galaxy Luminosity Functions to $z \sim 1$ from DEEP2 and COMBO-17: Implications for Red Galaxy Formation. *ApJ*, 665:265–294, August 2007. doi: 10.1086/519294.

L. Ferrarese and D. Merritt. A Fundamental Relation between Supermassive Black Holes and Their Host Galaxies. *ApJ*, 539:L9–L12, August 2000. doi: 10.1086/312838.

I. Ferreras, T. Lisker, C. M. Carollo, S. J. Lilly, and B. Mobasher. Evolution of Field Early-Type Galaxies: The View from GOODS CDFS. *ApJ*, 635: 243–259, December 2005. doi: 10.1086/497292.

P. Franzetti, M. Scodeggio, B. Garilli, D. Vergani, D. Maccagni, L. Guzzo, L. Tresse, O. Ilbert, F. Lamareille, T. Contini, O. Le Fèvre, G. Zamorani,

J. Brinchmann, S. Charlot, D. Bottini, V. Le Brun, J. P. Picat, R. Scaramella, G. Vettolani, A. Zanichelli, C. Adami, S. Arnouts, S. Bardelli, M. Bolzonella, A. Cappi, P. Ciliegi, S. Foucaud, I. Gavignaud, A. Iovino, H. J. McCracken, B. Marano, C. Marinoni, A. Mazure, B. Meneux, R. Merighi, S. Paltani, R. Pellò, A. Pollo, L. Pozzetti, M. Radovich, E. Zucca, O. Cucciati, and C. J. Walcher. The VIMOS-VLT deep survey. Color bimodality and the mix of galaxy populations up to $z \sim 2$. *A&A*, 465:711–723, April 2007. doi: 10.1051/0004-6361:20065942.

W. L. Freedman and M. S. Turner. Colloquium: Measuring and understanding the universe. *Reviews of Modern Physics*, 75:1433–1447, November 2003. doi: 10.1103/RevModPhys.75.1433.

C. S. Frenk, S. D. M. White, G. Efstathiou, and M. Davis. Cold dark matter, the structure of galactic haloes and the origin of the Hubble sequence. *Nat*, 317:595–597, October 1985. doi: 10.1038/317595a0.

C. S. Frenk, S. D. M. White, M. Davis, and G. Efstathiou. The formation of dark halos in a universe dominated by cold dark matter. *ApJ*, 327:507–525, April 1988. doi: 10.1086/166213.

Y. Fujita and M. Nagashima. Effects of Ram Pressure from the Intracluster Medium on the Star Formation Rate of Disk Galaxies in Clusters of Galaxies. *ApJ*, 516:619–625, May 1999. doi: 10.1086/307139.

K. R. Gabriel. The biplot graphic display of matrices with application to principal component analysis. *Biometrika*, 58 (3):453–467, 1971. doi: 10.1093/biomet/58.3.453. URL `http://biomet.oxfordjournals.org/cgi/content/abstract/58/3/453`.

I. Gath and A.B. Geva. Unsupervised Optimal Fuzzy Clustering. *IEEE Transactions on Pattern Analysis and Machine Intelligence*, 11:773–780, 1989. ISSN 0162-8828. doi: http://doi.ieeecomputersociety.org/10.1109/34.192473.

A. B. Geva, Y. Steinberg, S. Bruckmair, and G. Nahum. A comparison of cluster validity criteria for a mixture of normal distributed data. *Pattern Recognition Letters*, 21(6-7):511 – 529, 2000. ISSN 0167-8655. doi: DOI: 10.1016/S0167-8655(00)00016-7. URL `http://www.sciencedirect.com/science/article/B6V15-48CPF3D-4X/2/82b8`

S. Ghigna, B. Moore, F. Governato, G. Lake, T. Quinn, and J. Stadel. Dark matter haloes within clusters. *MNRAS*, 300:146–162, October 1998. doi: 10.1046/j.1365-8711.1998.01918.x.

C. Gini. Variabilità e mutabilità. *Memorie di metodologia statistica*, 1912.

J. Gorgas, N. Cardiel, S. Pedraz, and J. J. González. Empirical calibration of the lambda 4000 Å break. *A&AS*, 139:29–41, October 1999. doi: 10.1051/aas:1999375.

S. Gottlöber, A. Klypin, and A. V. Kravtsov. Merging History as a Function of Halo Environment. *ApJ*, 546:223–233, January 2001. doi: 10.1086/318248.

A. W. Graham and S. P. Driver. A Concise Reference to (Projected) Sérsic $R^{1/n}$ Quantities, Including Concentration, Profile Slopes, Petrosian Indices, and Kron Magnitudes. *Publications of the Astronomical Society of Australia*, 22: 118–127, 2005. doi: 10.1071/AS05001.

J. E. Gunn and J. R. Gott, III. On the Infall of Matter Into Clusters of Galaxies and Some Effects on Their Evolution. *ApJ*, 176:1–+, August 1972. doi: 10.1086/151605.

A. Heavens, B. Panter, R. Jimenez, and J. Dunlop. The star-formation history of the Universe from the stellar populations of nearby galaxies. *Nat*, 428: 625–627, April 2004. doi: 10.1038/nature02474.

S. F. Helsdon and T. J. Ponman. The morphology-density relation in X-ray-bright galaxy groups. *MNRAS*, 339:L29–L32, March 2003. doi: 10.1046/j.1365-8711.2003.06300.x.

L. Hernquist. Tidal triggering of starbursts and nuclear activity in galaxies. *Nat*, 340:687–691, August 1989. doi: 10.1038/340687a0.

L. Hernquist and J. C. Mihos. Excitation of Activity in Galaxies by Minor Mergers. *ApJ*, 448:41–+, July 1995. doi: 10.1086/175940.

L. C. Ho, A. V. Filippenko, and W. L. W. Sargent. A Search for "Dwarf" Seyfert Nuclei. V. Demographics of Nuclear Activity in Nearby Galaxies. *ApJ*, 487: 568–+, October 1997. doi: 10.1086/304638.

P. F. Hopkins, L. Hernquist, T. J. Cox, T. Di Matteo, B. Robertson, and V. Springel. A Unified, Merger-driven Model of the Origin of Starbursts, Quasars, the Cosmic X-Ray Background, Supermassive Black Holes, and Galaxy Spheroids. *ApJS*, 163:1–49, March 2006. doi: 10.1086/499298.

P. F. Hopkins, T. J. Cox, D. Kereš, and L. Hernquist. A Cosmological Framework for the Co-evolution of Quasars, Supermassive Black Holes, and Elliptical Galaxies. II. Formation of Red Ellipticals. *ApJS*, 175:390–422, April 2008a. doi: 10.1086/524363.

P. F. Hopkins, L. Hernquist, T. J. Cox, and D. Kereš. A Cosmological Framework for the Co-Evolution of Quasars, Supermassive Black Holes, and Elliptical Galaxies. I. Galaxy Mergers and Quasar Activity. *ApJS*, 175: 356–389, April 2008b. doi: 10.1086/524362.

H. Hotelling. Analysis of a complex of statistical variables into principal components. *Journal of Educational Psychology*, 24:417–441,498–520, 1933.

E. P. Hubble. Extragalactic nebulae. *ApJ*, 64:321–369, December 1926. doi: 10.1086/143018.

O. Ilbert, S. Arnouts, H. J. McCracken, M. Bolzonella, E. Bertin, O. Le Fèvre, Y. Mellier, G. Zamorani, R. Pellò, A. Iovino, L. Tresse, V. Le Brun, D. Bottini, B. Garilli, D. Maccagni, J. P. Picat, R. Scaramella, M. Scodeggio, G. Vettolani, A. Zanichelli, C. Adami, S. Bardelli, A. Cappi, S. Charlot, P. Ciliegi, T. Contini, O. Cucciati, S. Foucaud, P. Franzetti, I. Gavignaud, L. Guzzo, B. Marano, C. Marinoni, A. Mazure, B. Meneux, R. Merighi, S. Paltani, A. Pollo, L. Pozzetti, M. Radovich, E. Zucca, M. Bondi, A. Bongiorno, G. Busarello, S. de La Torre, L. Gregorini, F. Lamareille, G. Mathez, P. Merluzzi, V. Ripepi, D. Rizzo, and D. Vergani. Accurate photometric redshifts for the CFHT legacy survey calibrated using the VIMOS VLT deep survey. *A&A*, 457:841–856, October 2006. doi: 10.1051/0004-6361:20065138.

O. Ilbert, P. Capak, M. Salvato, H. Aussel, H. J. McCracken, D. B. Sanders, N. Scoville, J. Kartaltepe, S. Arnouts, E. L. Floc'h, B. Mobasher, Y. Taniguchi, F. Lamareille, A. Leauthaud, S. Sasaki, D. Thompson, M. Zamojski, G. Zamorani, S. Bardelli, M. Bolzonella, A. Bongiorno, M. Brusa, K. I. Caputi, C. M. Carollo, T. Contini, R. Cook, G. Coppa, O. Cucciati, S. de la Torre, L. de Ravel, P. Franzetti, B. Garilli, G. Hasinger, A. Iovino, P. Kampczyk, J.-P. Kneib, C. Knobel, K. Kovac, J. F. Le Borgne, V. Le Brun, O. L. Fèvre, S. Lilly, D. Looper, C. Maier, V. Mainieri, Y. Mellier, M. Mignoli, T. Murayama, R. Pellò, Y. Peng, E. Pérez-Montero, A. Renzini, E. Ricciardelli, D. Schiminovich, M. Scodeggio, Y. Shioya, J. Silverman, J. Surace, M. Tanaka, L. Tasca, L. Tresse, D. Vergani, and E. Zucca. Cosmos Photometric Redshifts with 30-Bands for 2-deg^2. *ApJ*, 690:1236–1249, January 2009. doi: 10.1088/0004-637X/690/2/1236.

R. Jesseit, T. Naab, R. F. Peletier, and A. Burkert. 2D kinematics of simulated disc merger remnants. *MNRAS*, 376:997–1020, April 2007. doi: 10.1111/j.1365-2966.2007.11524.x.

S. Jogee. The Fueling and Evolution of AGN: Internal and External Triggers. In D. Alloin, editor, *Physics of Active Galactic Nuclei at all Scales*, volume 693 of *Lecture Notes in Physics, Berlin Springer Verlag*, pages 143–+, 2006.

W. Kapferer, T. Kronberger, J. Weratschnig, S. Schindler, W. Domainko, E. van Kampen, S. Kimeswenger, M. Mair, and M. Ruffert. Metal enrichment of the intra-cluster medium over a Hubble time for merging and relaxed galaxy clusters. *A&A*, 466:813–821, May 2007. doi: 10.1051/0004-6361:20066804.

N. Katz and J. E. Gunn. Dissipational galaxy formation. I - Effects of gasdynamics. *ApJ*, 377:365–381, August 1991. doi: 10.1086/170367.

G. Kauffmann. The observed properties of high-redshift cluster galaxies. *MNRAS*, 274:161–170, May 1995.

G. Kauffmann, T. M. Heckman, S. D. M. White, S. Charlot, C. Tremonti, J. Brinchmann, G. Bruzual, E. W. Peng, M. Seibert, M. Bernardi, M. Blanton, J. Brinkmann, F. Castander, I. Csábai, M. Fukugita, Z. Ivezic, J. A. Munn, R. C. Nichol, N. Padmanabhan, A. R. Thakar, D. H. Weinberg, and D. York. Stellar masses and star formation histories for 10^5 galaxies from the Sloan Digital Sky Survey. *MNRAS*, 341:33–53, May 2003a. doi: 10.1046/j.1365-8711.2003.06291.x.

G. Kauffmann, T. M. Heckman, S. D. M. White, S. Charlot, C. Tremonti, E. W. Peng, M. Seibert, J. Brinkmann, R. C. Nichol, M. SubbaRao, and D. York. The dependence of star formation history and internal structure on stellar mass for 10^5 low-redshift galaxies. *MNRAS*, 341:54–69, May 2003b. doi: 10.1046/j.1365-8711.2003.06292.x.

G. Kauffmann, S. D. M. White, T. M. Heckman, B. Ménard, J. Brinchmann, S. Charlot, C. Tremonti, and J. Brinkmann. The environmental dependence of the relations between stellar mass, structure, star formation and nuclear activity in galaxies. *MNRAS*, 353:713–731, September 2004. doi: 10.1111/j.1365-2966.2004.08117.x.

T. Kenesei, B. Balasko, and J. Abonyi. A matlab toolbox and its web based variant for fuzzy cluster analysis. 2008. URL `http://citeseerx.ist.psu.edu/viewdoc/summary?doi=?doi=10.1.1.104.8532`.

R. C. Kennicutt, Jr. Star Formation in Galaxies Along the Hubble Sequence. *ARA&A*, 36:189–232, 1998. doi: 10.1146/annurev.astro.36.1.189.

D. Kereš, N. Katz, D. H. Weinberg, and R. Davé. How do galaxies get their gas? *MNRAS*, 363:2–28, October 2005. doi: 10.1111/j.1365-2966.2005.09451.x.

L. J. Kewley, M. J. Geller, and R. A. Jansen. [O II] as a Star Formation Rate Indicator. *AJ*, 127:2002–2030, April 2004. doi: 10.1086/382723.

T. Kodama, N. Arimoto, A. J. Barger, and A. Aragón-Salamanca. Evolution of the colour-magnitude relation of early-type galaxies in distant clusters. *A&A*, 334:99–109, June 1998.

R. A. Koopmann and J. D. P. Kenney. Massive Star Formation Rates and Radial Distributions from Hα Imaging of 84 Virgo Cluster and Isolated Spiral Galaxies. *ApJ*, 613:851–865, October 2004. doi: 10.1086/423190.

K. Kovač, S. J. Lilly, O. Cucciati, C. Porciani, A. Iovino, G. Zamorani, P. Oesch, M. Bolzonella, C. Knobel, A. Finoguenov, Y. Peng, C. M. Carollo, L. Pozzetti, K. Caputi, J. D. Silverman, L. A. M. Tasca, M. Scodeggio, D. Vergani, N. Z. Scoville, P. Capak, T. Contini, J.-P. Kneib, O. Le Fèvre, V. Mainieri, A. Renzini, S. Bardelli, A. Bongiorno, G. Coppa, S. de la Torre, L. de Ravel, P. Franzetti, B. Garilli, L. Guzzo, P. Kampczyk, F. Lamareille, J.-F. Le Borgne, V. Le Brun, C. Maier, M. Mignoli, R. Pello, E. Perez Montero, E. Ricciardelli, M. Tanaka, L. Tresse, E. Zucca, U. Abbas, D. Bottini, A. Cappi, P. Cassata, A. Cimatti, M. Fumana, A. M. Koekemoer, D. Maccagni, C. Marinoni, H. J. McCracken, P. Memeo, B. Meneux, and R. Scaramella. The Density Field of the 10k zCOSMOS Galaxies. *ApJ*, 708: 505–533, January 2010. doi: 10.1088/0004-637X/708/1/505.

C. Lacey and S. Cole. Merger rates in hierarchical models of galaxy formation. *MNRAS*, 262:627–649, June 1993.

F. Lamareille, T. Contini, J.-F. Le Borgne, J. Brinchmann, S. Charlot, and J. Richard. Spectrophotometric properties of galaxies at intermediate redshifts ($z \sim 0.2 - 1.0$). I. Sample description, photometric properties and spectral measurements. *A&A*, 448:893–906, March 2006. doi: 10.1051/0004-6361:20053601.

R. B. Larson. Models for the formation of elliptical galaxies. *MNRAS*, 173: 671–699, December 1975.

R. B. Larson, B. M. Tinsley, and C. N. Caldwell. The evolution of disk galaxies and the origin of S0 galaxies. *ApJ*, 237:692–707, May 1980. doi: 10.1086/157917.

O. Le Fèvre, G. Vettolani, B. Garilli, L. Tresse, D. Bottini, V. Le Brun, D. Maccagni, J. P. Picat, R. Scaramella, M. Scodeggio, A. Zanichelli, C. Adami, M. Arnaboldi, S. Arnouts, S. Bardelli, M. Bolzonella, A. Cappi, S. Charlot, P. Ciliegi, T. Contini, S. Foucaud, P. Franzetti, I. Gavignaud, L. Guzzo, O. Ilbert, A. Iovino, H. J. McCracken, B. Marano, C. Marinoni, G. Mathez, A. Mazure, B. Meneux, R. Merighi, S. Paltani, R. Pellò, A. Pollo, L. Pozzetti, M. Radovich, G. Zamorani, E. Zucca, M. Bondi, A. Bongiorno, G. Busarello, F. Lamareille, Y. Mellier, P. Merluzzi, V. Ripepi, and D. Rizzo. The VIMOS VLT deep survey. First epoch VVDS-deep survey: 11 564 spectra with $17.5 \leq I_{\rm AB} \leq 24$, and the redshift distribution over $0 \leq z \leq 5$. *A&A*, 439:845–862, September 2005. doi: 10.1051/0004-6361:20041960.

J. Lequeux, M. Peimbert, J. F. Rayo, A. Serrano, and S. Torres-Peimbert. Chemical composition and evolution of irregular and blue compact galaxies. *A&A*, 80:155–166, December 1979.

S. J. Lilly, O. Le Fèvre, A. Renzini, G. Zamorani, M. Scodeggio, T. Contini, C. M. Carollo, G. Hasinger, J.-P. Kneib, A. Iovino, V. Le Brun, C. Maier, V. Mainieri, M. Mignoli, J. Silverman, L. A. M. Tasca, M. Bolzonella, A. Bongiorno, D. Bottini, P. Capak, K. Caputi, A. Cimatti, O. Cucciati, E. Daddi, R. Feldmann, P. Franzetti, B. Garilli, L. Guzzo, O. Ilbert, P. Kampczyk, K. Kovac, F. Lamareille, A. Leauthaud, J.-F. L. Borgne, H. J. McCracken, C. Marinoni, R. Pello, E. Ricciardelli, C. Scarlata, D. Vergani, D. B. Sanders, E. Schinnerer, N. Scoville, Y. Taniguchi, S. Arnouts, H. Aussel, S. Bardelli, M. Brusa, A. Cappi, P. Ciliegi, A. Finoguenov, S. Foucaud, R. Franceschini, C. Halliday, C. Impey, C. Knobel, A. Koekemoer, J. Kurk, D. Maccagni, S. Maddox, B. Marano, G. Marconi, B. Meneux, B. Mobasher, C. Moreau, J. A. Peacock, C. Porciani, L. Pozzetti, R. Scaramella, D. Schiminovich, P. Shopbell, I. Smail, D. Thompson, L. Tresse, G. Vettolani, A. Zanichelli, and E. Zucca. zCOSMOS: A Large VLT/VIMOS Redshift Survey Covering $0 < z < 3$ in the COSMOS Field. *ApJS*, 172:70–85, September 2007. doi: 10.1086/516589.

S. J. Lilly, V. Le Brun, C. Maier, V. Mainieri, M. Mignoli, M. Scodeggio, G. Zamorani, M. Carollo, T. Contini, J.-P. Kneib, O. Le Fèvre, A. Renzini, S. Bardelli, M. Bolzonella, A. Bongiorno, K. Caputi, G. Coppa, O. Cucciati, S. de la Torre, L. de Ravel, P. Franzetti, B. Garilli, A. Iovino, P. Kampczyk, K. Kovac, C. Knobel, F. Lamareille, J.-F. Le Borgne, R. Pello, Y. Peng, E. Pérez-Montero, E. Ricciardelli, J. D. Silverman, M. Tanaka, L. Tasca, L. Tresse, D. Vergani, E. Zucca, O. Ilbert, M. Salvato, P. Oesch, U. Abbas, D. Bottini, P. Capak, A. Cappi, P. Cassata, A. Cimatti, M. Elvis, M. Fumana,

L. Guzzo, G. Hasinger, A. Koekemoer, A. Leauthaud, D. Maccagni, C. Marinoni, H. McCracken, P. Memeo, B. Meneux, C. Porciani, L. Pozzetti, D. Sanders, R. Scaramella, C. Scarlata, N. Scoville, P. Shopbell, and Y. Taniguchi. The zCOSMOS 10k-Bright Spectroscopic Sample. *ApJS*, 184: 218–229, October 2009. doi: 10.1088/0067-0049/184/2/218.

T. Lisker, K. Glatt, P. Westera, and E. K. Grebel. Virgo Cluster Early-Type Dwarf Galaxies with the Sloan Digital Sky Survey. II. Early-Type Dwarfs with Central Star Formation. *AJ*, 132:2432–2452, December 2006. doi: 10.1086/508414.

J. M. Lotz, J. Primack, and P. Madau. A New Nonparametric Approach to Galaxy Morphological Classification. *AJ*, 128:163–182, July 2004. doi: 10.1086/421849.

L. M. Lubin, J. B. Oke, and M. Postman. Evidence for Cluster Evolution from an Improved Measurement of the Velocity Dispersion and Morphological Fraction of Cluster 1324+3011 at $z = 0.76$. *AJ*, 124:1905–1917, October 2002. doi: 10.1086/342542.

M.-M. Mac Low and A. Ferrara. Starburst-driven Mass Loss from Dwarf Galaxies: Efficiency and Metal Ejection. *ApJ*, 513:142–155, March 1999. doi: 10.1086/306832.

R. Mandelbaum, U. Seljak, G. Kauffmann, C. M. Hirata, and J. Brinkmann. Galaxy halo masses and satellite fractions from galaxy-galaxy lensing in the Sloan Digital Sky Survey: stellar mass, luminosity, morphology and environment dependencies. *MNRAS*, 368:715–731, May 2006. doi: 10.1111/j.1365-2966.2006.10156.x.

D. Marcillac, D. Elbaz, S. Charlot, Y. C. Liang, F. Hammer, H. Flores, C. Cesarsky, and A. Pasquali. The star formation history of luminous infrared galaxies. *A&A*, 458:369–383, November 2006. doi: 10.1051/0004-6361:20064996.

A. Marcolini, F. Brighenti, and A. D'Ercole. Three-dimensional simulations of the interstellar medium in dwarf galaxies - I. Ram pressure stripping. *MNRAS*, 345:1329–1339, November 2003. doi: 10.1046/j.1365-2966.2003.07054.x.

A. Marcolini, A. D'Ercole, F. Brighenti, and S. Recchi. Star formation feedback and metal enrichment by Types Ia and II supernovae in dwarf spheroidal galaxies: the case of Draco. *MNRAS*, 371:643–658, September 2006. doi: 10.1111/j.1365-2966.2006.10671.x.

C. L. Martin and R. C. Kennicutt, Jr. Star Formation Thresholds in Galactic Disks. *ApJ*, 555:301–321, July 2001. doi: 10.1086/321452.

D. C. Martin, T. K. Wyder, D. Schiminovich, T. A. Barlow, K. Forster, P. G. Friedman, P. Morrissey, S. G. Neff, M. Seibert, T. Small, B. Y. Welsh, L. Bianchi, J. Donas, T. M. Heckman, Y.-W. Lee, B. F. Madore, B. Milliard, R. M. Rich, A. S. Szalay, and S. K. Yi. The UV-Optical Galaxy Color-Magnitude Diagram. III. Constraints on Evolution from the Blue to the Red Sequence. *ApJS*, 173:342–356, December 2007. doi: 10.1086/516639.

K. L. Masters, M. Mosleh, A. K. Romer, R. C. Nichol, S. P. Bamford, K. Schawinski, C. J. Lintott, D. Andreescu, H. C. Campbell, B. Crowcroft, I. Doyle, E. M. Edmondson, P. Murray, M. J. Raddick, A. Slosar, A. S. Szalay, and J. Vandenberg. Galaxy Zoo: Passive Red Spirals. *ArXiv e-prints*, October 2009.

C. Mastropietro, B. Moore, L. Mayer, V. P. Debattista, R. Piffaretti, and J. Stadel. Morphological evolution of discs in clusters. *MNRAS*, 364:607–619, December 2005. doi: 10.1111/j.1365-2966.2005.09579.x.

C. Maulbetsch, V. Avila-Reese, P. Colín, S. Gottlöber, A. Khalatyan, and M. Steinmetz. The Dependence of the Mass Assembly History of Cold Dark Matter Halos on Environment. *ApJ*, 654:53–65, January 2007. doi: 10.1086/509706.

L. Mayer, F. Governato, M. Colpi, B. Moore, T. Quinn, J. Wadsley, J. Stadel, and G. Lake. The Metamorphosis of Tidally Stirred Dwarf Galaxies. *ApJ*, 559:754–784, October 2001. doi: 10.1086/322356.

L. Mayer, C. Mastropietro, J. Wadsley, J. Stadel, and B. Moore. Simultaneous ram pressure and tidal stripping; how dwarf spheroidals lost their gas. *MNRAS*, 369:1021–1038, July 2006. doi: 10.1111/j.1365-2966.2006.10403.x.

J. Melnick and W. L. W. Sargent. The radial distribution of morphological types of galaxies in X-ray clusters. *ApJ*, 215:401–407, July 1977. doi: 10.1086/155369.

E. Merlin and C. Chiosi. Formation and evolution of early-type galaxies. II. Models with quasi-cosmological initial conditions. *A&A*, 457:437–453, October 2006. doi: 10.1051/0004-6361:20054486.

M. Mignoli, A. Cimatti, G. Zamorani, L. Pozzetti, E. Daddi, A. Renzini, T. Broadhurst, S. Cristiani, S. D'Odorico, A. Fontana, E. Giallongo, R. Gilmozzi, N. Menci, and P. Saracco. The K20 survey. VII. The

spectroscopic catalogue: Spectral properties and evolution of the galaxy population. *A&A*, 437:883–897, July 2005. doi: 10.1051/0004-6361:20042434.

M. Mignoli, G. Zamorani, M. Scodeggio, A. Cimatti, C. Halliday, S. J. Lilly, L. Pozzetti, D. Vergani, C. M. Carollo, T. Contini, O. Le Févre, V. Mainieri, A. Renzini, S. Bardelli, M. Bolzonella, A. Bongiorno, K. Caputi, G. Coppa, O. Cucciati, S. de La Torre, L. de Ravel, P. Franzetti, B. Garilli, A. Iovino, P. Kampczyk, J.-P. Kneib, C. Knobel, K. Kovač, F. Lamareille, J.-F. Le Borgne, V. Le Brun, C. Maier, R. Pellò, Y. Peng, E. Perez Montero, E. Ricciardelli, C. Scarlata, J. D. Silverman, M. Tanaka, L. Tasca, L. Tresse, E. Zucca, U. Abbas, D. Bottini, P. Capak, A. Cappi, P. Cassata, M. Fumana, L. Guzzo, A. Leauthaud, D. Maccagni, C. Marinoni, H. J. McCracken, P. Memeo, B. Meneux, P. Oesch, C. Porciani, R. Scaramella, and N. Scoville. The zCOSMOS redshift survey: the three-dimensional classification cube and bimodality in galaxy physical properties. *A&A*, 493:39–49, January 2009. doi: 10.1051/0004-6361:200810520.

J. C. Mihos and L. Hernquist. Ultraluminous starbursts in major mergers. *ApJ*, 431:L9–L12, August 1994. doi: 10.1086/187460.

J. C. Mihos and L. Hernquist. Gasdynamics and Starbursts in Major Mergers. *ApJ*, 464:641–+, June 1996. doi: 10.1086/177353.

R. G. Miller. *Simultaneous statistical inference*. McGraw-Hill New York,, 1966.

B. Moore, N. Katz, G. Lake, A. Dressler, and A. Oemler. Galaxy harassment and the evolution of clusters of galaxies. *Nat*, 379:613–616, February 1996. doi: 10.1038/379613a0.

B. Moore, G. Lake, T. Quinn, and J. Stadel. On the survival and destruction of spiral galaxies in clusters. *MNRAS*, 304:465–474, April 1999. doi: 10.1046/j.1365-8711.1999.02345.x.

T. Naab and A. Burkert. Statistical Properties of Collisionless Equal- and Unequal-Mass Merger Remnants of Disk Galaxies. *ApJ*, 597:893–906, November 2003. doi: 10.1086/378581.

K. Nandra, A. Georgakakis, C. N. A. Willmer, M. C. Cooper, D. J. Croton, M. Davis, S. M. Faber, D. C. Koo, E. S. Laird, and J. A. Newman. AEGIS: The Color-Magnitude Relation for X-Ray-selected Active Galactic Nuclei. *ApJ*, 660:L11–L14, May 2007. doi: 10.1086/517918.

J. E. Nelan, R. J. Smith, M. J. Hudson, G. A. Wegner, J. R. Lucey, S. A. W. Moore, S. J. Quinney, and N. B. Suntzeff. NOAO Fundamental Plane Survey. II. Age and Metallicity along the Red Sequence from Line-Strength Data. *ApJ*, 632:137–156, October 2005. doi: 10.1086/431962.

K. G. Noeske, S. M. Faber, B. J. Weiner, D. C. Koo, J. R. Primack, A. Dekel, C. Papovich, C. J. Conselice, E. Le Floc'h, G. H. Rieke, A. L. Coil, J. M. Lotz, R. S. Somerville, and K. Bundy. Star Formation in AEGIS Field Galaxies since $z = 1.1$: Staged Galaxy Formation and a Model of Mass-dependent Gas Exhaustion. *ApJ*, 660:L47–L50, May 2007a. doi: 10.1086/517927.

K. G. Noeske, B. J. Weiner, S. M. Faber, C. Papovich, D. C. Koo, R. S. Somerville, K. Bundy, C. J. Conselice, J. A. Newman, D. Schiminovich, E. Le Floc'h, A. L. Coil, G. H. Rieke, J. M. Lotz, J. R. Primack, P. Barmby, M. C. Cooper, M. Davis, R. S. Ellis, G. G. Fazio, P. Guhathakurta, J. Huang, S. A. Kassin, D. C. Martin, A. C. Phillips, R. M. Rich, T. A. Small, C. N. A. Willmer, and G. Wilson. Star Formation in AEGIS Field Galaxies since $z = 1.1$: The Dominance of Gradually Declining Star Formation, and the Main Sequence of Star-forming Galaxies. *ApJ*, 660:L43–L46, May 2007b. doi: 10.1086/517926.

A. Oemler, Jr. The Systematic Properties of Clusters of Galaxies. Photometry of 15 Clusters. *ApJ*, 194:1–20, November 1974. doi: 10.1086/153216.

D. E. Osterbrock. Interstellar Matter in Elliptical Galaxies. II. *ApJ*, 132: 325–+, September 1960. doi: 10.1086/146930.

B. Panter, R. Jimenez, A. F. Heavens, and S. Charlot. The star formation histories of galaxies in the Sloan Digital Sky Survey. *MNRAS*, 378:1550–1564, July 2007. doi: 10.1111/j.1365-2966.2007.11909.x.

K. Pearson. On Lines and Planes of Closest Fit to Points in Space. *Philosophical Magazine*, 2:559–572, 1901.

L. S. Pilyugin and F. Ferrini. The oxygen abundance deficiency in irregular galaxies. *A&A*, 354:874–880, February 2000.

B. M. Poggianti and H. Wu. Optical Spectral Signatures of Dusty Starburst Galaxies. *ApJ*, 529:157–169, January 2000. doi: 10.1086/308243.

M. Postman and M. J. Geller. The morphology-density relation - The group connection. *ApJ*, 281:95–99, June 1984. doi: 10.1086/162078.

L. Pozzetti, M. Bolzonella, E. Zucca, G. Zamorani, S. Lilly, A. Renzini, M. Moresco, M. Mignoli, P. Cassata, L. Tasca, E. Lamareille, C. Maier,

B. Meneux, P. Oesch, D. Vergani, K. Caputi, K. Kovac, A. Cimatti, O. Cucciati, A. Iovino, Y. Peng, M. Carollo, T. Contini, J. P. Kneib, O. Le Fevre, V. Mainieri, M. Scodeggio, S. Bardelli, A. Bongiorno, G. Coppa, S . de la Torre, L. de Ravel, P. Franzetti, B. Garilli, P. Kampczyk, C. Knobel, J. F. Le Borgne, V. Le Brun, R. Pello, E. Perez Montero, E. Ricciardelli, J. Silverman, M. Tanaka, L. Tresse, U. Abbas, D. Bottini, A. Cappi, L. Guzzo, C. Halliday, A. Leauthaud, A. Koekemoer, D. Maccagni, C. Marinoni, H. McCracken, P. Memeo, C. Porciani, R. Scaramella, C. Scarlata, and N. Scoville. zCOSMOS - 10k-bright spectroscopic sample. The bimodality in the Galaxy Stellar Mass Function: exploring its evolution with redshift. *ArXiv e-prints*, July 2009.

R Development Core Team. *R: A Language and Environment for Statistical Computing*. R Foundation for Statistical Computing, Vienna, Austria, 2009. URL `http://www.R-project.org`. ISBN 3-900051-07-0.

E. Roediger and G. Hensler. Ram pressure stripping of disk galaxies. From high to low density environments. *A&A*, 433:875–895, April 2005. doi: 10.1051/0004-6361:20042131.

K. Roettiger, J. O. Burns, and C. Loken. The Observational Consequences of Merging Clusters of Galaxies. *ApJ*, 473:651–+, December 1996. doi: 10.1086/178179.

E. E. Salpeter. The Luminosity Function and Stellar Evolution. *ApJ*, 121: 161–+, January 1955. doi: 10.1086/145971.

D. B. Sanders and I. F. Mirabel. Luminous Infrared Galaxies. *ARA&A*, 34: 749–+, 1996. doi: 10.1146/annurev.astro.34.1.749.

M. J. Sawicki, H. Lin, and H. K. C. Yee. Evolution of the Galaxy Population Based on Photometric Redshifts in the Hubble Deep Field. *AJ*, 113:1–12, January 1997. doi: 10.1086/118231.

C. Scannapieco, P. B. Tissera, S. D. M. White, and V. Springel. Feedback and metal enrichment in cosmological SPH simulations - II. A multiphase model with supernova energy feedback. *MNRAS*, 371:1125–1139, September 2006. doi: 10.1111/j.1365-2966.2006.10785.x.

C. Scarlata, C. M. Carollo, S. Lilly, M. T. Sargent, R. Feldmann, P. Kampczyk, C. Porciani, A. Koekemoer, N. Scoville, J.-P. Kneib, A. Leauthaud, R. Massey, J. Rhodes, L. Tasca, P. Capak, C. Maier, H. J. McCracken, B. Mobasher, A. Renzini, Y. Taniguchi, D. Thompson, K. Sheth, M. Ajiki,

H. Aussel, T. Murayama, D. B. Sanders, S. Sasaki, Y. Shioya, and M. Takahashi. COSMOS Morphological Classification with the Zurich Estimator of Structural Types (ZEST) and the Evolution Since $z = 1$ of the Luminosity Function of Early, Disk, and Irregular Galaxies. *ApJS*, 172: 406–433, September 2007. doi: 10.1086/516582.

K. Schawinski. Do AGN suppress star formation in early-type galaxies? *ArXiv e-prints*, February 2010.

K. Schawinski, D. Thomas, M. Sarzi, C. Maraston, S. Kaviraj, S.-J. Joo, S. K. Yi, and J. Silk. Observational evidence for AGN feedback in early-type galaxies. *MNRAS*, 382:1415–1431, December 2007. doi: 10.1111/j.1365-2966.2007.12487.x.

M. Schmidt. The Rate of Star Formation. *ApJ*, 129:243–+, March 1959. doi: 10.1086/146614.

F. Schweizer. Interactions as a driver of galaxy evolution. In *Astronomy, physics and chemistry of H_3^+*, volume 358 of *Royal Society of London Philosophical Transactions Series A*, pages 2063–+, July 2000. doi: 10.1098/rsta.2000.0630.

F. Schweizer. Colliding and Merging Galaxies. III. The Dynamically Young Merger Remnant NGC 3921. *AJ*, 111:109–+, January 1996. doi: 10.1086/117765.

F. Schweizer and P. Seitzer. Correlations between UBV colors and fine structure in E and S0 galaxies - A first attempt at dating ancient merger events. *AJ*, 104:1039–1067, September 1992. doi: 10.1086/116296.

J. L. Sérsic. Influence of the atmospheric and instrumental dispersion on the brightness distribution in a galaxy. *Boletin de la Asociacion Argentina de Astronomia La Plata Argentina*, 6:41–+, 1963.

Joseph Silk. *The big bang : the creation and evolution of the universe*. W. H. Freeman, San Francisco :, 1980. ISBN 0716710846 0716710854.

J. D. Silverman, V. Mainieri, B. D. Lehmer, D. M. Alexander, F. E. Bauer, J. Bergeron, W. N. Brandt, R. Gilli, G. Hasinger, D. P. Schneider, P. Tozzi, C. Vignali, A. M. Koekemoer, T. Miyaji, P. Popesso, P. Rosati, and G. Szokoly. The Evolution of AGN Host Galaxies: From Blue to Red and the Influence of Large-Scale Structures. *ApJ*, 675:1025–1040, March 2008. doi: 10.1086/527283.

I. Smail, R. S. Ellis, A. Dressler, W. J. Couch, A. Oemler, Jr., R. M. Sharples, and H. Butcher. A Comparison of Direct and Indirect Mass Estimates for Distant Clusters of Galaxies. *ApJ*, 479:70–+, April 1997. doi: 10.1086/303844.

G. P. Smith, T. Treu, R. S. Ellis, S. M. Moran, and A. Dressler. Evolution since $z = 1$ of the Morphology-Density Relation for Galaxies. *ApJ*, 620:78–87, February 2005. doi: 10.1086/426930.

V. Springel, S. D. M. White, G. Tormen, and G. Kauffmann. Populating a cluster of galaxies - I. Results at $z = 0$. *MNRAS*, 328:726–750, December 2001. doi: 10.1046/j.1365-8711.2001.04912.x.

V. Springel, T. Di Matteo, and L. Hernquist. Modelling feedback from stars and black holes in galaxy mergers. *MNRAS*, 361:776–794, August 2005a. doi: 10.1111/j.1365-2966.2005.09238.x.

V. Springel, S. D. M. White, A. Jenkins, C. S. Frenk, N. Yoshida, L. Gao, J. Navarro, R. Thacker, D. Croton, J. Helly, J. A. Peacock, S. Cole, P. Thomas, H. Couchman, A. Evrard, J. Colberg, and F. Pearce. Simulations of the formation, evolution and clustering of galaxies and quasars. *Nat*, 435:629–636, June 2005b. doi: 10.1038/nature03597.

I. Strateva, Ž. Ivezić, G. R. Knapp, V. K. Narayanan, M. A. Strauss, J. E. Gunn, R. H. Lupton, D. Schlegel, N. A. Bahcall, J. Brinkmann, R. J. Brunner, T. Budavári, I. Csabai, F. J. Castander, M. Doi, M. Fukugita, Z. Győry, M. Hamabe, G. Hennessy, T. Ichikawa, P. Z. Kunszt, D. Q. Lamb, T. A. McKay, S. Okamura, J. Racusin, M. Sekiguchi, D. P. Schneider, K. Shimasaku, and D. York. Color Separation of Galaxy Types in the Sloan Digital Sky Survey Imaging Data. *AJ*, 122:1861–1874, October 2001. doi: 10.1086/323301.

M. Takamiya. Galaxy Structural Parameters: Star Formation Rate and Evolution with Redshift. *ApJS*, 122:109–150, May 1999. doi: 10.1086/313216.

M. Tanaka, T. Kodama, N. Arimoto, S. Okamura, K. Umetsu, K. Shimasaku, I. Tanaka, and T. Yamada. The build-up of the colour-magnitude relation as a function of environment. *MNRAS*, 362:268–288, September 2005. doi: 10.1111/j.1365-2966.2005.09300.x.

L. A. M. Tasca, J.-P. Kneib, A. Iovino, O. Le Fèvre, K. Kovač, M. Bolzonella, S. J. Lilly, R. G. Abraham, P. Cassata, O. Cucciati, L. Guzzo, L. Tresse,

G. Zamorani, P. Capak, B. Garilli, M. Scodeggio, K. Sheth, E. Zucca, C. M. Carollo, T. Contini, V. Mainieri, A. Renzini, S. Bardelli, A. Bongiorno, K. Caputi, G. Coppa, S. de La Torre, L. de Ravel, P. Franzetti, P. Kampczyk, C. Knobel, A. M. Koekemoer, F. Lamareille, J.-F. Le Borgne, V. Le Brun, C. Maier, M. Mignoli, R. Pello, Y. Peng, E. Perez Montero, E. Ricciardelli, J. D. Silverman, D. Vergani, M. Tanaka, U. Abbas, D. Bottini, A. Cappi, A. Cimatti, O. Ilbert, A. Leauthaud, D. Maccagni, C. Marinoni, H. J. McCracken, P. Memeo, B. Meneux, P. Oesch, C. Porciani, L. Pozzetti, R. Scaramella, and C. Scarlata. The zCOSMOS redshift survey: the role of environment and stellar mass in shaping the rise of the morphology-density relation from $z \sim 1$. *A&A*, 503:379–398, August 2009. doi: 10.1051/0004-6361/200912213.

K. Tassis, A. V. Kravtsov, and N. Y. Gnedin. Scaling Relations of Dwarf Galaxies without Supernova-driven Winds. *ApJ*, 672:888–903, January 2008. doi: 10.1086/523880.

A. Toomre. Mergers and some consequences. In B. M. Tinsley and R. B. Larson, editors, *The Evolution Of Galaxies And Stellar Populations*, pages 401–426, New Haven, 1977. Yale Univ. Observatory.

C. A. Tremonti, T. M. Heckman, G. Kauffmann, J. Brinchmann, S. Charlot, S. D. M. White, M. Seibert, E. W. Peng, D. J. Schlegel, A. Uomoto, M. Fukugita, and J. Brinkmann. The Origin of the Mass-Metallicity Relation: Insights from 53,000 Star-forming Galaxies in the Sloan Digital Sky Survey. *ApJ*, 613:898–913, October 2004. doi: 10.1086/423264.

T. Treu, R. S. Ellis, J.-P. Kneib, A. Dressler, I. Smail, O. Czoske, A. Oemler, and P. Natarajan. A Wide-Field Hubble Space Telescope Study of the Cluster Cl 0024+16 at $z = 0.4$. I. Morphological Distributions to 5 Mpc Radius. *ApJ*, 591:53–78, July 2003. doi: 10.1086/375314.

R. B. Tully, J. R. Mould, and M. Aaronson. A color-magnitude relation for spiral galaxies. *ApJ*, 257:527–537, June 1982. doi: 10.1086/160009.

S. van den Bergh. Photoelectric Spectrophotometry of Stars. *AJ*, 68:295–+, 1963. doi: 10.1086/109055.

S. van den Bergh. A new classification system for galaxies. *ApJ*, 206:883–887, June 1976. doi: 10.1086/154452.

S. van den Bergh and I. J. Sackmann. The Abundance of Carbon, Nitrogen, and the Metals in Main Sequence Stars. *AJ*, 70:133–+, March 1965. doi: 10.1086/109686.

P. G. van Dokkum and M. Franx. Morphological Evolution and the Ages of Early-Type Galaxies in Clusters. *ApJ*, 553:90–102, May 2001. doi: 10.1086/320645.

P. G. van Dokkum and S. A. Stanford. The Fundamental Plane at $z = 1.27$: First Calibration of the Mass Scale of Red Galaxies at Redshifts $z < 1$. *ApJ*, 585:78–89, March 2003. doi: 10.1086/345989.

P. G. van Dokkum, M. Franx, D. Fabricant, G. D. Illingworth, and D. D. Kelson. Hubble Space Telescope Photometry and Keck Spectroscopy of the Rich Cluster MS 1054-03: Morphologies, Butcher-Oemler Effect, and the Color-Magnitude Relation at $z = 0.83$. *ApJ*, 541:95–111, September 2000. doi: 10.1086/309402.

L. van Zee. The Evolutionary Status of Isolated Dwarf Irregular Galaxies. II. Star Formation Histories and Gas Depletion. *AJ*, 121:2003–2019, April 2001. doi: 10.1086/319947.

W. N. Venables and B. D. Ripley. *Modern Applied Statistics with S. Fourth Edition*. Springer, New York, 2002. URL `http://www.stats.ox.ac.uk/pub/MASS4/`. ISBN 0-387-95457-0.

D. Vergani, G. Zamorani, S. Lilly, F. Lamareille, C. Halliday, M. Scodeggio, C. Vignali, P. Ciliegi, M. Bolzonella, M. Bondi, K. Kovač, C. Knobel, E. Zucca, K. Caputi, L. Pozzetti, S. Bardelli, M. Mignoli, A. Iovino, C. M. Carollo, T. Contini, J.-P. Kneib, O. Le Fèvre, V. Mainieri, A. Renzini, A. Bongiorno, G. Coppa, O. Cucciati, S. de La Torre, L. de Ravel, P. Franzetti, B. Garilli, P. Kampczyk, J.-F. Le Borgne, V. Le Brun, C. Maier, R. Pello, Y. Peng, E. Perez Montero, E. Ricciardelli, J. D. Silverman, M. Tanaka, L. Tasca, L. Tresse, U. Abbas, D. Bottini, A. Cappi, P. Cassata, A. Cimatti, L. Guzzo, A. M. Koekemoer, A. Leauthaud, D. Maccagni, C. Marinoni, H. J. McCracken, P. Memeo, B. Meneux, P. Oesch, C. Porciani, R. Scaramella, P. Capak, D. Sanders, N. Scoville, and Y. Taniguchi. K+a galaxies in the zCOSMOS survey . Physical properties of systems in their post-starburst phase. *A&A*, 509(26):A260000+, January 2010. doi: 10.1051/0004-6361/200912802.

B. Vollmer, V. Cayatte, C. Balkowski, and W. J. Duschl. Ram Pressure Stripping and Galaxy Orbits: The Case of the Virgo Cluster. *ApJ*, 561: 708–726, November 2001. doi: 10.1086/323368.

S. D. M. White and M. J. Rees. Core condensation in heavy halos - A two-

stage theory for galaxy formation and clustering. *MNRAS*, 183:341–358, May 1978.

R. L. Wildey, E. M. Burbidge, A. R. Sandage, and G. R. Burbidge. On the Effect of Fraunhofer Lines on u, b, V Measurements. *ApJ*, 135:94–+, January 1962. doi: 10.1086/147251.

J. D. Younger, P. F. Hopkins, T. J. Cox, and L. Hernquist. The Self-Regulated Growth of Supermassive Black Holes. *ApJ*, 686:815–828, October 2008. doi: 10.1086/591639.

M. A. Zamojski, D. Schiminovich, R. M. Rich, B. Mobasher, A. M. Koekemoer, P. Capak, Y. Taniguchi, S. S. Sasaki, H. J. McCracken, Y. Mellier, E. Bertin, H. Aussel, D. B. Sanders, O. Le Fèvre, O. Ilbert, M. Salvato, D. J. Thompson, J. S. Kartaltepe, N. Scoville, T. A. Barlow, K. Forster, P. G. Friedman, D. C. Martin, P. Morrissey, S. G. Neff, M. Seibert, T. Small, T. K. Wyder, L. Bianchi, J. Donas, T. M. Heckman, Y.-W. Lee, B. F. Madore, B. Milliard, A. S. Szalay, B. Y. Welsh, and S. K. Yi. Deep GALEX Imaging of the COSMOS HST Field: A First Look at the Morphology of $z \sim 0.7$ Star-forming Galaxies. *ApJS*, 172:468–493, September 2007. doi: 10.1086/516593.

E. Zucca, S. Bardelli, M. Bolzonella, G. Zamorani, O. Ilbert, L. Pozzetti, M. Mignoli, K. Kovač, S. Lilly, L. Tresse, L. Tasca, P. Cassata, C. Halliday, D. Vergani, K. Caputi, C. M. Carollo, T. Contini, J.-P. Kneib, O. Le Fèvre, V. Mainieri, A. Renzini, M. Scodeggio, A. Bongiorno, G. Coppa, O. Cucciati, S. de La Torre, L. de Ravel, P. Franzetti, B. Garilli, A. Iovino, P. Kampczyk, C. Knobel, F. Lamareille, J.-F. Le Borgne, V. Le Brun, C. Maier, R. Pellò, Y. Peng, E. Perez-Montero, E. Ricciardelli, J. D. Silverman, M. Tanaka, U. Abbas, D. Bottini, A. Cappi, A. Cimatti, L. Guzzo, A. M. Koekemoer, A. Leauthaud, D. Maccagni, C. Marinoni, H. J. McCracken, P. Memeo, B. Meneux, M. Moresco, P. Oesch, C. Porciani, R. Scaramella, S. Arnouts, H. Aussel, P. Capak, J. Kartaltepe, M. Salvato, D. Sanders, N. Scoville, Y. Taniguchi, and D. Thompson. The zCOSMOS survey: the role of the environment in the evolution of the luminosity function of different galaxy types. *A&A*, 508:1217–1234, December 2009. doi: 10.1051/0004-6361/200912665.